PERFORMANCE BASED SEISMIC DESIGN OF R.C.C. BUILDING

BY

Jigar R. Zala

09MCL018

DEPARTMENT OF CIVIL ENGINEERING

AHMEDABAD-382481

May 2011

PERFORMANCE BASED SEISMIC DESIGN OF R.C.C. BUILDING

Major Project

Submitted in partial fulfillment of the requirements

For the degree of

Master of Technology in Civil Engineering

(Computer Aided Structural Analysis And Design)

By

Jigar R. Zala

09MCL018

DEPARTMENT OF CIVIL ENGINEERING

AHMEDABAD-382481

May 2011

Declaration

This is to certify that

a. The thesis comprises my original work towards the Degree of Master of Technology in Civil Engineering (Computer Aided Structural Analysis and Design) at Nirma University and has not been submitted elsewhere for a degree.

b. Due acknowledgement has been made in the text to all other material used.

Jigar R. Zala

Certificate

This is to certify that the Major project entitled "Performance Based Seismic Design of R.C.C. Building" submitted by Jigar R. Zala (09MCL018), towards the partial fulfillment of the requirement for the degree of Master of Technology in civil Engineering (Computer Aided Structural Analysis and Design) of Nirma University, Ahmedabad, is the record of work carried out by him under my supervision and guidance. In my opinion, the submitted work has reached a level required for being accepted for examination. The results embodied in this major project, to the best of my knowledge, haven't been submitted to any other university or institution for award of any degree or diploma.

Dr. S. P. Purohit
Guide and Associate Professor,
Department of Civil Engineering,
Institute of Technology,
Nirma University, Ahmedabad.

Dr. P. H. Shah
Professor and Head,
Department of Civil Engineering,
Institute of Technology,
Nirma University, Ahmedabad.

Dr K Kotecha
Director,
Institute of Technology,
Nirma University,
Ahmedabad

____
Examiner

____
Date of Examintion

Abstract

Earthquakes are known to produce one of the most destructive forces on the earth. It can causes loss of life and property and economical loss of the country. Earthquake cannot be prevented, since it is unpredictable, but loss of life of people and damage to the structures can be prevented if later is designed properly.

Among various seismic design philosophies exists, Performance Based Design (PBD) of structure is the modern approach to earthquake resistant design. PBD explicitly evaluates how a building is likely to perform, given the potential hazard it is likely to experience, considering uncertainties inherent in the quantification of potential hazard and uncertainties in assessment of the actual building response. PBD is applicable to design of new buildings or retrofit to existing buildings. PBD defines various limit state of performance for the building and hence gives clearcut idea about its performance under hazards that is considered. However, PBD is not to be considered as an alternate to rigorous nonlinear time history analysis.

Present study is an attempt to understand PBD of building and its importance in quantifying its performance under considered seismic hazards. The aim of the study is to obtain performance of 3D multistorey building using PBD. Also, assess the performance of the building under different seismic hazards through fragility curves showing probability of exceeding particular limit state due to such seismic hazards. Fragility Curves are generated for building analyzed by PBD as well as nonlinear Time History Analysis, using specified limit states as per ATC-40 and Indian code. Analysis has beeb carried out using ETABS (version 9.5). Fragility Curves obtained for limit state specification on response quantities like peak interstorey drift and peak displacement are generated and reviewed in details, in order to conclude the work. Additionally, a parametric study regarding lateral load pattern to Pushover Analysis, modeling and capacity uncertainty to obtained fragility curves are also included.

Acknowledgements

I would first of all like to thanks **Dr. S. P. Purohit**, Guide M.Tech. Department of Civil Engineering (CASAD), Institute of Technology, Nirma University, Ahmedabad whose keen interest and excellent knowledge base helped me to carry out the dissertation work. His constant support and interest in the subject equipped me with a great understanding of different aspects of the required architecture for the project work. He has shown keen interest in this dissertation work right from beginning and has been a great motivating factor in outlining the flow of my work.

My sincere thanks and gratitude to **Prof. G. N. Patel**, Formerly Professor, Department of Civil Engineering, **Dr. P. V. Patel**, Professor, Department of Civil Engineering, and **Prof. N. C. Vyas**, Professor, Department of Civil Engineering, **Shri Himat Solanki**, Visiting Faculty, Department of Civil Engineering, and **Dr. U. V. Dave**, Associate Professor, Civil Engineering Department, Institute of Technology, Nirma University, Ahmedabad for his continual kind words of encouragement and motivation throughout the Dissertation work.

I further extend my thanks to **Dr. P. H. Shah**, Head, Department of Civil Engineering, Institute of Technology, Nirma University, Ahmedabad and **Dr K Kotecha**, Director, Institute of Technology, Nirma University, Ahmedabad for providing all kind of required resources during my study.

I would like to thank The Almighty, my family and all my friends, for supporting and encouraging me in all possible ways throughout the dissertation work.

- Jigar R. Zala

09MCL018

Abbreviation Notation and Nomenclature

ADRS .... Acceleration Displacement Response-Spectra

ATC .... Applied Technology Council

ABS .... Absolute Method

BF .... Base Force

CP .... Collapse Prevention

CQC .... Complete Quadratic Combination

Ca .... Coefficient of Acceleration

Cv .... Coefficient of Velocity

CSM .... Capacity Spectrum Method

D .... Response demand

E_D .... Energy dissipated by damping

E_{SO} .... Maximum strain energy

FEMA .... Federal Emergency Management Egency

GMC .... General Modal Combination

GMI .... Ground Motion Intensity

HAZUS .... Hazard Loss Estimation Software, US

IO .... Immediate Occupancy

LS .... Life Safety

M3 Hinge .... Default Moment hinge

MAEC .... Mid-American Earthquake Center

PBD .... Performance Based Design

PGA .... Peak Ground Acceleration

P Hinge .... Axial hinge

PMM Hinge .... Axial Moment Interaction hinge

PEERC .... Pacific Earthquake Engineering Research Center

PF_1 .... Participation factor

$P(LS_i/GMI)$ .... Probability of exceeding a particular limit state

PGV .... Peak Ground Velocity

PGD . . . . Peak Ground Displacement
RCC . . . . Reinforced Cement Concrete
SEAOC . . . . Structural Engineers Associations of California
SRSS . . . . Square Root of the Sum of Square
S . . . . Earthquake intensity
Sa_i . . . . Spectral Acceleration
Sd_i . . . . Spectral Displacement
S_v . . . . Spectral Velocity
V_i . . . . Base Shear
V2 Hinge . . . . Default Shear hinge
V/W . . . . Base Shear to Seismic Weight Ratio
SRSS . . . . Square Root of the Sum of Square
δ_i . . . . Roof-Displacement
α_1 . . . . Model mass coefficient
$\phi_{1,roof}$ . . . . Roof level amplitude
λ . . . . Modification factor
β_{eff} . . . . Effective damping
Φ . . . . Standard normal distribution function
λ_{CL} . . . . Median drift capacity for a particular limit state
β_{CL} . . . . Uncertainty associated with drift capacity criteria
β_M . . . . Uncertainty associated with modeling of the structure
$\beta_{D/GMI}$ . . . . Square root of the standard error

Contents

List of Tables

List of Figures

Chapter 1

Introduction

1.1 General

Historically, introduction and enforcement of structural design codes and standards has been the responsibility of competent Authorities, with public safety as their overriding consideration. So, traditional seismic design codes or standards, especially for buildings, aim at protecting human life by preventing local or global collapse under a specific earthquake level with low probability of exceedance. However, in the 1960's the international earthquake engineering community was already aware of the importance of property loss and other economic consequences caused by more frequent seismic events. Recognizing that it is not feasible to avoid any damage under strong earthquakes, the Structural Engineers Association of California (SEAOC) adopted in its 1968 recommendations the following requirements for seismic design:[**1**]

Structures should, in general, be able to:

- Resist a minor level of earthquake ground motion without damage.
- Resist a moderate level of earthquake ground motion without structural damage, but possibly experience some nonstructural damage.
- Resist a major level of earthquake ground motion having an intensity equal to the strongest either experienced or forecast for the building site, without collapse, but possibly with some structural as well as nonstructural damage.

Major earthquakes that hit developed countries in the second half of the 1980's and the first half of the 1990's caused relatively few casualties but very large damage to property and other economic losses. In response to this, Performance Based Earthquake Engineering emerged in the SEAOC Vision 2000 document and developed into the single most important idea of recent years for seismic design or retrofitting of buildings.

"Performance Based Earthquake Engineering" in particular tries to maximize the utility from the use of a facility by minimizing its expected total cost, including the short-term cost of the work and the expected value of the loss in future earthquakes (in terms of casualties, cost of repair or replacement, disruption of use, etc.).

Ideally we should take into account all possible future seismic events with their annual probability of occurrence and carry out a convolution with the corresponding consequences during the design working life of the facility. Therefore, at present performance-based earthquake engineering advocates replacing the traditional single-tier design against collapse and its prescriptive rules, with a transparent multi-tier seismic design, meeting several discrete performance levels, each one under a different seismic event with its own annual probability of exceedance.

Seismic analysis methods of the structures can be characterized as, Seismic coefficient method and Dynamic Analysis. Seismic coefficient method is an equivalent static analysis considering a design seismic coefficient. The design seismic coefficients include factors such as Importance Factor, Soil-foundation Factor, Response Reduction Factor and Zone Factor. In order to simplify the methods of analysis for determining earthquake effects on structures, codes of practice recommend Seismic Coefficient Method. Dynamic analysis can be characterized as, Response Spectrum analysis for linear structures and Time History analysis for linear or non-linear Structures.

1.2 Background

Performance-based Design specifically intended to limit the consequences of one or more hazards to acceptable levels likes Earthquake, Blast Effect, Fire Effect and

Wind Load. The causalities from the earthquakes suffered during the last decade has made it necessary to control and access buildings that have been constructed without any regard to appropriate seismic design characteristics. Thus, in recent years there has been an extensive examination of performance of structures during an earthquake using performance based techniques. The widely used method to evaluate performance of structures is Nonlinear Static Analysis known as "Pushover Analysis."

The basic concept of PBD is to provide the capability to design buildings that have a predictable and reliable performance in earthquakes. PBD is an attempt to predict the performance of buildings under expected seismic event. A structure designed with PBD concept does not developed undesirable failure mechanism during earthquake. The analysis can be performed on new as well as existing buildings and the performance of buildings in future earthquake can be evaluated.

Most buildings today are designed to resist earthquakes through conformance to procedures specified by the building codes.The code-specified procedures are intended to protect life safety in the most severe earthquakes ever likely to affect buildings and reduce property damage and loss in more frequent, moderate earthquakes.

These nonlinear static procedures constitute an inelastic analysis that considers what happens to buildings after they begin to crack and yield in response to realistic earthquake motions.

This approach differs from traditional linear static procedures that reduce seismic forces to levels that allow engineers to design buildings under the assumption.

1.3 Objective of the study

As mentioned above, each building need to access for its seismic capacity and characteristic performance of building is required to understand. Hence, performance based seismic analysis is essential for the buildings to understand its behavior and response during earthquake.

The main objective of study is to perform performance based seismic analysis i.e. to obtain performance levels of buildings for the future earthquake and to provide a new framework for developing fragility relationships of buildings, in order to quantify limit state levels. As shown in Figure 1.1, Pushover curves and time histories con-

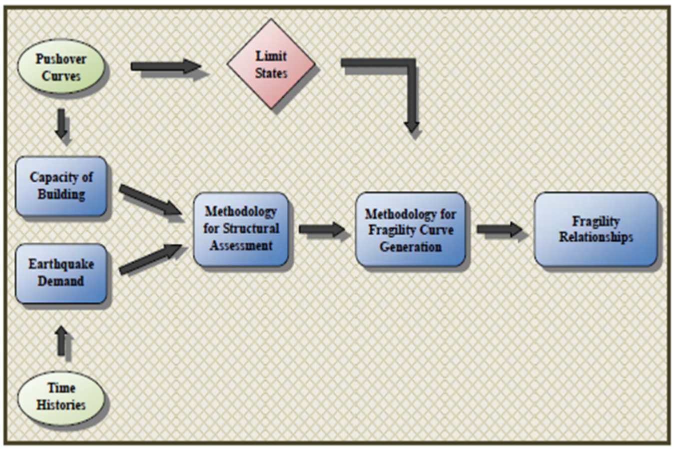

Figure 1.1: Flowchart for the proposed procedure of fragility analysis[2]

stitute the capacity of building and earthquake demand respectively. These first two components can be considered as inputs to the simulation engine which is the third component, i.e. the methodology for structural assessment. Structural response data obtained by analyzing the building capacity under the earthquake demand is processed by the methodology for fragility curve generation (fourth component) to yield the results. Limit states, which are determined from the pushover curves, are required at this step. The ETABS (version 9.5) is capable of performing performance based seismic analysis.

1.4 Scope of the work

The scope of work includes, performance based analysis of a new G+4 storey Reinforced Cement Concrete (RCC) building. Assessment of its performance using Pushover Analysis needs to be carried out. Also, traditional Time History Analysis is to be carried out for G+4 storey RCC building. A Fragility Curve defining performance of the building in terms of interstorey drift and displacement is to be obtained.

In view to fulfill the above outlined objective of work, following work are performed.

- Selection of an appropriate structural layout for new G+4 storey RCC building.
- Carryout Nonlinear Static Analysis (Pushover Analysis) of G+4 storey RCC building.
- Generate pushover curve (Base Shear-Displacement) of RCC building.
- Obtain Demand curve by converting Response Spectrum into ADRS (Acceleration Displacement Response Spectrum) format.
- Superposition of Capacity curve and Demand Curve to obtain performance point for a specific level of earthquake.
- Evaluation of building performance with reference to performance point of the RCC building.
- Understanding the collapse mechanism of different structural members of a RCC building.
- Evaluation of influence of lateral load patterns on Pushover analysis of the RCC building.
- Carryout Time History Analysis of the same RCC building for different earthquake ground motion records. (20 in nos.)
- Generation of fragility curves using Conventional fragility method.
- Compilation of important observations and conclusions of the study.

1.5 Organization of the report

The report may be viewed as divided into seven chapters.

In the **second chapter**, the literature review of the various technical papers, books and journals are dealt with. This includes the specific points from technical papers, books, journals and reports by Applied Technical Council (ATC-40) and Federal Emergency Management Agency (FEMA 273).

Chapter Three is devoted to explain the fundamentals of Nonlinear Static Analysis. Important definition of Demand and Capacity in detailed and also, procedure for performing Pushover analysis and evaluating performance point.

Fourth chapter includes Pushover Analysis of new G+4 storey RCC building. Three different types of building i.e, building with bare frame, building with masonry wall modeled as membrane element and equivalent strut element are considered. The performance point for above mentioned building are obtained under three different types of lateral loading patterns, namely, rectangular, parabolic and triangular.

Chapter Five covers Time History analysis of G+4 storey RCC building. Twenty earthquake ground motions are considered. Response of building under these earthquake ground motion in terms of peak interstorey drift and peak displacement are obtained.

Chapter Six essentially analyze generation of fragility curve methodology as available in literature. The chapter also discuss the modeling uncertainty and capacity uncertainty that need to be incorporate while generating fragility curves. It also includes fragility curve generated for limit state on peak interstorey drift and peak displacement of G+4 storey RCC building.

Chapter Seven includes important observations and conclusions derived out of study. It also includes possible extension of present study as future scope of work is mentioned.

Chapter 2

Literature Review

2.1 General

Literature survey is essential to review the work done in the area of performance based engineering. To take up the specific need to perform the analysis, the literature like technical papers, journals and books need to be referred. The prime important in the review was to understand the analysis and different concept of performance based engineering.

Focus of the chapter is to reviewed in brief, methodology of PBD, concept of nonlinearity, various methods of seismic analysis of the structure, extraction of performance point, various limit states of building performance and fragility curves.

2.2 Performance Based Design

Performance based design provides a systematic methodology for assessing the performance capability of a building, system or component. It can be used to verify the equivalent performance of alternatives, deliver standard performance at a reduced cost, or confirm higher performance needed for critical facilities. In performance based design, identifying and assessing the performance capability of a building is an integral part of the design process, and guides the many design decisions that must be made. **FEMA 445 [3]** describes a flowchart that presents the key steps in the perfor-

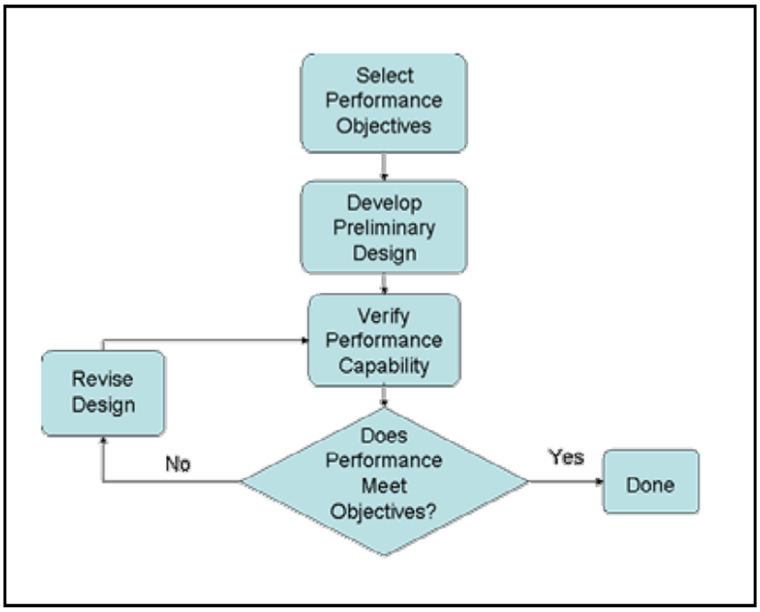

Figure 2.1: Performance based design flow diagram [3]

mance based design process. It is an iterative process that begins with the selection of performance objectives, followed by the development of a preliminary design, an assessment as to whether or not the design meets the performance objectives, and finally redesign and reassessment, if required, until the desired performance level is achieved.

Performance based design begins with the selection of design criteria stated in the form of one or more performance objectives. Each performance objective is a statement of the acceptable risk of incurring specific levels of damage, and the consequential losses that occur as a result of this damage, at a specified level of seismic hazard.

2.2.1 Nonlinearity

As it is required to know the ultimate capacity of building, the analysis is essential to be carried out up to the plastic zone. The nonlinearities in RCC members can be geometric as well as material. Both of these become more important at higher deformations.

E.D. Thomson, A.J. Carr and P.J. Moss [4] describes Geometric nonlinearity as a change in the elastic load-deformation characteristics of the structure caused by the change in the structural shape due to large deformation. It appears when the deflections of the structure are large enough to cause significant changes in the geometry of the structure, requiring the equilibrium equations to be formulated for the deformed configuration. These geometric nonlinearities can become significant in frames, which are displaced laterally due to seismic load or by wind load. The interaction between the gravity load induced axial forces in the columns and moments and forces produced due to lateral displacements in addition to those determined in a common first order analysis. This additional effect is commonly referred as $P - \Delta$ effects, where P refers to the gravity loading and Δ the lateral displacements.

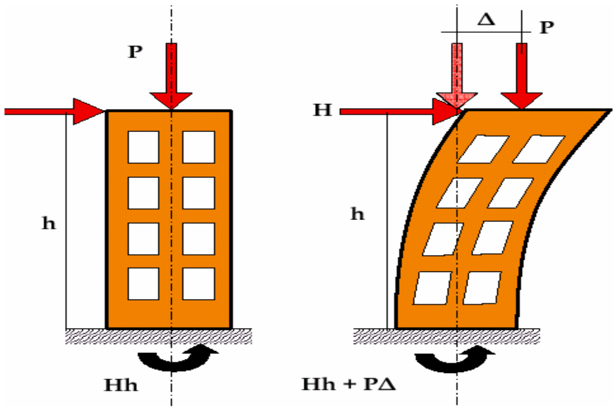

Figure 2.2: Geometric Nonlinearity, $P - \Delta$ Effect [4]

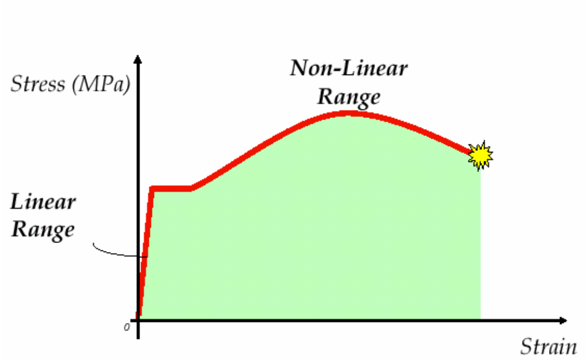

Figure 2.3: Material Nonlinearity [4]

Concrete and steel are the two constituents of RCC. Since concrete and steel are both strongly nonlinear materials, the material nonlinearity of RCC is a complex combination of both.

2.2.2 Methods of Analysis

The various methods available for nonlinear analysis as described by **Yogendra Singh** [**5**] are Code Procedure, Demand Capacity Ratio, Capacity Spectrum Method, Secant Method, and Time History Analysis. The most basic nonlinear analysis procedure is the complete nonlinear time history analysis. However, this method has difficulty in selection of design time history, as the codes give design response spectrum and not the design time history. Further, this method is considered to be too complex and impractical for general uses.

Farzad Naeim [**6**] considers Capacity Spectrum Method, a most popular method. The method is also known as Nonlinear Static Procedure, Nonlinear Pushover Analysis or simply Pushover analysis method. In a technical literature, **Farzad Naeim** [**6**] has described pushover analysis techniques in various points:

- Push-over analysis is a technique by which a computer model of the building is subjected to a lateral load of a certain shape (i.e., inverted triangular or uniform or parabolic pattern).

- The intensity of the lateral load is slowly increased and the sequence of cracks, yielding, plastic hinge formations, and failure of various structural components is recorded.

- Push-over analysis can provide a significant insight into the weak links in seismic performance of a structure.

- A series of iterations are usually required during which, the structural deficiencies observed in one iteration, are rectified and followed by another.

- This iterative analysis and design process continues until the design satisfies prestablished performance criteria.

- The performance criterion for pushover analysis is generally established as the desired state of the building given roof-top or spectral displacement amplitude.

ATC-40 [7] describes Pushover analysis as a basic tool for the performance based seismic design of the building structures. By pushover analysis the base shear versus the top displacement curve of the structure, usually called capacity curve, is obtained. The basic demand and capacity parameter for the analysis is the lateral displacement of the building.

The generation of capacity curve defines the capacity of the building uniquely for an assumed force distribution and displacement pattern.

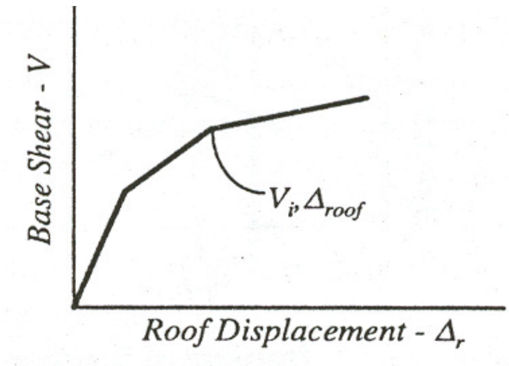

Figure 2.4: Pushover Curve [7]

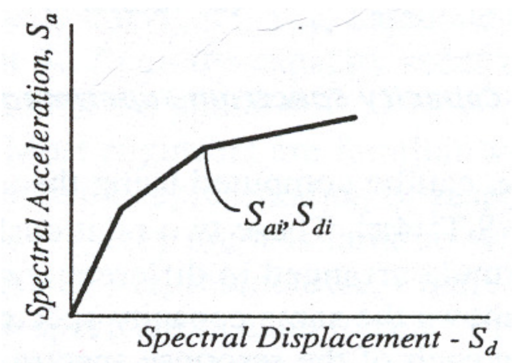

Figure 2.5: Capacity Spectrum Curve [7]

The Capacity Spectrum Method compares the capacity spectrum of the structure and demand spectrum of earthquake ground motion using visual graphic procedure.

This visual graphic procedure is easy to understand for the seismic performance of the structures existing or to be designed.

2.2.3 Methods of Obtaining Performance Point

No building can be pushed to infinity without failure. Performance point is where the Seismic Capacity and the Seismic Demand curves meet. If the performance point exists and damage state at that point is acceptable, the building satisfies the pushover criterion. If not, the building is required to alter to satisfy the pushover criteria.

According to **ATC-40** [**7**], the location of performance point must satisfy two relationships:

1) The point must lie on the capacity spectrum curve in order to represent the structure at a given displacement, and

2) The point must lie on a spectral demand curve, reduced from the elastic, 5 percent damped design spectrum that represents the nonlinear demand at the same structural displacement.

There are three methods of obtaining performance point given in **ATC-40** [**7**]. They are: Procedure A, Procedure B, Procedure C

Procedure A is more transparent and most direct application of the methodology. It is truly iterative, but is formula based and easily be programmed into a spreadsheet. It is more an analytical method than a graphical method. It is the best method for beginners as it is most direct and easiest to understand.

Procedure B is also an analytical method but is simpler than Procedure A. simplification is introduced in the bilinear modeling of the capacity curve that enables a relatively direct solution for the performance point with little iteration. It assumes that not only the initial slope of bilinear representation of capacity curve remains constant, but also the post yield slope remains constant.

Procedure C is graphical method and is most convenient for hand analysis. It is not particularly convenient for spreadsheet programming. It is the least transparent application of the methodology.

Farzad Naeim [6] gives some solution if the performance point dose not exist. There are three solutions.

- Add Strength or Stiffness or both to the building: As shown in Figure (2.6) of the reasons for not getting performance point is that the demand is more and capacity is less. Adding strength or stiffness to the building raises the capacity of the building and subsequently the capacity curve of the building which intersects the demand curve.

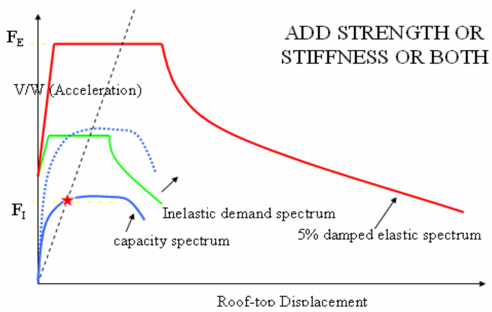

Figure 2.6: Obtaining performance point by adding strength to system [8]

- Enhance System Ductility: Enhancing ductility in the building will increase the capacity of building to resist more loads in nonlinear range. As shown in Figure (2.7) the capacity spectrum of this building will be elongated as it will be able to deform more under the constant load.

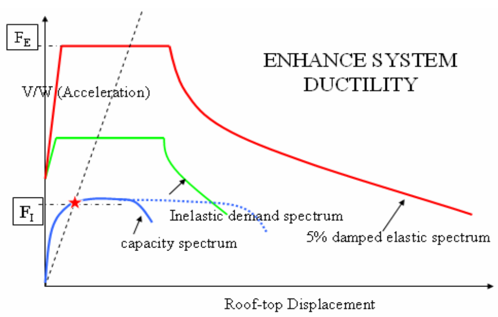

Figure 2.7: Obtaining performance point by enhancing ductility to system [8]

- Reduce Seismic Demand by adding Damping or Isolation: Adding damping will reduce the demand as there will be more energy dissipation. This will bring down the demand curve as shown in Figure (2.8)

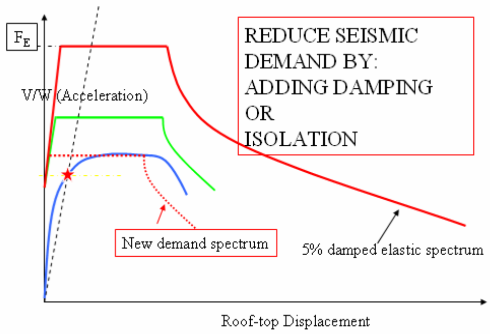

Figure 2.8: Obtaining performance point by adding damping to system [8]

2.2.4 Building Performance

ATC-40 [**7**] also gives guidelines regarding performance objectives. Performance objective specifies the desired seismic performance of the building. It includes consideration of damage states for several levels of ground motion. Performance level describes a limiting damage condition which may be considered satisfactory for a given building and a given ground motion. Target performance level is specified independently. Structural performance levels are given names and number designations while nonstructural performance levels are given names and letter designations.

Performance of building can be evaluated by combination of evaluation of Structural performance and Nonstructural performance. **Farzad Naeim** [**6**] has describes this performance levels in brief.

Structural performance levels are defined as:

Immediate Occupancy (SP-1): limited structural damage with the basic vertical and lateral force resisting system retaining most of their pre-earthquake characteristics and capacities.

Damage Control (SP-2): a placeholder for a state of damage somewhere between Immediate Occupancy and Life Safety.

Life Safety (SP-3): significant damage with some margin against total or partial collapse. Injuries may occur with the risk of life-threatening injury being low. Repair may not be economically feasible.

Limited Safety (SP-4): a placeholder for a state of damage somewhere between Life Safety and Structural Stability.

Structural Stability (SP-5): substantial structural damage in which the structural system is on the verge of experiencing partial or total collapse. Significant risk of injury exists. Repair may not be technically or economically feasible.

Not considered (SP-6): placeholder for situations where only non-structural seismic evaluation or retrofit is performed.

Non-Structural performance levels are defined as:

Operational (NP-A): non-structural elements are generally in place and functional. Back-up systems for failure of external utilities, communications and transportation have been provided.

Immediate Occupancy (NP-B): non-structural elements are generally in place but may not be functional. No back-up systems for failure of external utilities are provided.

Life Safety (NP-C): considerable damage to non-structural components and systems but no collapse of heavy items. Secondary hazards such as breaks in high-pressure, toxic or fire suppression piping should not be present.

Reduced Hazards (NP-D): extensive damage to non-structural components but should not include collapse of large and heavy items that can cause significant injury to groups of people.

Not considered (NP-E): non-structural elements, other than those that have an effect on structural response, are not evaluated.

2.2.5 Fragility Curves

The behavior of reinforced concrete structures under the effect of ground motions has always been investigation in seismic regions. The damage to buildings from recent earthquakes has emphasized the need for risk assessment of existing building stock to estimate the potential damage from future earthquakes.

According to **Murat Serdar Kircil and Zekeriya Polat** [**8**] seismic risk analysis of a building is important for identifying the seismic vulnerability of a structural system under the effect of potential seismic ground motions. For this purpose, fragility curves are useful tools for risk assessment studies. Fragility analysis are allows to estimation of the probability of structural damage due to earthquakes as a function of ground motion records or various design parameters, e.g, peak ground acceleration (PGA), spectral acceletation (Sa), and spectral displacement (Sd).

According to **Sathish K. Ramamoorthy, Paolo Gardoni, and Joseph M. Bracci** [**9**] fragility is defined as the conditional probability of attaining or exceeding a specified limit state of a structural member or system for a given set of demand variables. Fragility curves are constructed to assess the seismic vulnerability of a hypothetical reinforced concrete frame building. Fragility curves are also developed for the the building which is retrofitted by means of column strengthening.

B.Gencturk, A.S.Elnashai and J.Song [**2**] describes a new procedure for fragility analysis of buildings. The procedure is divided into four components, namely (i) capacity of building, (ii) earthquake demand, (iii) structural assessment and (iv) fragility curve generation. In this procedure the capacity of building is represented using either analytically-derived or software based pushover curves. Earthquake demand is modeled by synthetically generated site specific ground motions or peak ground acceleration recorded during earthquake event. Structural assessment is carried out using an advanced Capacity Spectrum Method (CSM). Finally, fragility curves are presented in two different formats, conventional and HAZUS-compatible. The uniformly derived fragility relationships are proposed as a reliable tool for earthquake impact assessment.

Figure 1.1 shows the flowchart for the proposed procedure of fragility analysis. In which, pushover curves and time histories form the capacity of building and earthquake demand, respectively. These two components are inputs to the methodology for structural assessment. Then statical analysis of structural response data is performed under the component and the methodology for fragility curve generation provides the desired relationships. Limit states which are determined using the pushover curves are also utilized in this step.

According to report on "Fragility Relationship for Population of Building Based on Inelastic Response" by **Bora Gencturk, Amr S. Elnashai, and Junho Song** (**Mid-American Earthquake Center**) [**10**] fragility curve generation is basically statistical analysis of the results obtained from the structural response assessment i.e, of the variations of capacity of buildings under various ground motion using the methodology for structural response assessment. The structural earthquake fragility relationship is classify into two methods. The commonly adopted approach is to directly associate the exceedance probabilities of certain performance levels with the ground motion parameters, e.g, peak ground acceleration (PGA), peak ground velocity (PGV), spectral acceleration(Sa) and spectral displacement(Sd). This first method is known as "conventional fragility relationships." On the other hand, the widely used loss estimation software HAZUS in USA prefers a description where the exceedance probabilities are related to structural response which is called as "HAZUS compatible fragility relationships."

2.3 Summary

All the different papers gives an idea about the amount of various research works carried out on this topic so far, current trends of research works and further scope of detailed studies required in in this topic, it also gives an idea about the performance level of new as well as existing building, for future seismic hazards.

Chapter 3

Nonlinear Static Analysis

3.1 Introduction

There are various elastic and inelastic methods available for analysis of existing concrete buildings. Elastic analysis methods include code based static lateral force procedures, code based dynamic lateral force procedures and elastic procedures using demand capacity ratio. The most basic inelastic analysis method is the complete nonlinear time history analysis. Other simplified nonlinear analysis methods includes the Capacity Spectrum Method (CSM) that uses the intersection of the capacity (pushover) curve and a reduced response spectrum to estimate maximum displacement.

Ashraf Habibullah and Stephen Pyle [11] describes, the recent advent of performance based design has brought the nonlinear static pushover analysis procedure to the forefront. Pushover analysis is a static, nonlinear procedure in which the magnitude of the structural loading is incrementally increased in accordance with a certain predefined pattern. With the increase in the magnitude of the loading, weak links and failure modes of the structures are found. The loading is monotonic with the effects of the cyclic behavior and load reversals being estimated by using a modified monotonic force-deformation criteria and with damping approximations.

Static pushover analysis is an attempt by the structural engineering profession to evaluate the real strength of the structure and it promises to be a useful and effective tool for performance based design.

Performance based seismic design appears to be the future direction of seismic design codes. In the newly developed performance based seismic design approach, nonlinear analysis procedure become important in identifying the patterns and levels of damage for assessing a structures inelastic behavior and for understanding the failure modes of the structure during severe seismic events.

The Capacity Spectrum Method, a nonlinear static procedure that provides a graphical representation of the global force-displacement capacity curve of the structure and compares it to the response spectra representation of the earthquake demands, is a very useful tool in the evaluation and retrofit design of existing concrete building. The graphical representation provides a clear picture of how a building responds to earthquake ground motion, and it provides an immediate and clear picture of how various retrofit strategies, such as adding stiffness or strength, will impact the buildings response to earthquake.

3.2 Demand, Capacity and Performance

The key elements of a performance based seismic design procedure are demand and capacity. Demand is a representative of the earthquake ground motion. Capacity is a representation of the structures ability to resist the seismic demand. The performance is dependent on the manner that the capacity is able to handle the demand.

Determination of three primary elements: capacity, demand (displacement) and performance are required for Nonlinear Static (Pushover) Analysis. Each of these is briefly described below.

3.2.1 Capacity

Capacity is the expected ultimate strength (in flexure, shear, or axial loading) of a structural component excluding the reduction factors commonly used in design of concrete members. The capacity usually refers to the strength at the yield point of the element or structure's capacity curve. For deformation-controlled components, capacity beyond the elastic limit generally includes the effects of strain hardening.

The overall capacity of a structure depends on the strength and deformation capacities of the individual components of the structure. In order to determine capacities beyond the elastic limits, some form of nonlinear analysis, such as the pushover procedure, is required. This procedure uses a series of sequential elastic analysis, superimposed to approximate a force-displacement capacity diagram of the overall structure. The mathematical model of the structure is modified to account for reduced resistance of yielding components. A lateral force distribution is again applied until additional components yield. This process is continued until the structure becomes unstable or until a predetermined limit is reached.

3.2.2 Demand

A representation of the earthquake ground motion or shaking that the building is subjected to. In nonlinear static analysis procedures, demand is represented by an estimation of the displacements or deformations that the structure is expected to undergo. This is in contrast to conventional, linear elastic analysis procedures in which demand is represented by prescribed lateral forces applied to the structure.

The traditional design methods use equivalent lateral forces to represent the design condition. For nonlinear methods it is easier and more direct to use a set of lateral displacements as the design condition. For a given structure and ground motion, the displacement demand is an estimate of the maximum expected response of the building during the ground motion.

3.2.3 Performance

Once, a capacity curve and demand displacement, are defined, a performance check can be done. A performance check verifies that structural and nonstructural components are not damaged beyond the acceptable limits of the performance objective for the forces and displacements implied by the displacement demand.

3.3 Pushover Analysis

Under the Nonlinear Static analysis, also called as Pushover analysis, a model directly incorporating inelastic material response is displaced to a target displacement, and resulting internal deformations and forces are determined. The nonlinear load-deformation characteristics of individual components and elements of the building are modeled directly.

The mathematical model of the building is subjected to monotonically increasing lateral forces or displacements until either a target displacement is exceeded or the building collapses. The target displacement is intended to represent the maximum displacement likely to be experienced during the design earthquake. The target displacement may be calculated by any procedure that accounts for the effects of nonlinear response on displacement amplitude. Because the mathematical model accounts directly for effects of material inelastic response, the calculated internal forces will be reasonable approximations of those expected during the design earthquake.

Results of the Nonlinear static analysis are to be checked. Calculated displacements and internal forces are compared directly with allowable values.

3.4 Pushover Analysis Procedure

ATC-40 [7] provides detailed guidelines about how to perform a nonlinear static pushover analysis. The most important parts of this method are the generation of the Capacity Spectrum and the design Response Spectra and finding of the point of intersection of the capacity and the response spectra. The intersection defines the performance level of the structure for the design earthquake. The procedure is mention below.

- Form the analytical model of the nonlinear structure.
- Set the performance criteria, like drift at specific floor levels, limiting plastic hinge rotation at specific plastic hinge points, etc.
- Apply the gravity load and analyze for the internal forces.
- Assign the equivalent static seismic lateral load to the structure incrementally. There is guideline how to distribute loads between different floor levels. This is either based on the current code specified load or equivalent static load computed based on modal analysis.
- Select a control point (usually at the top floor) to observe displacement.
- Apply the lateral load gradually using incremental iteration procedure.
- Draw the Base Shear vs. Controlled Displacement curve, This is called Pushover Curve.
- Convert the pushover curve to the Acceleration-Displacement Response-Spectra (ADRS) format, this is called Capacity Spectrum.
- Obtain the equivalent damping based on the expected performance level.
- Get the design Response Spectra for different levels of damping and adjust the spectra for the nonlinearity based on the damping in the Capacity Spectrum.
- The capacity spectrum and the design response spectra can be plotted together when they are expressed in the ADRS format.
- The intersection of the capacity spectrum and the response spectra defines the performance level. If the performance level satisfies the design, the design is okay, otherwise adjustment to the structures is required.

3.5 Capacity Spectrum Method

One of the methods used to determine the performance point is the Capacity Spectrum Method, also known as the Acceleration-Displacement Response Spectrum method (ADRS). The Capacity Spectrum Method requires that both the capacity curve and the demand curve be represented in response spectral ordinates.

The point at which the capacity curve intersects the reduced demand curve represents the performance point at which capacity and demand are equal.

To convert a spectrum from the standard Sa (Spectral Acceleration) vs. T (Time) format found in the building codes to ADRS format, it is necessary to determine the value of Sd_i (Spectral Displacement) for each point on the curve, (Sa_i, T_i). This can be done with the equations:

$$Sd_i = \frac{T_i^2}{4\pi^2} Sa_i g \tag{3.1}$$

Standard demand response spectra contain a range of constant spectral acceleration and a second range of constant spectral velocity, Sv. Spectral acceleration and displacement at period Ti are given by:

$$Sa_i g = \frac{2\pi}{T_i} Sv \tag{3.2}$$

$$Sd_i = \frac{T_i}{2\pi} Sv \tag{3.3}$$

The capacity spectrum can be developed from the pushover curve by a point by point conversion to the first mode spectral coordinates. Any point V_i (Base Shear), δ_i (Roof-Displacement) on the capacity curve is converted to the corresponding point Sa_i, Sd_i on the capacity spectrum using the equations:

$$Sa_i = \frac{V_i/W}{\alpha_1} \tag{3.4}$$

$$Sd_i = \frac{\delta_i}{PF_1 \times \phi_{1,roof}} \tag{3.5}$$

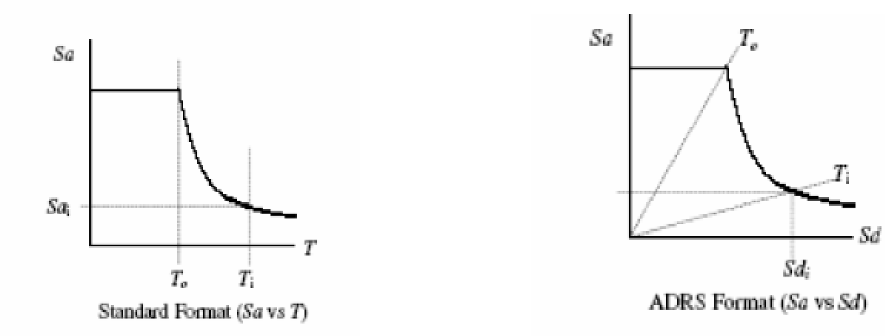

Figure 3.1: Response Spectrum Conversion [6]

Where α_1 and PF_1 are the modal mass coefficient and participation factors for the first natural mode of the structure respectively. $\phi_{1,roof}$ is the roof level amplitude of the first mode.

The damping that occurs when the structure is pushed into the inelastic range can be viewed as a combination of viscous and hysteretic damping. Hysteretic damping can be represented as equivalent viscous damping. Thus, the total effective damping can be estimated as:

$$\beta_{eff} = \lambda\beta_0 + 0.05 \tag{3.6}$$

Where β_0 is the hysteretic damping and 0.05 is the assumed 5% viscous damping inherent in the RCC structure. The λ factor is the modification factor to account for the extent to which the actual building hysteresis is well represented by the bilinear representation of the capacity spectrum. The term β_0 can be calculated using:

$$\beta_0 = \frac{E_D}{4\pi * E_{S0}} \tag{3.7}$$

Where E_D is the energy dissipated by damping and E_{S0} is the maximum strain energy.

To account for the damping, the response spectrum is reduced by reduction factors SR_A and SR_V which is given by:

$$SR_A = \frac{1}{B_S} = \frac{3.21 - 0.68 l_n(\beta_{eff})}{2.12} \tag{3.8}$$

$$SR_V = \frac{1}{B_L} = \frac{2.31 - 0.41 l_n(\beta_{eff})}{1.65} \tag{3.9}$$

The elastic response spectrum (5% damped) is thus reduced to a response spectrum with damping values greater than 5% critically damped.

3.6 Performance Point

In pushover curve a point on the curve defines a specific damage state for the structure, since the deformation for all components can be related to the global displacement of the structure. By correlating this capacity curve to the seismic demand generated by a specific earthquake or ground shaking intensity, a point can be found on the capacity curve that estimates the maximum displacement of the building the earthquake will cause. This defines the performance point.

There are three procedures described in **ATC-40** [**7**] to find the performance point. The most transparent is the Procedure A. To find the performance point using Procedure A the following steps are used:

a. A 5% damped response spectrum appropriate for the site for the hazard level required for the performance objective is developed and converted to ADRS format.

b. The capacity curve obtained from the nonlinear analysis is converted to a capacity spectrum using the above given equations.

c. A trial performance point Sa_{pi}, Sd_{pi} is selected. This may be done using the equal displacement approximation as shown in Figure 3.2

d. The reduced demand spectrum is plotted together with the capacity spectrum.

e. If the reduced demand spectrum intersects the capacity spectrum at Sa_{pi}, Sd_{pi} or if the intersection point Sd_p is within 5% of Sd_{pi}, then this point represents the performance point.

f. If the intersection point does not lie within acceptable tolerance (5% of Sd_{pi} or other) then select another point and repeat steps d to f. The intersection point obtained in step e can be used as starting point for the next iteration.

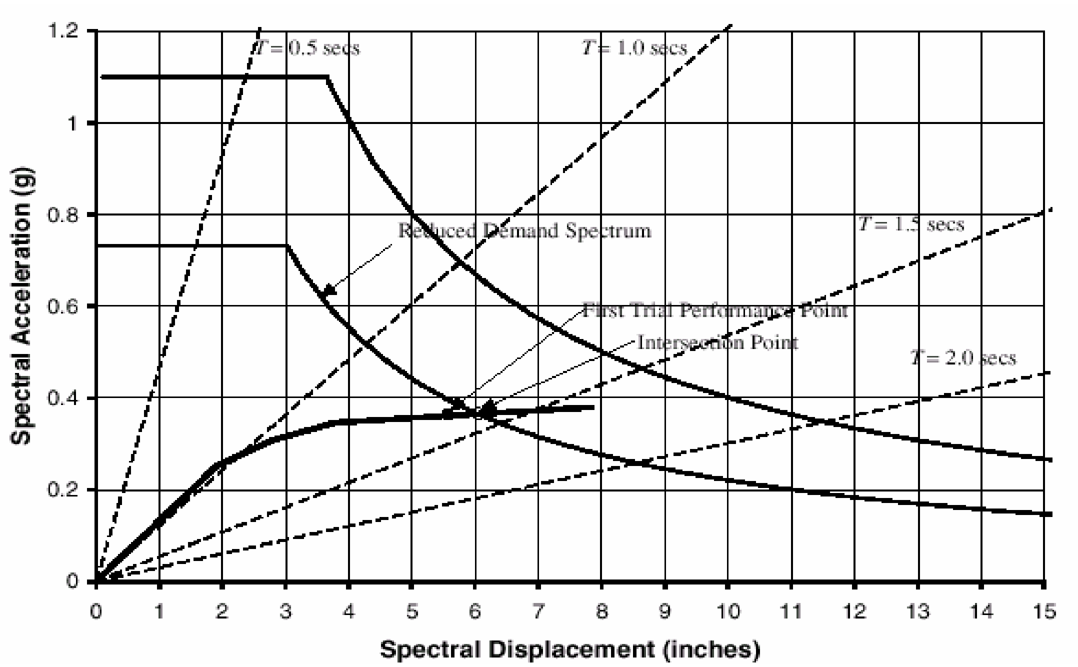

Figure 3.2: Performance Point evaluation by Procedure A [7]

3.7 Summary

In this chapter, important definition of Demand, Capacity, procedure for performing Pushover analysis, evaluating performance point is described. This chapter also, includes generation of capacity curve, demand curve, numerical found spectral acceleration Vs. time format to ADRS format, which is necessary to determine the value of spectral displacement for each point on the curve.

Chapter 4

Pushover Analysis of G+4 Storey R.C.C. Building

4.1 Configuration of building

A ground plus four storey RC building of plan dimension 20 m x 15 m having 4 bay in x-direction and 3 bay in Y-direction, each of 5m in length, located in seismic zone III on medium soil is considered. Seismic analysis is performed using the codal based seismic coefficient method. The structure is a regular building with storey height 3m and slabs are of 150 mm thickness. Brick wall below all beams are 115 mm thick. Concrete and steel grade considered are M25 and Fe415, respectively.

Plan of the building is shown in Figure (4.1). The sizes of the beams, columns and live load supported by slab are given in Table 4.1.

Table 4.1: Geometric Properties of frame and live loads on slab

Floor	Column size (mm)	Beam size (mm)	Live load on slab (KN/m^2)
G.F.	230x600	230x500	2
1^{st} floor	230x600	230x500	2
2^{nd} floor	230x500	230x450	1.5
3^{rd} floor	230x500	230x450	1.5
4^{th} floor	230x450	230x450	1.5

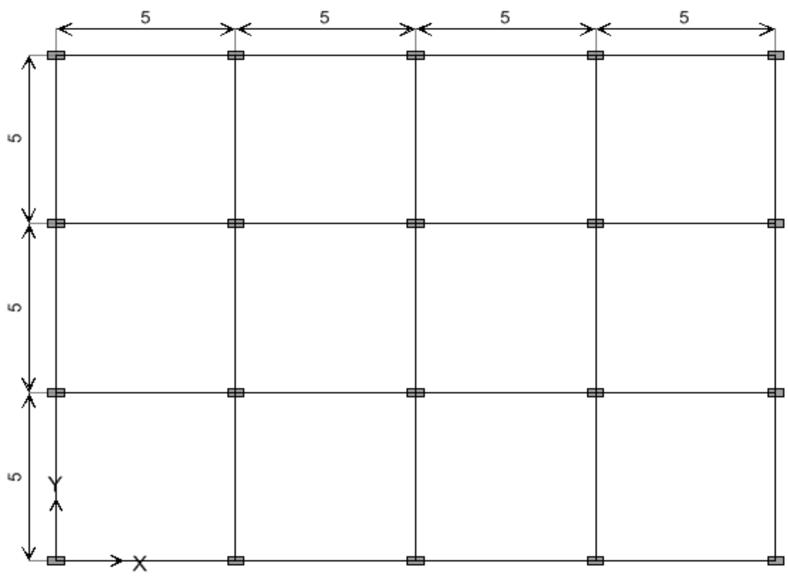

Figure 4.1: Plan of new G+4 storey R.C.C. building

4.2 Modeling of building

To carry out pushover analysis, firstly an analytical model of the building is required to be developed. Building elements like slabs, beams and columns are modelled as rigid diaphragm, beam element and column element, respectively. However, modelling of masonry infill wall is little bit complex. Various literature available about modelling of masonry infill walls. In present study, masonry wall is modelled by two approach, one it is considered as membrane element with inplane stiffness and second it is modelled as strut element of some width and thickness to produce stiffness. Thus, three analytical models are considered in present study, namely, Bare Frame (i.e, w/o masonry infill wall), Frame with infill wall as membrane and Frame with infill wall as strut. Each one of them is discussed in details as follows.

4.2.1 Bare Frame without infill wall

The model Bare Frame having beams, columns and slabs, but no infill walls. The geometric property assigned to all the beams and columns and loading on slabs are listed in Table 4.1. All structural members are of M25 grade concrete and Fe415 steel. The slabs are considered as rigid floor diaphragm.

As per the general practice followed in field, the column and beam sizes were reduced going from GF to 4^{th} floor, also the live loads are reduced as per IS:875(Part-II). Figure (4.2) shows the elevation of the building model. The storey height is 3m and the support condition at base is assumed to be fixed.

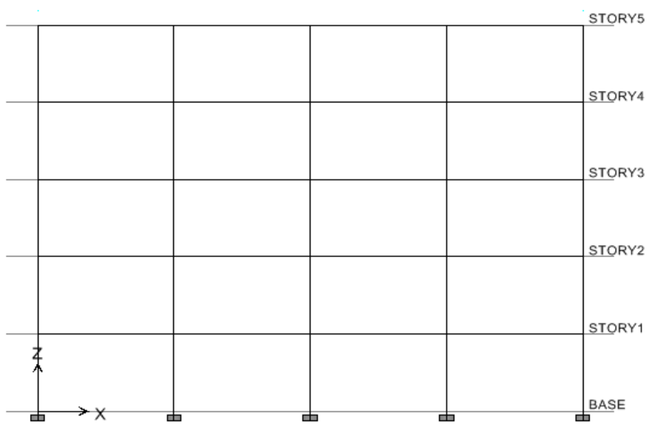

Figure 4.2: Elevation of G+4 bare frame model

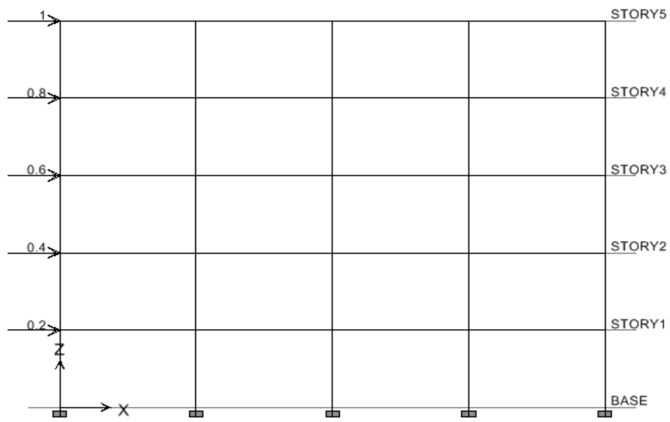

Figure 4.3: Lateral Loading Pattern

The lateral load is applied in X-direction. The lateral load profile applied through out the height of the building is inverted triangular shape. The unit load is applied at the top of the column which is reduced to zero at the base. The lateral load is applied at the junction of outer beams and columns as shown in Figure (4.3).

4.2.2 Building Frame with infill as membrane wall

This model incorporates infill wall as a membrane element. The property of membrane element is such that it has only inplane stiffness and outplane stiffness is voids. The infill walls are provided below all the beams except the first floor beams, in order to estimate real life problem. The thickness of wall is 115 mm. The material properties of masonry infill wall is listed below:

Modulus of Elasticity : 1237.5 N/mm^2

Density : 20 kN/m^3

Poissons ratio : 0.17

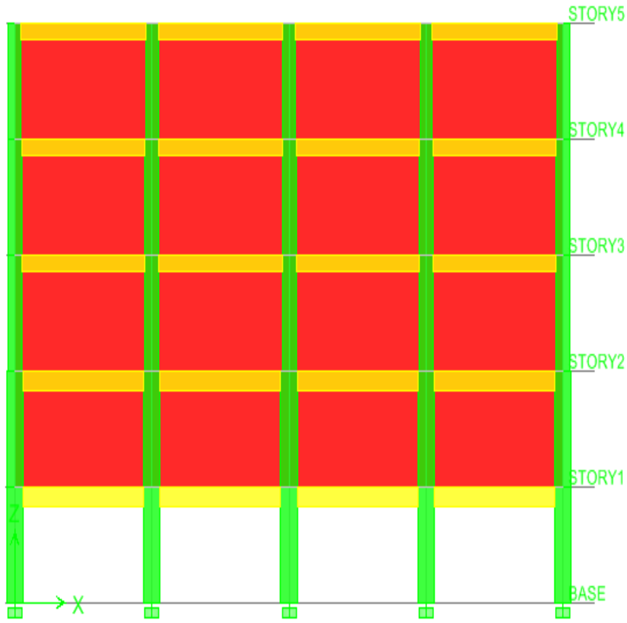

Figure 4.4: G+4 storey model with infill as membrane wall

The geometrical properties of beams, columns and loading are same as considered in Bare Frame. The reduction of size of the columns and beams are clearly observed from the Figure (4.4).

4.2.3 Building Frame with infill as equivalent strut

In this model, the equivalent compression strut is modeled in place of membrane wall having material property same as membrane wall. Figure (4.5) shows the elevation of analytical model with strut. The ends of diagonal struts are released for moments and torsion in all the directions, to make it as a pinned joint. The thickness of the strut is same as the thickness of the membrane wall. The equivalent width should be taken as one third of the diagonal length of strut, as per literature. The width of strut is calculated as 1.94 m, for present case. The dot at the end of strut as shown

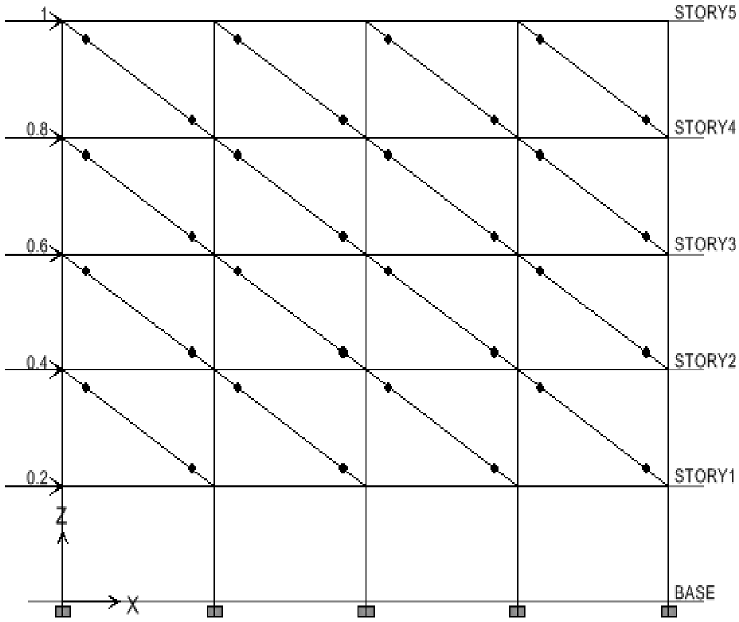

Figure 4.5: G+4 storey with infill as equivalent strut

in Figure (4.5) represents the end releases. As shown in Figure (4.5), the orientation of the diagonal strut was such that it takes only axial compressive load under lateral loading.

4.3 Static Load Cases

Once model is ready with geometric and sectional properties of elements, loading cases needs to be defined. The software (ETABS) calculates apply Dead Load automatically while Live load need to be applied to each floor as per IS:875(Part-II). The other load cases required to be define are Lateral loads in two horizontal (X and Y) directions. These lateral loads are required while carrying out Pushover analysis. The shape of loading pattern bears a lots of importance in pushover analysis. This is, generally, like the lateral forces distributed across height of building. ATC-40/FEMA 273 prescribed two types of loading pattern, namely Rectangular and Triangular. However, IS:1893(Part 1)2002 distribute lateral forces parabolically across the height of building. Therefore, for present study three different types of loading patterns are considered to carry out pushover analysis.

4.4 Response Spectrum Cases

For earthquake analysis, Response Spectrum Case is to be defined. As ETABS (version 9.5) supports IS 1893(Part 1):2002, the response spectrum for 5% damping is applied automatically. Response Spectrum Curve shown in Figure (4.6) is for 5% damping and medium soil as per IS 1893(Part 1):2002.

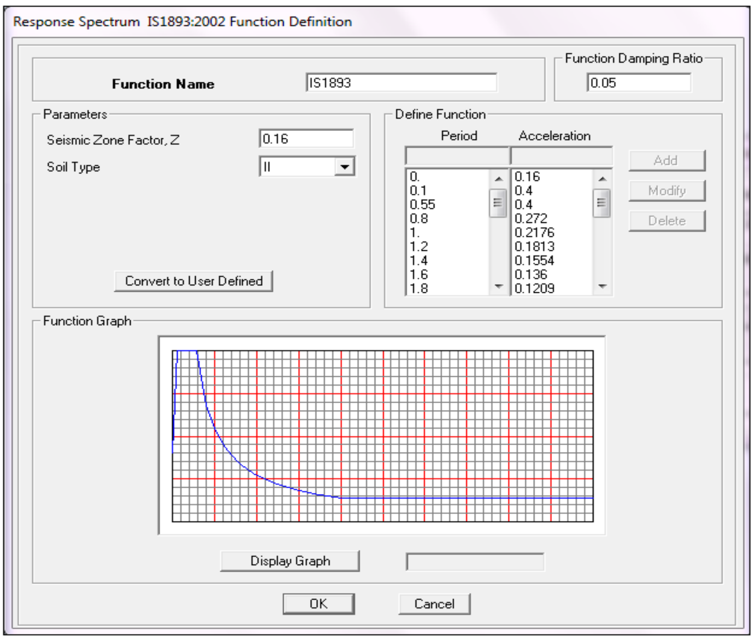

Figure 4.6: Response Spectrum Curve of IS 1893(Part 1):2002

The response spectrum cases are required to be define in two horizontal (X and Y) direction. Response spectrum case includes the modal combination options like Complete Quadratic Combination (CQC), Square Root of the Sum of the Square (SRSS), Absolute Method (ABS) and General Modal Combination (GMC) method. Response spectrum analysis needs to be carried out for both horizontal directions.

4.5 Nonlinear Hinge Property Assignment

Nonlinear hinge properties are most essential part of Pushover analysis, because they ensure Nonlinear Static Analysis of the buildings. Nonlinear hinges are added to beams, columns and diagonal struts. From the analysis it was concluded that the probable location of hinge formations in beams are at the ends. Also the governing forces in beams are Shear force and Bending Moments and thus, default Moment (M3) hinges and Shear (V2) hinges are added at relative distance zero and one, i.e. at both the ends. The columns are provided with default Axial Moment Interaction (PMM) hinges at base as column in subjected to interaction of axial force and biaxial moments. The diagonal struts were provided with default Axial Hinges (P) property, as the orientation of the diagonal strut is such that it takes only axial compressive load under lateral loading.

Figure (4.7) shows the default hinge properties available with the software (ETABS). There are three types of hinge properties in the ETABS: Default hinge property, User defined hinge property and generated hinge property. Only default hinge property and user defined hinge property can be assigned to the frame elements. When a default or user defined hinge property is assigned to any frame element, it will automatically creates a new generated hinge property for each hinge.

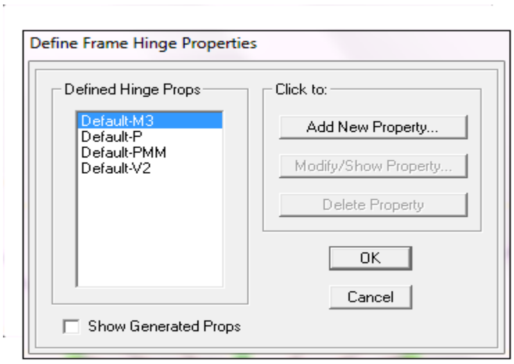

Figure 4.7: Default Hinge Types

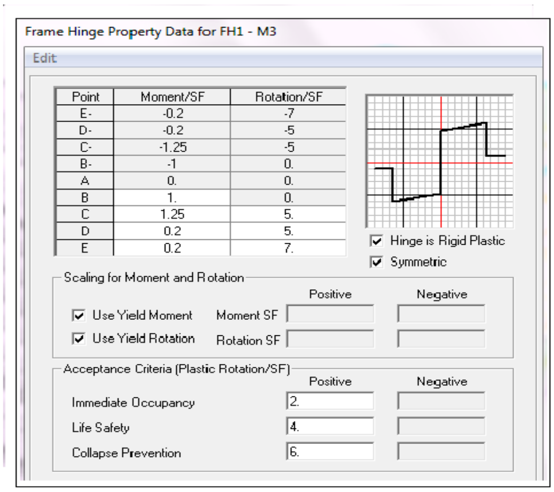

Figure 4.8: Frame Moment Hinge Property

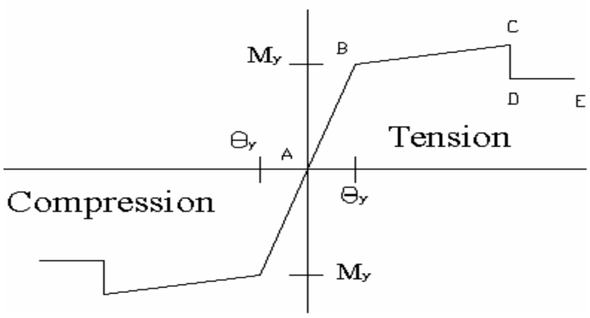

Figure 4.9: Moment Rotation Curve

Figure (4.8) and Figure (4.9) shows the default properties for M3 hinges. Point A is the starting point. Default hinge uses yield moment and yield rotation for scaling. Point B shows yield condition of the hinge. Point C is the ultimate condition of the hinge. It is 25% more than the yield Moment. The corresponding rotation is the ultimate rotation. After reaching to ultimate yielding hinge suddenly the moment degrades and reaches to point D having some residual strength (moment). For default hinge property the residual strength is taken as the 20% of the yield strength. Point E is the final deformation under residual strength. Similar kind of hinge properties is available for Shear and Axial-Moment Interaction hinge. These properties are as per ATC-40 and FEMA 273.

Figure 4.10: Nonlinear Hinges in beams and columns

Figure (4.10) shows the Nonlinear Hinges were provided in beams and columns.

4.6 Static Nonlinear Cases

Besides static load cases, static nonlinear cases are to be defined for performing Pushover analysis. For analysis of all the models, i.e, three analytical models, two nonlinear cases are defined namely, PUSH1 and PUSH2.

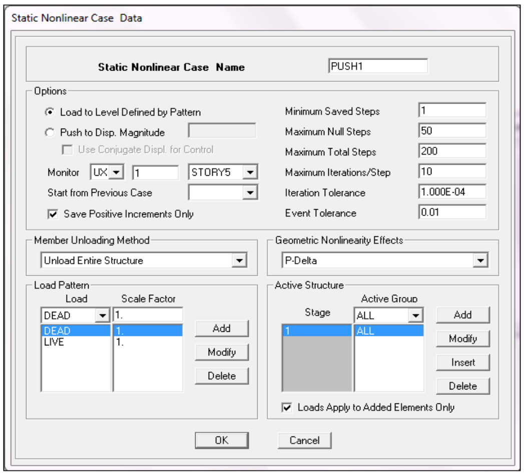

Figure 4.11: PUSH1 case for G+4 storey model

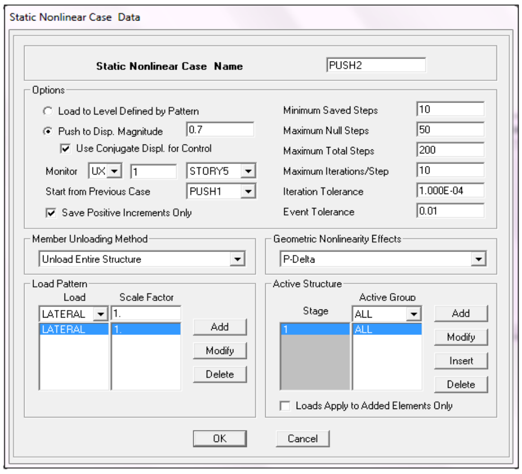

Figure 4.12: PUSH2 case for G+4 storey model

Figure (4.11) shows first nonlinear case PUSH1 for gravity loads. It is load controlled as the magnitude of applied gravity load are known. The displacement of 1^{st} node of top storey is monitored for analysis. Member unloading method used is Unload Entire Structure. Geometric Nonlinearity is also considered in analysis.

As shown in Figure (4.12), (P-Δ effects) PUSH2 considers lateral loads and it is displacement controlled as applied lateral load are not known. The analysis starts at the end of PUSH1 analysis. Member unloading Method and Geometric Nonlinearity are taken same as in PUSH1 case.

4.7 Pushover Curve and Capacity Spectrum Curve

The static pushover curve is the single force-displacement curve obtained from a static nonlinear analysis. The ideal pushover curve is shown in Figure (4.13). A-B range is the linear range, B-C is the nonlinear range which includes different performance levels such as IO, LS and CP. Point C indicates the ultimate failure after which the residual strength remains indicated by point D. Point E is the final displacement under residual strength.

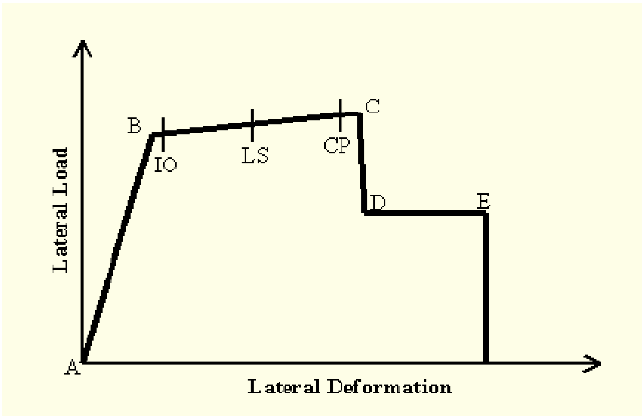

Figure 4.13: Ideal Pushover Curve

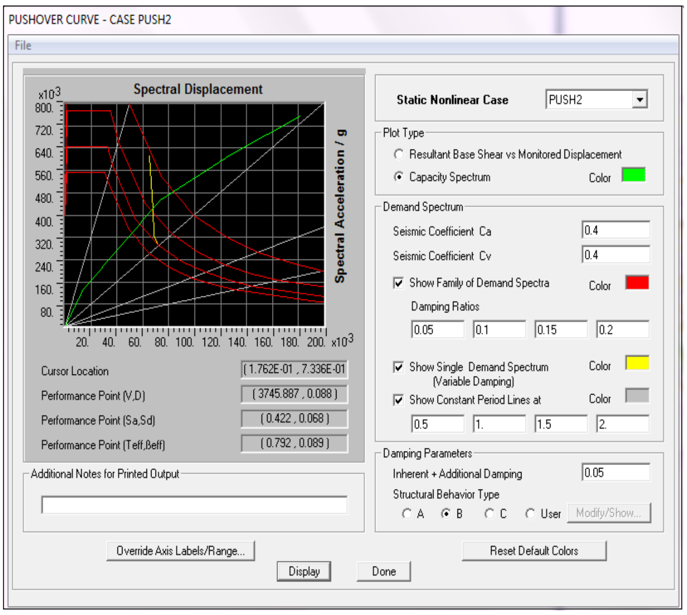

Figure 4.14: Pushover Curve and Capacity Curve

Figure (4.14) shows various parameters need to be defining for getting pushover curve and capacity spectrum curve. On upright top corner, the static nonlinear case is selected for which the pushover curve is to be displayed. If the plot type is Resultant Based Reaction Vs Monitored Displacement, the Damping Parameters and Demand Spectrum option becomes inactive. As the plot type is changed to capacity spectrum, four type of curves are displayed in the displayed area. Each curve on the plot type area is having some color code which can be changed. The default color for each curve are green for Capacity spectrum curve, red curve for demand spectrum curve, yellow for single demand spectrum curve and grey is the constant period line.

The currently displayed pushover curve can be display in tabular format from file menu provided at the top of the window. If the displayed curve is Resultant Base Reaction Vs Monitored Displacement, then the displayed tabular format includes, Base Reaction, Monitored Displacement and the number of hinges beyond the certain control points (B, IO, LS, CP, C, D and E). If the currently displayed curve is in ADRS format, the displayed table includes the information regarding Effective period, Effective Damping, Spectral coordinates of capacity curve, Spectral coordinates of single modified demand spectrum curve, the scaling factor used for converting the force-displacement curve to the ADRS format. The edit box in the Additional Notes For Printed Output area is used to include the additional notes required to be included in the output.

Damping Period and Demand Spectra Parameters:

When the Capacity Spectrum option is chosen as the Plot Type on the Pushover Curve form, the Demand Spectrum and Damping Parameters areas of the form become active. The shape of demand spectra with 5% damping is controlled by the values input in the seismic coefficient Ca, and seismic coefficient Cv edit box. Checking show the family of demand spectra box in demand spectrum area overlays a family of demand spectra on the capacity curve in ADRS format. The family of curves can include up to four demand-spectra curves, each with a different effective damping ratio, β_{eff}. By default, the software plots curves with β_{eff} = 0.05, 0.1, 0.15 and 0.2.

The damping ratios for any of the four curves can be changed by editing the value in one of the four Damping Ratios, β_{eff} edit boxes. The values input into the β_{eff} edit boxes must be between 0 and 1, inclusively. A value of 0, or a blank edit box, means to omit that demand spectrum curve.

Checking Show Single Demand Spectra (Variable Damping) displays the demand spectra as single curve. The method of constructing single demand spectra is similar to the Procedure B in ATC-40 except that the software does not make the simplifying assumption that post yield stiffness remains constant.

Check the Show Constant Period Lines At check box to display lines of constant period. These lines appear as radial lines on the capacity spectrum plot. By default the program plots lines for T = 0.5, 1, 1.5 and 2 seconds. The periods for any of the four curves can be changed by editing the value in one of the four associated edit boxes. A value of 0, or a blank edit box, means to omit that period line.

In the Damping Parameters area, the value of Inherent/Additional Damping is to be provided. The value input into this box must be between 0 and 1, inclusively. The default value is 0.05. The β_0 term is automatically included by the ETABS analysis method, and the 5% inherent viscous damping term can be specified in the Inherent/Additional Damping edit box as 0.05. If there is additional viscous damping provided in the structure, perhaps by viscous dampers that are not specifically included in the model, and then this damping should also be included in the Inherent/Additional Damping edit box. Thus if the damping inherent in the structure is assumed to be 5% of critical damping, and dampers which provide an additional 7% of critical damping are assumed to be added to the structure (although they are not actually in the model), then the value input in the Inherent/Additional Damping edit box should be 0.12, since 0.05 + 0.07 = 0.12.

Structural Behavior type is also available. The Structural Behavior types A, B and C defaults to the value defined for those structural behavior types in ATC-40.

4.8 Obtaining Performance Point

The intersection of the single demand spectra curve and capacity curve is the performance point. The single demand spectrum (variable damping) curve is constructed by doing the following for each point on the ADRS pushover curve:

a. Draw a radial line through the point on the ADRS pushover curve. This is a line of constant period.

b. Calculate the damping associated with the point on the curve based on the area under the curve up to that point.

c. Construct the demand spectrum, plotting it for the same damping level as associated with the point on the pushover curve.

d. The intersection point of the radial line and the associated demand spectrum represents a point on the Single Demand Spectrum (Variable Damping) curve.

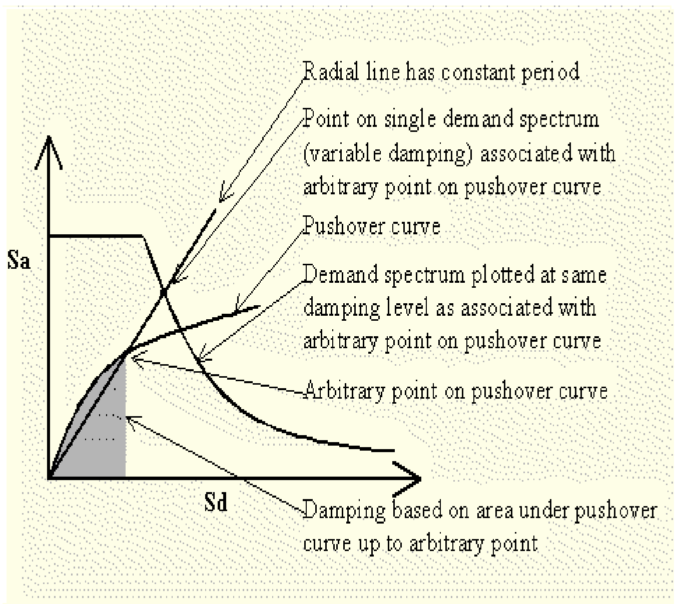

Figure 4.15: Construction of Single Demand Spectrum curve [12]

The software shows performance point in two units. There are four boxes below the displayed area in the pushover curve window. First box displays the coordinate of the cursor when it is positioned in the plot area. Second box shows the Performance point in base shear Vs monitored displacement coordinate. Third box shows the performance point in spectral acceleration Vs spectral displacement coordinate and fourth box shows the effective period and effective damping at the performance point.

4.9 Pushover Analysis and Results of building without Infill Wall

4.9.1 Linear static and dynamic analysis

Once the model is created, the linear static, dynamic and response spectrum analysis is performed. Analysis gives storey shear, lateral force at each storey, diaphragm (CM) displacement, storey drift, no. of modes, time period for each mode and mode participation factor in two horizontal (X and Y) direction. As it is a new RCC building model, the design is carried out as per IS 456-2000. All the section are found safe for the applied forces.

4.9.2 Pushover Curve, Capacity Spectrum Curve and Performance Point

Pushover curve obtained for G+4 storey building model without infill walls i.e. Bare Frame is as shown in Figure (4.16). The ultimate base shear the building can take before failure is around 7210 kN and the corresponding roof displacement is 235mm.

The capacity spectrum curve of the same model is shown in Figure (4.17). Red curve in the Figure (4.17) shows the response spectrum curve for various damping values. The Response Spectrum curves are governed by the values of Coefficient of Acceleration (Ca) and Coefficient of Velocity (Cv). For getting the response spectrum curve as per IS:1893(Part 1):2002, the value of Ca and Cv are calculated and assigned to the ETABS. For medium soil and Zone III, Ca and Cv values calculated are 0.16 and 0.4 respectively, as per Appendix B.

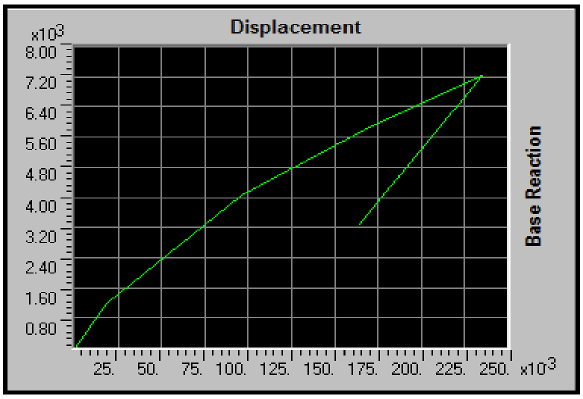

Figure 4.16: Pushover Curve for G+4 storey Bare Frame

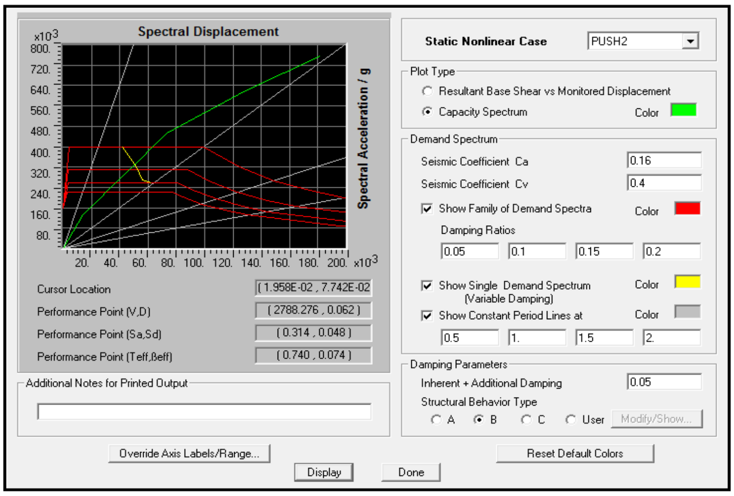

Figure 4.17: Capacity Spectrum Curve for G+4 storey Bare Frame

In Figure (4.17), the green curve is the capacity spectrum curve, red curves are response spectrum curve for various damping ratios and yellow curve is Single Demand Spectra. The intersection point of Single Demand Spectra with the Capacity Spectrum Curve is the Performance Point. The base shear at performance point is 2788.27 kN and corresponding displacement is 62 mm. Table 4.2 shows the step wise base shear, corresponding roof displacement and number of hinges formed in different nonlinear ranges.

The pushover analysis has included five steps. It has been observed that, on subsequent push to building, hinges started forming in beams first. Initially hinges were in B-IO stage and subsequently proceeding to IO-LS and LS-CP stages. On further

Table 4.2: Tabular format of pushover curve for G+4 storey Bare Frame

Step	Displ (mm)	BF (KN)	A-B	B-IO	IO-LS	LS-CP	CP-C	C-D	D-E	$> E$	T
0	0.00	0	718	2	0	0	0	0	0	0	720
1	18.3	1165.8	586	62	72	0	0	0	0	0	720
2	95.8	4042.3	540	44	76	60	0	0	0	0	720
3	167.2	5783.3	534	38	36	108	0	4	0	0	720
4	234.7	7209.8	534	38	36	102	0	2	6	2	720
5	163.6	3255.1	720	0	0	0	0	0	0	0	720

pushing of building the hinges that formed initially, moved to higher stage of hinge property. At performance point, where the capacity and demand meets, out of 720 assigned hinges 534 were in AB stage, 38, 36, and 102 hinges are in B-IO, IO-LS and LS-CP stages, respectively. From Figure (4.18) it is evident that building has good capacity to resist future earthquake as demand seen less. At performance point, hinges were in LS-CP range, therefore overall performance of building is said to be Life Safety to Collapse Prevention. Also it has been observed that, at ultimate capacity of building hinges formed were in columns. At ultimate load, columns capacity exhausted and analysis stopped. Hinges formation are shown in Figure (4.18).

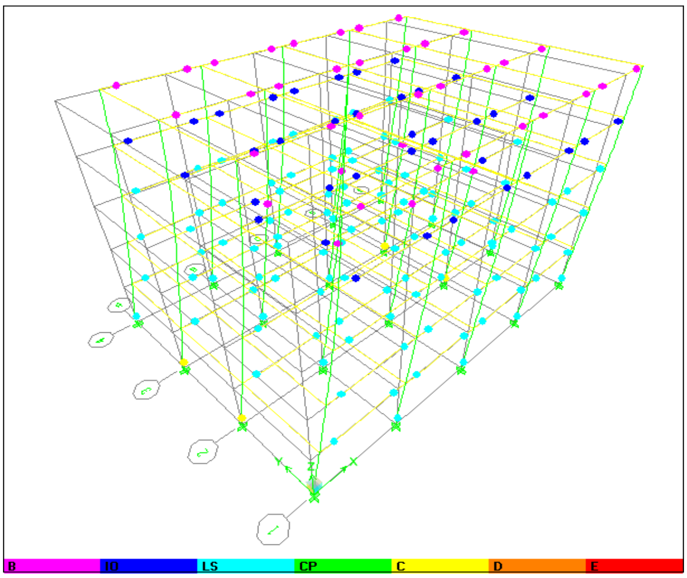

Figure 4.18: Hinge Formation at Performance Point in Bare Frame model

4.10 Pushover Analysis and Results of building with Infill Wall

In this model, the infill walls are modeled as membrane element with in-plane stiffness and no out of plane stiffness, and as equivalent compression strut. The behavior of infill wall was observed in both the cases.

4.10.1 Linear Static and Dynamic analysis

Once the model is created, the linear static, dynamic and response spectrum analysis need to be performed. Analysis gives storey shear, lateral force at each storey, diaphragm CM displacement, storey drift, no. of modes, time period for each mode and mode participation factor in two horizontal (X and Y) direction. From analysis it was observed that the infill wall models gives higher storey shear and lateral force as compared to bare frame model. Since, it is a new RCC building model, the design is carried out as per IS 456-2000. and the sections are found safe for the applied forces.

4.10.2 Pushover Curve, Capacity Spectrum Curve and Performance Point

Pushover curve obtained for G+4 storey building model with infill walls as a membrane element is as shown in Figure (4.19). The ultimate base shear the building can take before failure is around 11970 kN and the corresponding roof displacement is 70 mm which is less as compared to bare frame structure, as it has higher stiffness as compared to bare frame, because of the presence of infill walls. The drop in the pushover curve indicates the failure of some of the member, which suddenly reduces the applied load to the structure.

As mentioned above, the drop in the pushover curve comes at step 3 where six hinges are reaching to its failure stage. Because the G+4 storey building model do not have infill walls at ground floor and rest of all upper storey infill walls, it has anticipated a large displacement and formation of hinges (yielding of members) at

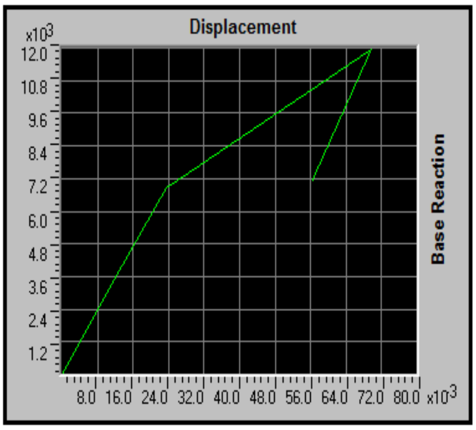

Figure 4.19: Pushover Curve for G+4 storey Infill Frame

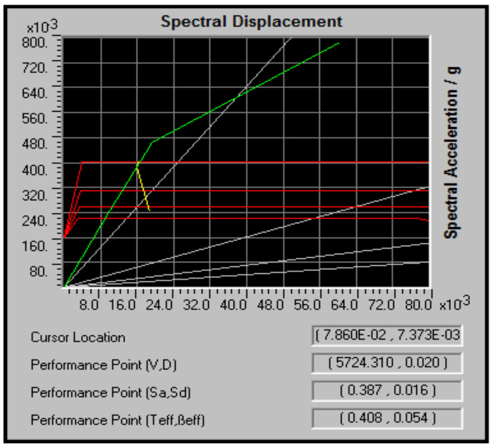

Figure 4.20: Capacity Spectrum Curve for G+4 storey Infill Frame

ground floor to first floor level. The same has been observed from the result. This is typical soft storey phenomenon of the building. Refer Figure (4.20) at performance point, the base shear was 5724.31 kN and corresponding roof displacement 20 mm.

Tabular format of pushover curve is shown in Table 4.3 It has been observed that the hinge formation starts from the lower storey because of the soft storey phenomena. Hinges started forming in column first and then subsequently to the beams of first floor. Initially the hinges were in B-IO stage. As analysis proceeds, the yielding of column occurs. In step three, out of 720 hinges 668 hinges are in A-B range, 24 and 16 hinges are in B-IO and LS-CP range respectively, while 4 hinges are in C-D range. The failure of these four hinges which were in C-D range in step two, occurs in step

Table 4.3: Tabular format of pushover curve for G+4 storey Infill Frame

Step	Displ (mm)	BF (KN)	A-B	B-IO	IO-LS	LS-CP	CP-C	C-D	D-E	$> E$	T
0	0.00	0	718	2	0	0	0	0	0	0	720
1	12.2	3650.11	672	48	0	0	0	0	0	0	720
2	23.5	6852.99	668	24	8	16	0	4	0	0	720
3	69.6	11969.94	668	24	8	8	0	6	4	2	720
4	56.1	7068.74	720	0	0	0	0	0	0	0	720

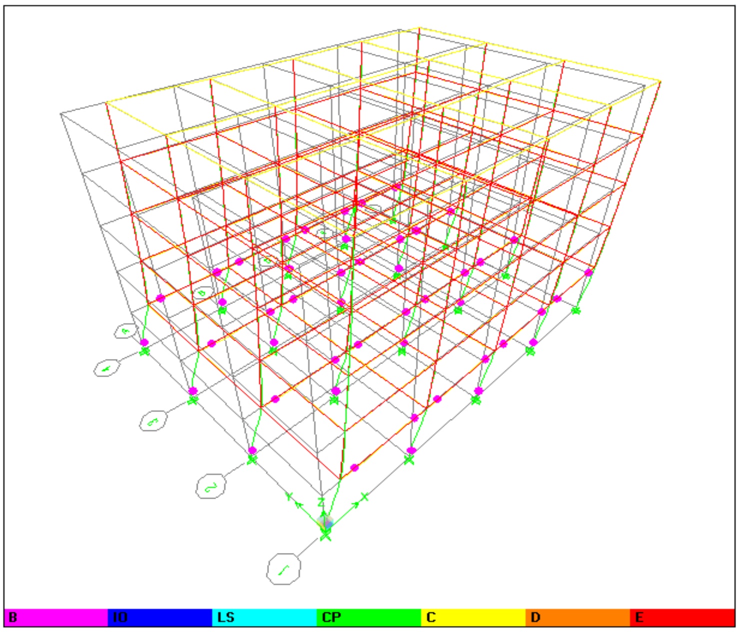

Figure 4.21: Hinge Formation at Performance Point in Infill Frame model

three as it moves to the D-E range. The analysis continues and the loads from those four failed hinges were redistributed to the other hinges.

The graphical representation of hinge formation at the step of performance point is shown in Figure (4.21). Overall performance of building is of Immediate Occupancy stage and hence, the building can be occupied immediately in predicted earthquake level.

Similarly, the pushover curve and capacity spectrum curve for G+4 storey building model with equivalent strut is shown in Figure (4.22) and (4.23).

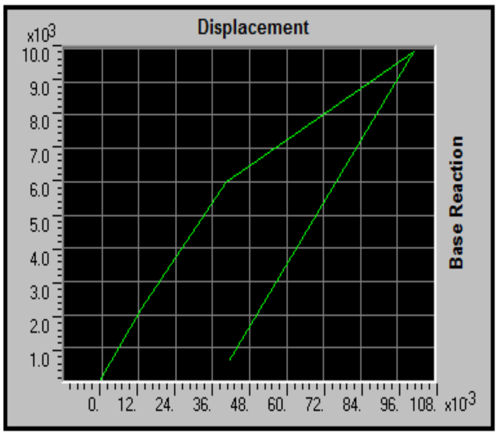

Figure 4.22: Pushover Curve for G+4 storey Equivalent Strut

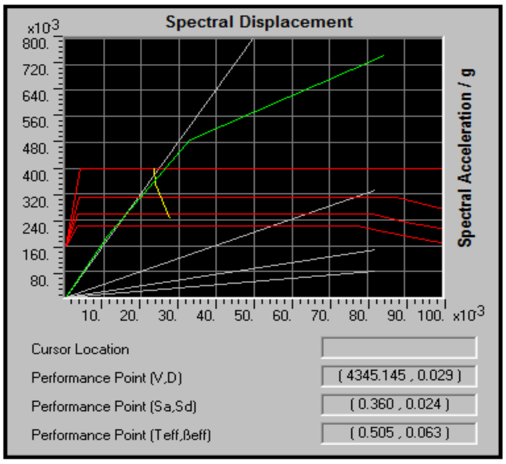

Figure 4.23: Capacity Spectrum Curve for G+4 storey Equivalent Strut

The ultimate base shear before failure is around 9899.36 KN and corresponding displacement is 101 mm which is less as compared to bare frame. The pushover analysis includes four steps. It has been observed and as tabulated in Table 4.4, initially the axial hinges have formed into the strut and were in A-B range, up to second step of analysis. In step three, out of 968 hinges assigned, 830 hinges were in A-B range, 86 hinges were in B-IO while 4 hinges were in D-E range. At performance point, the base shear was 4345.15 KN and corresponding displacement 29 mm.

Interesting point was that, the subsequent formation of hinges has not taken place. The reason was the brittle property of masonry strut. As shown in Figure (4.24) there was no hinge formation in columns, while the beams closer to the strut which were

Table 4.4: Tabular format of pushover curve for G+4 storey Equivalent Strut

Step	Displ (mm)	BF (KN)	A-B	B-IO	IO-LS	LS-CP	CP-C	C-D	D-E	$> E$	T
0	0.00	0	966	2	0	0	0	0	0	0	968
1	12.8	2155.75	872	96	0	0	0	0	0	0	968
2	40.4	6009.69	830	86	16	32	0	4	0	0	968
3	101.4	9899.36	830	86	16	30	0	0	4	2	968
4	41.2	607.14	968	0	0	0	0	0	0	0	968

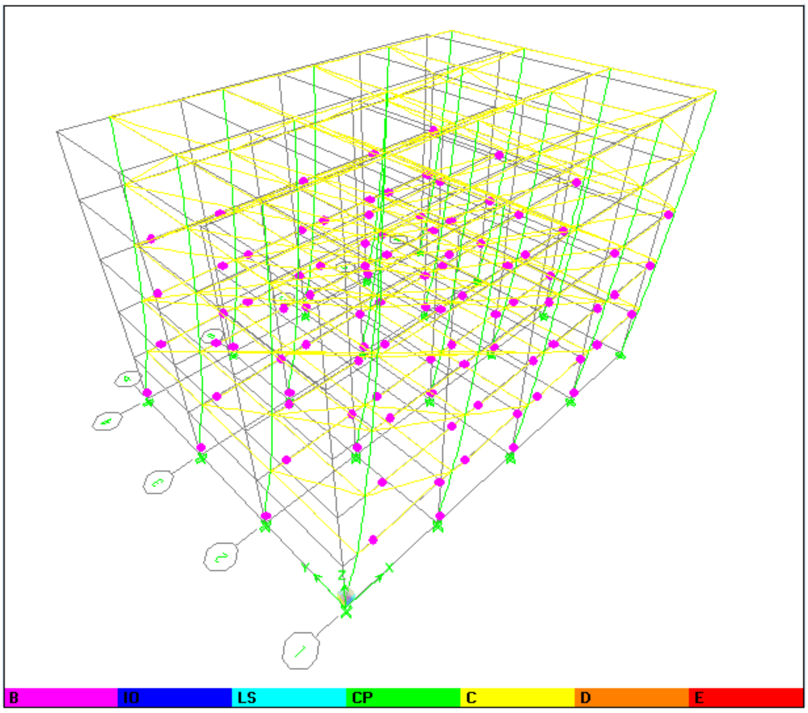

Figure 4.24: Hinge Formation at Performance Point in Equivalent Strut model

failing, started showing hinge formation at later stages because of the redistribution of the forces. Overall performance of building is of Immediate Occupancy.

4.11 Evaluation of Lateral Load Patterns for Pushover Analysis

The performance of a building depends on various parameters out of which lateral load pattern is most critical. FEMA-273 and ATC-40 adopts specific pattern of lateral loading for nonlinear static analysis, widely known as pushover analysis.

For a performance evaluation the load pattern selection is likely to be more critical than the accurate determination of the target displacement. Here, the evaluation of three different loading patterns namely, Rectangular and Triangular (k=1) as per FEMA-273 and ATC-40 and Parabolic (k=2) as per IS: 1893(Part 1)-2002 was applied on G+4 storey R.C.C. building for pushover analysis of three different types of building model likely Bare Frame, Infill Wall and Equivalent Strut. The capacity curve (V/W) to displacement for different levels was obtained for three different types of lateral loading patterns.

Table 4.5: Lateral Load Pattern Results for Bare Frame with Parabolic Loading

Roof		**Storey-4**		**Storey-3**		**Storey-2**		**Storey-1**	
V/W	**Displ** (m)	**V/W**	**Displ** (m)	**V/W**	**Displ** (m)	**V/W**	**Displ** (m)	**V/W**	**Displ** (m)
0	0	0	0	0	0	0	0	0	0
0.1	0.018	0.1	0.015	0.1	0.011	0.1	0.007	0.1	0.0028
0.35	0.094	0.37	0.089	0.41	0.078	0.41	0.044	0.39	0.015
0.58	0.2	0.58	0.18	0.59	0.14	0.59	0.08	0.42	0.017
0.64	**0.24**	**0.64**	**0.21**	**0.64**	**0.17**	**0.64**	**0.11**	**0.64**	**0.055**
0.44	0.17	0.44	0.15	0.44	0.13	0.44	0.09	0.44	0.048

The total weight of building for bare frame model was found to be 11255.84 KN. Table 4.5 indicates the variation of V/W and displacement of each floor level for bare frame with parabolic loading pattern.

As shown in Figure (4.25) the maximum displacement was obtained at roof level only. The displacements were goes on reducing while coming down from roof level to ground level of building. The maximum displacement obtained was about 0.24 m at a base shear of 7203.74 KN at ultimate capacity.

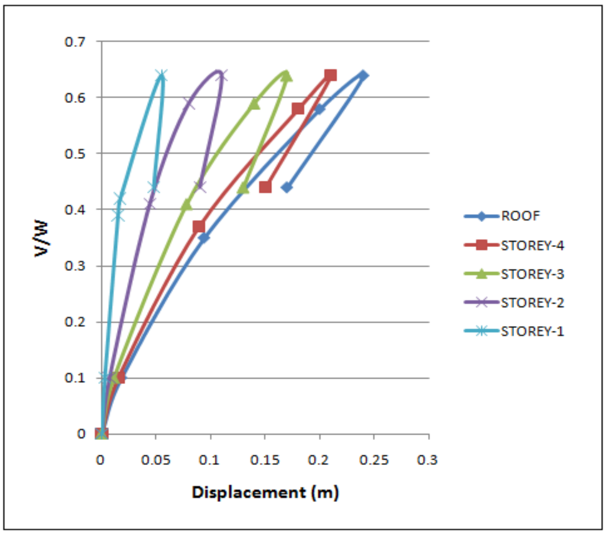

Figure 4.25: V/W Vs. Displacement Curve for Bare Frame with Parabolic Loading

Table 4.6: Lateral Load Pattern Results for Bare Frame with Triangular Loading

Roof		**Storey-4**		**Storey-3**		**Storey-2**		**Storey-1**	
V/W	**Displ** (m)	**V/W**	**Displ** (m)	**V/W**	**Displ** (m)	**V/W**	**Displ** (m)	**V/W**	**Displ** (m)
0	0	0	0	0	0	0	0	0	0
0.1	0.018	0.1	0.015	0.1	0.011	0.1	0.007	0.1	0.0028
0.34	0.09	0.37	0.086	0.42	0.077	0.41	0.044	0.4	0.015
0.53	0.17	0.53	0.14	0.59	0.13	0.61	0.11	0.42	0.017
0.64	**0.23**	**0.64**	**0.2**	**0.64**	**0.16**	**0.64**	**0.13**	**0.64**	**0.055**
0.22	0.14	0.22	0.13	0.22	0.1	0.22	0.076	0.22	0.042

Table 4.6 indicates the variation of V/W and displacement of each floor level for bare frame with triangular loading pattern. As shown in Figure (4.26) the maximum displacement of building was obtained about 0.23 m with base shear of 7203.74 KN.

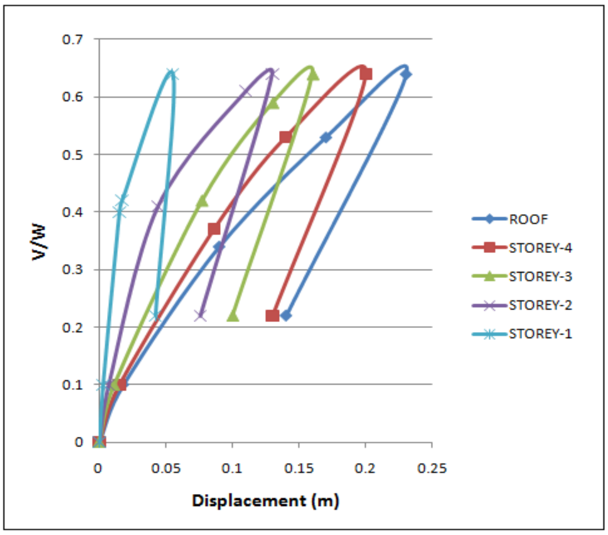

Figure 4.26: V/W Vs. Displacement Curve for Bare Frame with Triangular Loading

Table 4.7: Lateral Load Pattern Results for Bare Frame with Rectangular Loading

Roof		**Storey-4**		**Storey-3**		**Storey-2**		**Storey-1**	
V/W	**Displ** (m)	**V/W**	**Displ** (m)	**V/W**	**Displ** (m)	**V/W**	**Displ** (m)	**V/W**	**Displ** (m)
0	0	0	0	0	0	0	0	0	0
0.15	0.016	0.15	0.015	0.15	0.012	0.15	0.007	0.15	0.003
0.51	0.087	0.53	0.083	0.51	0.064	0.51	0.04	0.51	0.015
0.71	0.15	0.77	0.16	0.76	0.13	0.76	0.1	0.53	0.016
0.81	**0.19**	**0.81**	**0.18**	**0.81**	**0.15**	**0.81**	**0.13**	**0.81**	**0.055**
0.2	0.11	0.2	0.1	0.2	0.088	0.2	0.067	0.2	0.038

Table 4.7 indicates the variation of V/W and displacement of each floor level for bare frame with rectangular loading pattern. It was observed from Figure (4.27) that, the displacement of roof level was maximum. Also, it was evident that, the ultimate capacity of building estimated by rectangular loading pattern is more among all the loading pattern considered. The value of maximum displacement was about 0.19 m for the base shear value of 9117.23 KN.

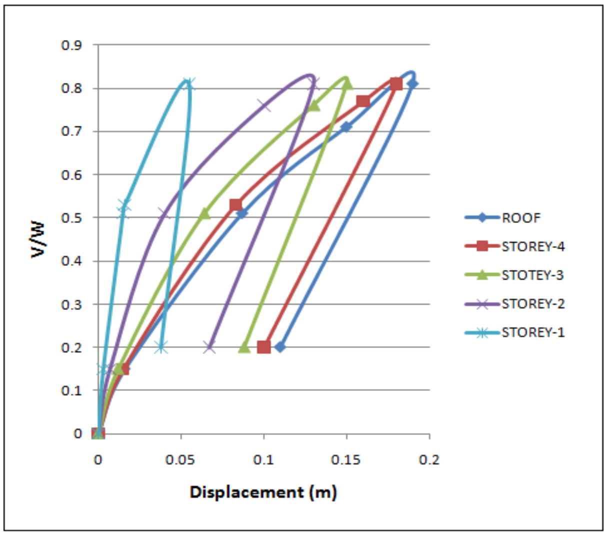

Figure 4.27: V/W Vs. Displacement Curve for Bare Frame with Rectangular Loading

Table 4.8: Lateral Load Pattern Results for Infill Wall with Parabolic Loading

Roof		**Storey-4**		**Storey-3**		**Storey-2**		**Storey-1**	
V/W	**Displ** (m)	**V/W**	**Displ** (m)	**V/W**	**Displ** (m)	**V/W**	**Displ** (m)	**V/W**	**Displ** (m)
0	0	0	0	0	0	0	0	0	0
0.075	0.017	0.075	0.015	0.075	0.017	0.075	0.007	0.075	0.0028
0.26	0.092	0.29	0.092	0.31	0.077	0.3	0.044	0.3	0.016
0.38	0.16	0.4	0.16	0.44	0.15	0.44	0.09	0.31	0.017
0.47	**0.23**	**0.47**	**0.21**	**0.47**	**0.17**	**0.47**	**0.11**	**0.47**	**0.055**
0.34	0.18	0.34	0.16	0.34	0.13	0.34	0.091	0.34	0.048

The total weight of building for infill wall model was found to be 15533.84 KN. Table 4.8 indicates the variation of V/W and displacement of each floor level for infill frame with parabolic loading pattern. As shown in Figure (4.28) the maximum displacement was obtained at roof level only. The displacements were goes on reducing while coming down from roof level to ground level of building. The maximum displacement obtained was about 0.23 m at a base shear of 7300.90 KN at ultimate capacity.

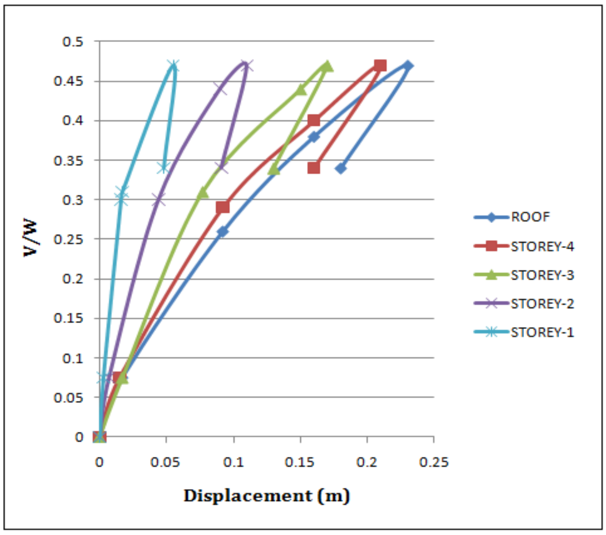

Figure 4.28: V/W Vs. Displacement Curve for Infill Wall with Parabolic Loading

Table 4.9: Lateral Load Pattern Results for Infill Wall with Triangular Loading

Roof		**Storey-4**		**Storey-3**		**Storey-2**		**Storey-1**	
V/W	**Displ** (m)	**V/W**	**Displ** (m)	**V/W**	**Displ** (m)	**V/W**	**Displ** (m)	**V/W**	**Displ** (m)
0	0	0	0	0	0	0	0	0	0
0.075	0.017	0.075	0.015	0.075	0.017	0.07	0.007	0.075	0.0028
0.27	0.095	0.29	0.094	0.31	0.076	0.3	0.044	0.29	0.016
0.38	0.16	0.41	0.16	0.44	0.13	0.43	0.08	0.31	0.017
0.47	**0.21**	**0.47**	**0.21**	**0.47**	**0.17**	**0.47**	**0.11**	**0.47**	**0.056**
0.14	0.13	0.14	0.12	0.13	0.1	0.14	0.074	0.14	0.042

Table 4.9 indicates the variation of V/W and displacement of each floor level for infill wall with triangular loading pattern. As shown in Figure (4.29) the maximum displacement of building was obtained about 0.21 m with base shear of 7300.90 KN.

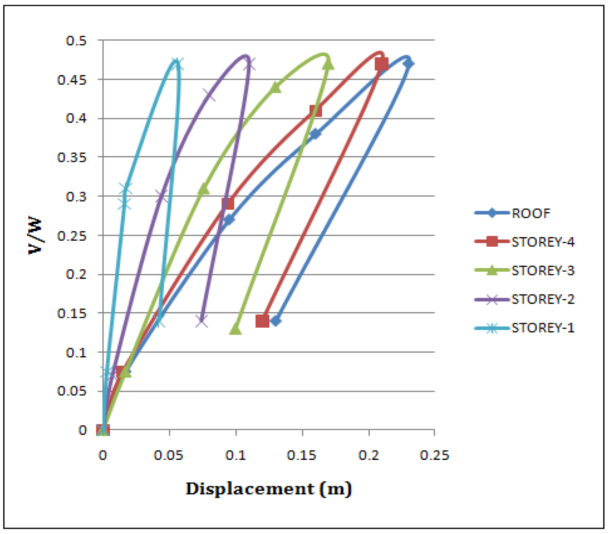

Figure 4.29: V/W Vs. Displacement Curve for Infill Wall with Triangular Loading

Table 4.10: Lateral Load Pattern Results for Infill Wall with Rectangular Loading

Roof		**Storey-4**		**Storey-3**		**Storey-2**		**Storey-1**	
V/W	**Displ** (m)	**V/W**	**Displ** (m)	**V/W**	**Displ** (m)	**V/W**	**Displ** (m)	**V/W**	**Displ** (m)
0	0	0	0	0	0	0	0	0	0
0.11	0.017	0.11	0.015	0.11	0.012	0.11	0.007	0.11	0.0032
0.37	0.087	0.39	0.083	0.38	0.06	0.38	0.041	0.38	0.015
0.53	0.15	0.54	0.14	0.58	0.13	0.58	0.08	0.39	0.016
0.6	**0.19**	**0.6**	**0.18**	**0.6**	**0.15**	**0.6**	**0.11**	**0.49**	**0.055**
0.19	0.13	0.19	0.11	0.2	0.1	0.2	0.078	0.2	0.046

Table 4.10 indicates the variation of V/W and displacement of each floor level for infill frame with rectangular loading pattern. It was observed from Figure (4.30) that, the displacement of roof level was maximum. Also, it was evident that, the ultimate capacity of building estimated by rectangular loading pattern is more among all the loading pattern considered. The value of maximum displacement was about 0.19 m for the base shear value of 9320.30 KN.

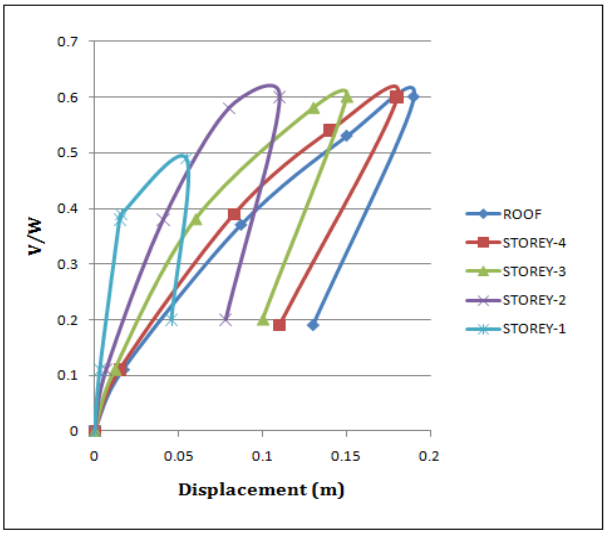

Figure 4.30: V/W Vs. Displacement Curve for Infill Wall with Rectangular Loading

Table 4.11: Lateral Load Pattern Results for Equivalent Strut with Parabolic Loading

Roof		**Storey-4**		**Storey-3**		**Storey-2**		**Storey-1**	
V/W	**Displ** (m)	**V/W**	**Displ** (m)	**V/W**	**Displ** (m)	**V/W**	**Displ** (m)	**V/W**	**Displ** (m)
0	0	0	0	0	0	0	0	0	0
0.082	0.018	0.082	0.015	0.082	0.011	0.082	0.007	0.082	0.0028
0.28	0.091	0.3	0.089	0.33	0.078	0.33	0.045	0.32	0.016
0.44	0.18	0.44	0.16	0.48	0.15	0.48	0.09	0.34	0.017
0.51	**0.23**	**0.51**	**0.21**	**0.51**	**0.17**	**0.51**	**0.11**	**0.51**	**0.055**
0.16	0.14	0.16	0.12	0.16	0.1	0.16	0.075	0.16	0.041

The total weight of building for equivalent strut model was found to be 14033.33 KN. Table 4.11 indicates the variation of V/W and displacement of each floor level for equivalent strut with parabolic loading pattern. As shown in Figure (4.31) the maximum displacement was obtained at roof level only. The displacements were goes on reducing while coming down from roof level to ground level of building. The maximum displacement obtained was about 0.23 m at a base shear of 7156.99 KN at ultimate capacity.

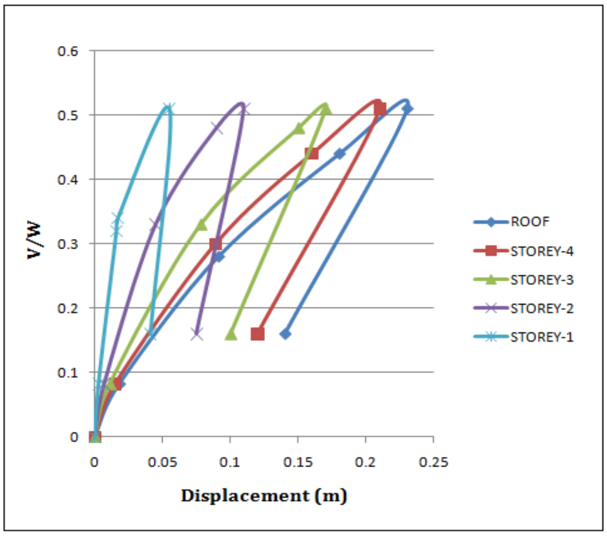

Figure 4.31: V/W Vs. Displacement Curve for Equivalent Strut with Parabolic Loading

Table 4.12 indicates the variation of V/W and displacement of each floor level for equivalent strut with triangular loading pattern. As shown in Figure (4.32) the maximum displacement of building was obtained about 0.22 m with base shear of 7156.99 KN.

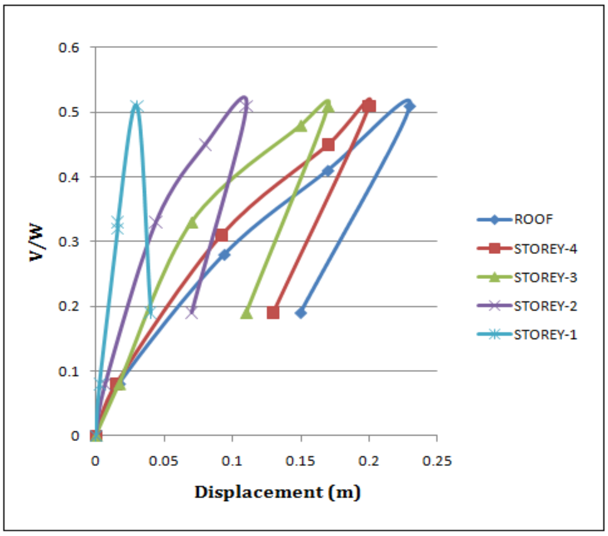

Figure 4.32: V/W Vs. Displacement Curve for Equivalent Strut with Triangular Loading

Table 4.12: Lateral Load Pattern Results for Equivalent Strut with Triangular Loading

Roof		**Storey-4**		**Storey-3**		**Storey-2**		**Storey-1**	
V/W	**Displ** (m)	**V/W**	**Displ** (m)	**V/W**	**Displ** (m)	**V/W**	**Displ** (m)	**V/W**	**Displ** (m)
0	0	0	0	0	0	0	0	0	0
0.08	0.017	0.08	0.015	0.08	0.017	0.08	0.007	0.08	0.0028
0.28	0.094	0.31	0.092	0.33	0.07	0.33	0.044	0.32	0.016
0.41	0.17	0.45	0.17	0.48	0.15	0.45	0.08	0.33	0.016
0.51	**0.22**	**0.51**	**0.2**	**0.51**	**0.17**	**0.51**	**0.11**	**0.51**	**0.03**
0.19	0.15	0.19	0.13	0.19	0.11	0.19	0.07	0.19	0.04

Table 4.13: Lateral Load Pattern Results for Equivalent Strut with Rectangular Loading

Roof		**Storey-4**		**Storey-3**		**Storey-2**		**Storey-1**	
V/W	**Displ** (m)	**V/W**	**Displ** (m)	**V/W**	**Displ** (m)	**V/W**	**Displ** (m)	**V/W**	**Displ** (m)
0	0	0	0	0	0	0	0	0	0
0.12	0.017	0.12	0.015	0.12	0.017	0.12	0.007	0.12	0.0032
0.41	0.08	0.42	0.084	0.41	0.064	0.41	0.041	0.41	0.015
0.58	0.16	0.63	0.16	0.63	0.14	0.63	0.09	0.43	0.016
0.65	**0.19**	**0.65**	**0.18**	**0.65**	**0.15**	**0.65**	**0.11**	**0.65**	**0.055**
0.15	0.11	0.15	0.1	0.15	0.087	0.15	0.067	0.15	0.04

Table 4.13 indicates the variation of V/W and displacement of each floor level for equivalent strut with rectangular loading pattern. It was observed from Figure (4.33) that, the displacement of roof level was maximum. Also, it was evident that, the ultimate capacity of building estimated by rectangular loading pattern is more among all the loading pattern considered. The value of maximum displacement was about 0.19 m for the base shear value of 9121.66 KN.

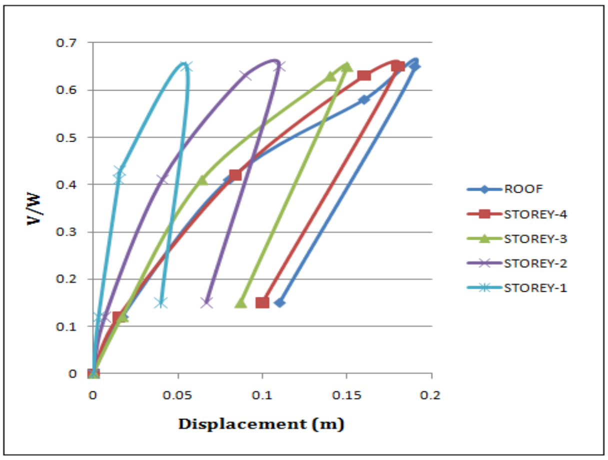

Figure 4.33: V/W Vs. Displacement Curve for Equivalent Strut with Rectangular Loading

4.12 Summary

This chapter includes Pushover Analysis of new G+4 storey RCC building for three different types of building i.e, building with bare frame, building with infill wall modelled as membrane element and equivalent strut element are considered. A procedure for modeling of building and Pushover analysis in ETABS is discussed. The performance point for above mentioned building are obtained. Also, the evaluation of three different types of lateral loading patterns for pushover analysis, namely, parabolic, triangular and rectangular are considered.

The results of the Pushover analysis shows that, building model without infill i.e, bare frame has an overall performance in Life Safety to Collapse Prevention, building model with infill as membrane wall has an overall performance in Immediate Occupancy level and building model with infill as equivalent strut has an overall performance in Immediate Occupancy level.

The results of the influence of lateral loading patterns on Pushover analysis shows that, a rectangular loading pattern gives higher base shear to weight ratio as compared to other loading patterns. Parabolic loading patterns gives the least base shear to weight ratio as compared to other loading patterns. It was observed that displacement capacity under parabolic loading pattern is maximum among all loading pattern considered.

Chapter 5

Time History Analysis of G+4 Storey R.C.C. Building

5.1 Configuration of Building

The plan dimensions of building, geometric properties of frame and live loads on slab are considered as described in chapter 4. The time history analysis of G+4 storey R.C.C. building is carried out for twenty number of different earthquake ground motion records. The three different types of models were prepared namely, bare frame, infill wall and equivalent strut for time history analysis.

5.2 Earthquake Ground Motion Records

Earthquake ground motion records are used to investigate the correlation between structural response and seismic intensity measures. A time history analysis should be performed to calculate a probabilistic demand curve to determine a relationship between the structural response demand and the intensity measure. Based on **Pacific Earthquake Engineering Research Center** [**13**], acceleration time histories of twenty numbers of earthquake ground motion records with different peak ground acceleration (PGA) are taken for time history analysis, as shown below:

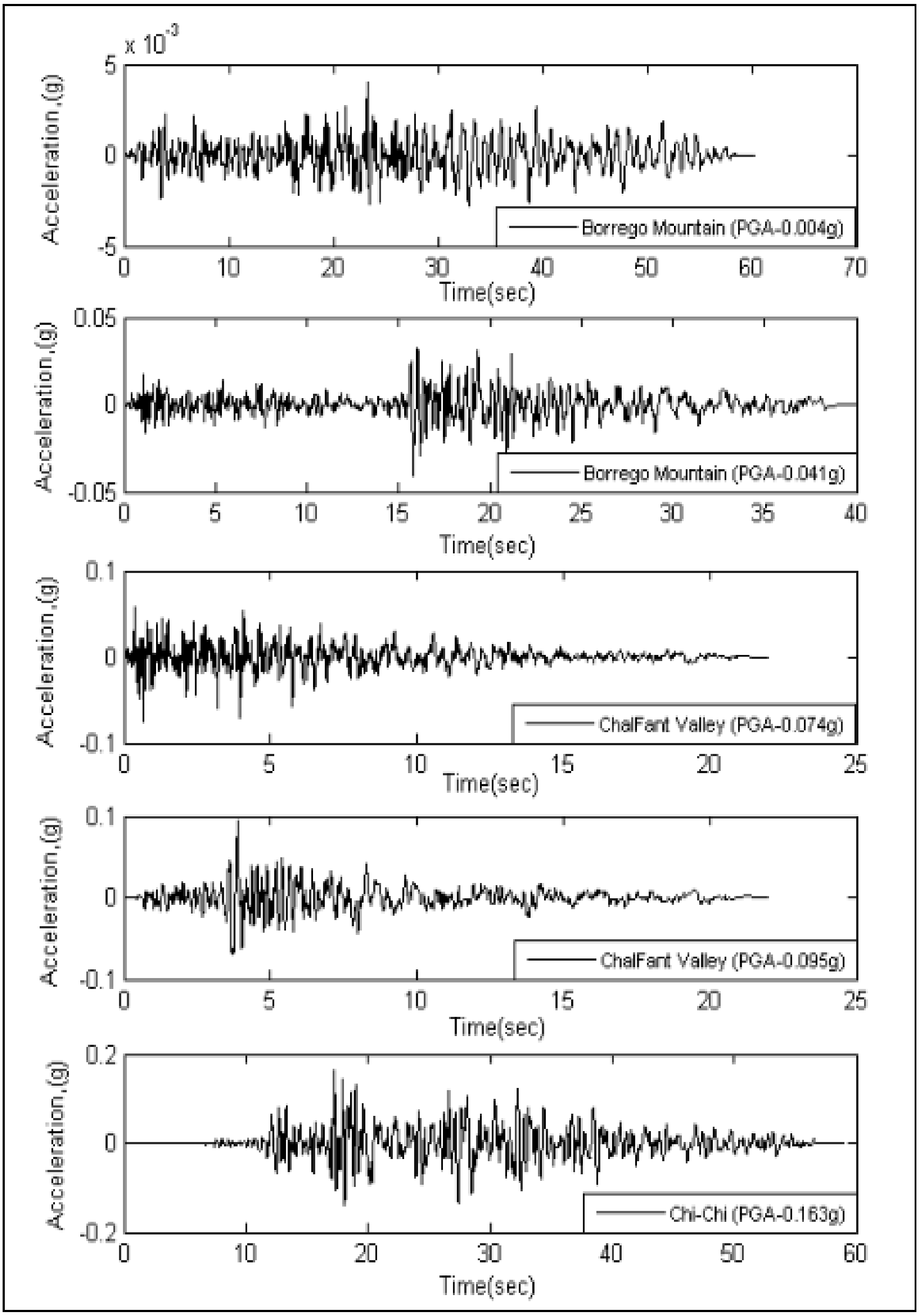

Figure 5.1: Acceleration time histories for five different PGA (0.004g-0.163g)

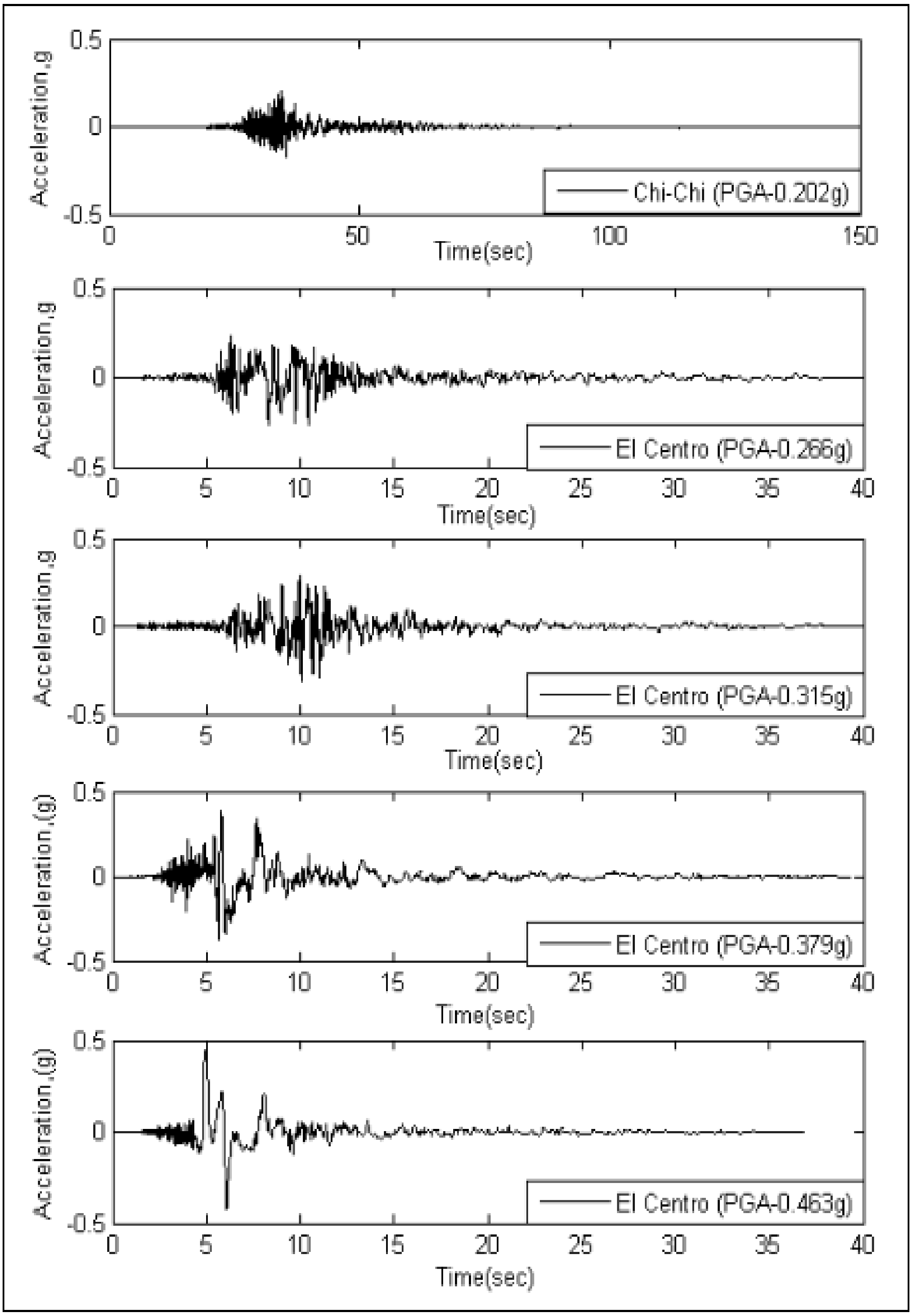

Figure 5.2: Acceleration time histories for five different PGA (0.202g-0.463g)

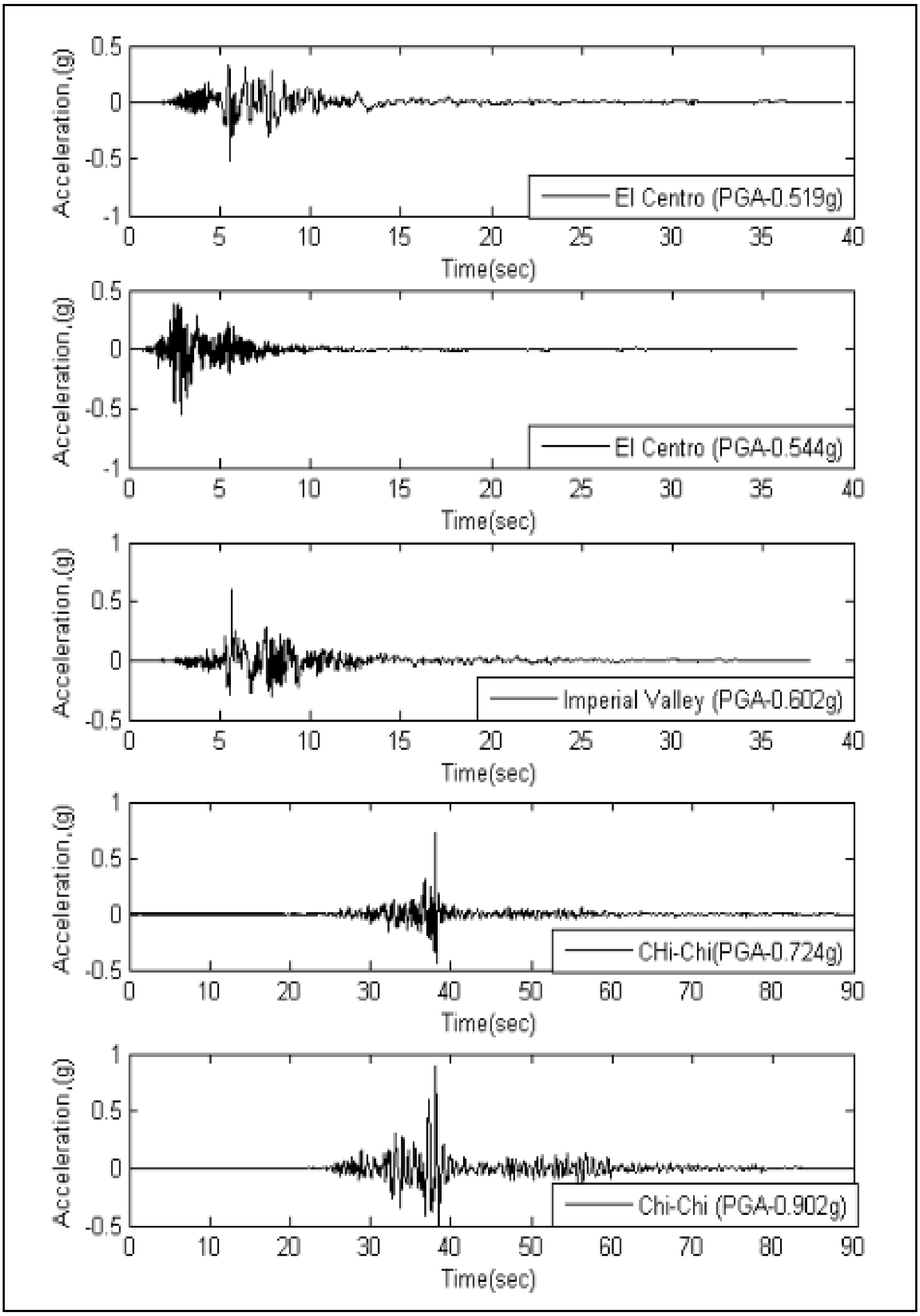

Figure 5.3: Acceleration time histories for five different PGA (0.519g-0.902g)

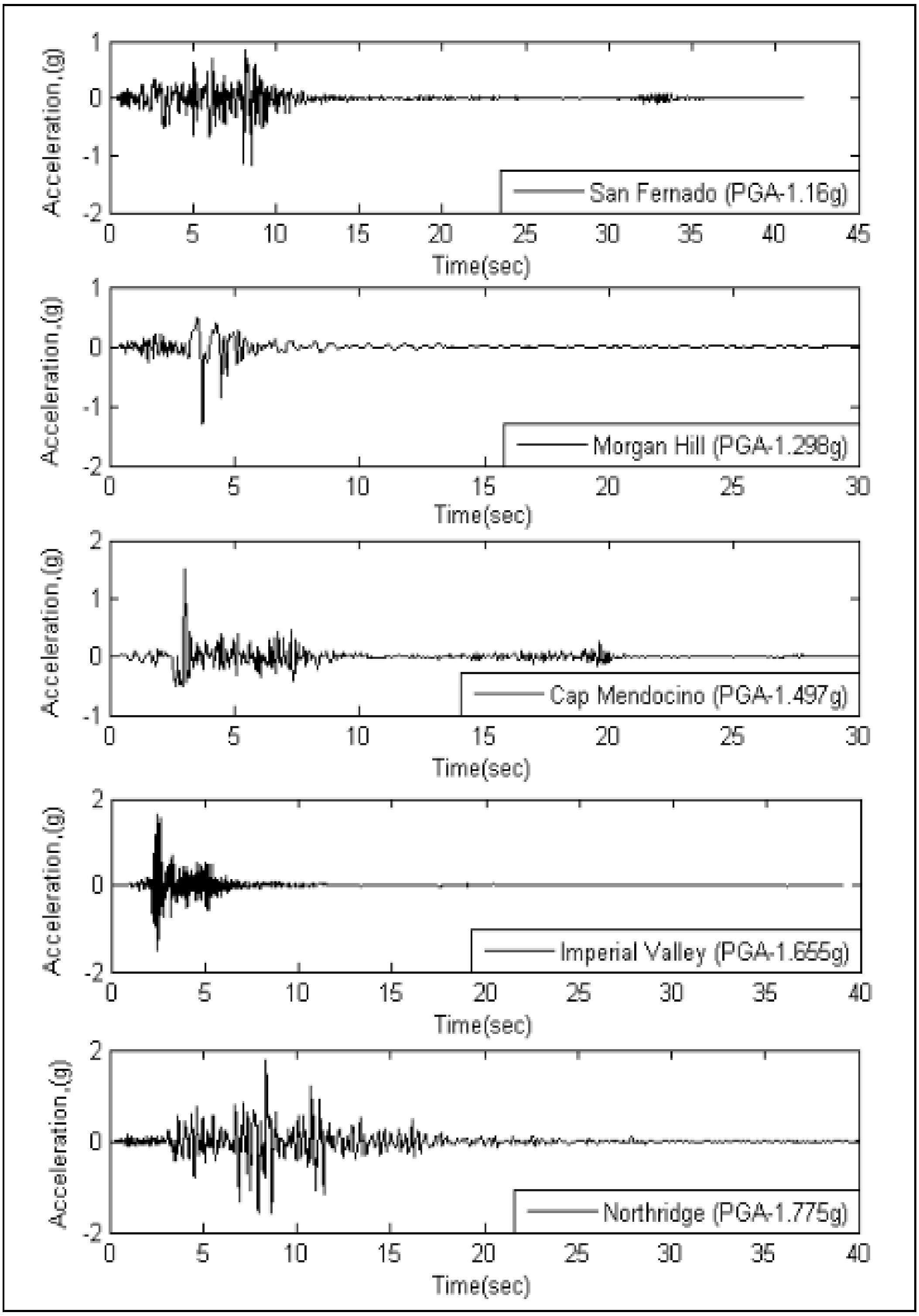

Figure 5.4: Acceleration time histories for five different PGA (1.16g-1.775g)

5.3 Static Load Cases

The model is created and the geometric properties are to be assigned. The ETABS calculates apply Dead Load automatically while Live load is to be applied to each floor as per IS:875(Part-II).

5.4 Time History Function and Cases

A time history function may be (a) a list of time and function values or (b) a list of function values that are assumed to occur at equal spaced intervals. The function values in a time history function may be (a) ground acceleration values or (b) multipliers for specified load cases (force or displacement).

An accelerogram is basically the time history of the acceleration experienced by the ground in a given direction during a seismic event. We need to input accelerogram as a generic function defined in ETABS starting from a TXT file.

Add a Time History Function Definition

- Add a time history function based on a text file of earthquake ground motion records by clicking the Add Function from File button.
- Add a time history function based on user specified parameters by selecting Add User Function from the drop-down list

Here, a time history function was assigned by input text file.

Modify/Show a Time History Function Definition

- Highlight the name of the function to be modified/shown in the list of function names in the Functions area of the Define Time History Functions form.

Figure 5.5 shows time history functions define in ETABS and Figure 5.6 shows definition of time history function in ETABS.

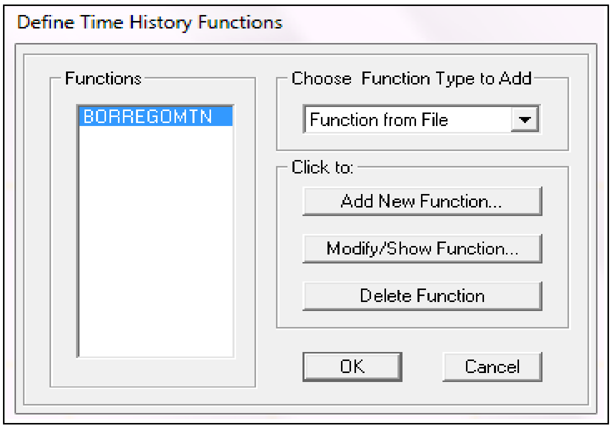

Figure 5.5: Define Time History Functions

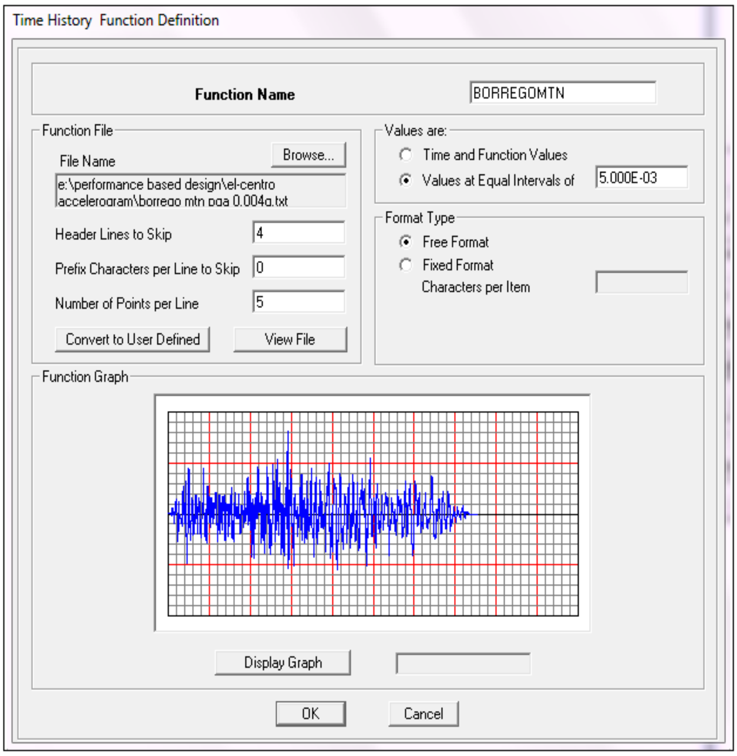

Figure 5.6: Time History Function Definition

As shown in Figure 5.6, We can select:

- Name of the function (e.g. BORREGO MOUNTAIN)
- Location of the file by using the button BROWSE.
- Number of lines to skip (4 for the PEER database).
- Number of points per line (5 for the PEER database).

By clicking on Display Graph we can visually check the waveform.

Time History Case Data

As shown in Figure 5.7 the time history case data form has the following areas:

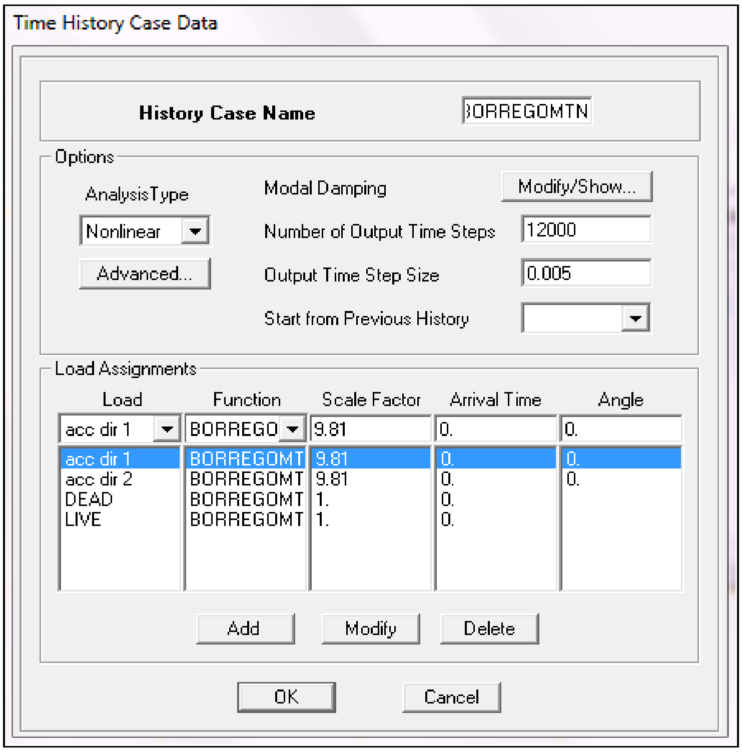

Figure 5.7: Time History Case Data

History Case Name Specify or modify the name of the time history case.

Options: Specify parameters for the following options.

Analysis Type:

- **Linear:** In a linear time history analysis, all objects behave linearly. Only the linear properties assigned to link elements are considered in a linear time history analysis.
- **Periodic:** A periodic time history analysis is a linear analysis. For this analysis, specify a single cycle of the periodic function and then ETABS assumes that the specified cycle continues indefinitely. ETABS shows time history results for a single cycle that occurs after the output has stabilized such that the conditions at the beginning of the cycle are equal to those at the end of the cycle. In a periodic time history analysis, all objects behave linearly. Only the linear properties assigned to link elements are considered in a periodic time history analysis.
- **Nonlinear:** In a nonlinear time history analysis the nonlinear dynamic properties assigned to link elements are considered. The mode shapes obtained for the analysis are based on linear properties only.

Model Damping:

Damping for All Modes: Enter the damping for all modes in this form. This is a percent critical damping. A damping that is 5% 0f critical damping is entered as 0.05.

Number of Output Time Steps: The number of output time steps is the number of equally spaced steps at which the output results are reported. Do not confuse this with the number of time steps in your input time history function. The number of output time steps can be different from the number of time steps in your input time history function. The number of output time steps times the output time step size is equal to the length of time over which output results are reported. The number of output time steps should be given by the duration of accelerogram divided by the sampling time.

Output Time Step Size: The output time step size is the time in seconds between each of the equally spaced output time steps. Do not confuse this with the time step size in your input time history function. The number of output time step size can be different from the input time step size in your input time history function. The number of output time steps time the output time step size is equal to the length of time over which output results are reported. The output time step size should be given by the sampling time of the accelerogram.

Start from Previous History: The Start from Previous History option allows you to set the initial conditions for the time history analysis to the conditions that exist at the end of a previously run analysis (in the same analysis run). This option is not available for periodic time history analysis. The advantage of the Start from Previous History option is that when you want to start several different time histories from the final conditions of another time history, such as a gravity load time history, you only have to run the other (gravity) time history once rather than multiple times.

Load Assignments:

- **To define a load assignment,** fill in the appropriate items in the Load, Function, Scale Factor, Arrival Time and Angle boxes and then click the Add button.

- **To modify an existing load assignment,** highlight the existing load assignment in the Load Assignment area of the form. Note that the data associated with that load assignment appears in the edit and drop-down boxes at the top of this area. Modify the load assignment data as desired. Then click the Modify button.

Specify parameters for the following options:

Load: The Load may either be a defined static load case, acceleration direction 1, acceleration direction 2 or acceleration direction 3. The three accelerations (acc dir 1, acc dir 2 and acc dir 3) are ground accelerations in the local axes directions of the time history. Positive acc dir 3 corresponds to the positive global Z direction always. When you specify one of these three ground accelerations your input function defines how the ground acceleration varies with time. The static load cases that you can specify in this area may be either force loads or displacement loads. In this case your input function defines how this load or displacement varies with time.

Function: This option shows the particular time history function define for analysis.

Scale Factor: The Scale Factor item is used as a multiplier on the input function values. The units for the scale factor depend on the type of load specified in the Load drop-down box. If the load is specified as a ground acceleration (that is, acc dir 1, acc dir 2 or acc dir 3), this scale factor has units of $meter/seconds^2$. If the load is a static load case, this scale factor is unitless. The scale factor can be any positive or negative number, or zero. Here, the records from PEER website are given in units of (g), so the scale factor for acceleration direction 1 and acceleration direction 2 would be 9.81 m/s^2.

Arrival Time: The arrival time is the time that a particular load assignment starts. Assume that you want to apply the same ground acceleration that lasts 30 seconds to your building in the global X and global Y directions. Further assume that you want the ground acceleration in the global Y direction to start 10 seconds after the ground acceleration in the global X direction begins. In that case you could specify an arrival time of 0 for the load assignment for the global X direction shaking and an arrival time of 10 for the load assignment for the global Y direction shaking.

The arrival time can be zero or any positive or negative time. The time history analysis for a given time history case always starts at time zero. Thus if you specify a negative arrival time for a load assignment, any portion of its associated input function that occurs before time zero is ignored. For example suppose a particular load assignment has an arrival time of -5 seconds. Then the first five seconds of the input function associated with that load assignment is ignored by the program.

Angle: The local 1 and 2 axes of the time history case coordinate system lie in the global XY plane. By default the local 1-axis is in the same direction as the positive global X-axis, the local 2-axis is in the same direction as the positive global Y-axis and the local 3-axis is in the same direction as the positive global Z-axis. You can rotate the local 1 and 2 axes of the time history coordinate system about the local 3 (global Z) axis. The Angle item specifies the angle in degrees measured from the positive global X-axis to the positive local 1-axis of the time history case coordinate system. Positive angles appear counterclockwise as you look down on the model.

5.5 Time History Analysis and Results of Building without Infill Wall

Table 5.1: Displacement in X-direction for Bare Frame

SR.No.	PGA (g)	Displacement (m) in X-direction				
		Storey-5	Storey-4	Storey-3	Storey-2	Storey-1
1	0.004	0.00096	0.00085	0.00065	0.00039	0.00016
2	0.041	0.0075	0.0064	0.0048	0.0028	0.0011
3	0.074	0.0070	0.0059	0.0045	0.0027	0.0011
4	0.095	0.010	0.0084	0.0062	0.0035	0.0014
5	0.163	0.057	0.049	0.037	0.021	0.0089
6	0.202	0.048	0.040	0.031	0.018	0.0075
7	0.266	0.057	0.050	0.042	0.023	0.010
8	0.315	0.091	0.076	0.056	0.032	0.013
9	0.379	0.080	0.071	0.055	0.034	0.014
10	0.463	0.15	0.13	0.10	0.060	0.024
11	0.519	0.067	0.058	0.045	0.027	0.011
12	0.544	0.036	0.031	0.024	0.014	0.006
13	0.602	0.099	0.087	0.067	0.041	0.016
14	0.724	0.13	0.11	0.081	0.042	0.011
15	0.902	0.23	0.19	0.15	0.089	0.036
16	1.16	0.17	0.14	0.10	0.056	0.022
17	1.298	0.23	0.19	0.14	0.090	0.036
18	1.497	0.18	0.14	0.096	0.052	0.032
19	1.655	0.076	0.053	0.042	0.032	0.015
20	1.775	0.28	0.24	0.18	0.10	0.042

Time History trace results of G+4 storey R.C.C. building for bare frame, includes maximum displacement, maximum storey drift and maximum acceleration in two horizontal X and Y direction respectively.

Table 5.1 shows maximum displacement of each storey in X-direction for bare frame. The maximum displacement obtained was 0.28 m at storey-5 for PGA 1.775g.

Table 5.2: Displacement in Y-direction for Bare Frame

SR.No.	**PGA (g)**	**Displacement (m) in Y-direction**				
		Storey-5	**Storey-4**	**Storey-3**	**Storey-2**	**Storey-1**
1	0.004	0.0036	0.0033	0.0026	0.0017	0.00084
2	0.041	0.012	0.011	0.0093	0.0065	0.0032
3	0.074	0.012	0.010	0.0082	0.0055	0.0027
4	0.095	0.019	0.017	0.013	0.0089	0.0046
5	0.163	0.11	0.096	0.079	0.054	0.026
6	0.202	0.086	0.077	0.062	0.040	0.019
7	0.266	0.11	0.096	0.074	0.050	0.025
8	0.315	0.12	0.11	0.087	0.059	0.029
9	0.379	0.23	0.21	0.16	0.11	0.053
10	0.463	0.24	0.21	0.16	0.10	0.047
11	0.519	0.14	0.12	0.10	0.076	0.039
12	0.544	0.11	0.10	0.080	0.052	0.025
13	0.602	0.12	0.11	0.097	0.063	0.034
14	0.724	0.13	0.12	0.10	0.07	0.034
15	0.902	0.55	0.50	0.39	0.25	0.11
16	1.16	0.28	0.24	0.19	0.13	0.063
17	1.298	0.33	0.29	0.23	0.15	0.070
18	1.497	0.24	0.22	0.19	0.12	0.064
19	1.655	0.15	0.13	0.099	0.068	0.0036
20	1.775	0.33	0.27	0.19	0.13	0.069

Table 5.2 shows maximum displacement of each storey in Y-direction for bare frame. The maximum displacement obtained was 0.33 m at storey-5 for PGA 1.775g.

Table 5.3 shows maximum storey drift of each storey in X-direction for bare frame. The maximum storey drift obtained was 0.077 m at storey-3 for PGA 1.775g.

Table 5.3: Storey Drift in X-direction for Bare Frame

SR.No.	**PGA (g)**	**Storey Drift (m) in X-direction**				
		Storey-5	**Storey-4**	**Storey-3**	**Storey-2**	**Storey-1**
1	0.004	0.00013	0.00020	0.00026	0.00055	0.00016
2	0.041	0.0011	0.0016	0.0019	0.0017	0.0012
3	0.074	0.0014	0.0017	0.0019	0.0016	0.0011
4	0.095	0.0018	0.0023	0.0026	0.0022	0.0014
5	0.163	0.0081	0.012	0.015	0.013	0.0089
6	0.202	0.0077	0.011	0.012	0.011	0.0075
7	0.266	0.011	0.015	0.018	0.015	0.010
8	0.315	0.016	0.021	0.024	0.019	0.014
9	0.379	0.010	0.016	0.021	0.019	0.0097
10	0.463	0.019	0.031	0.040	0.036	0.019
11	0.519	0.0099	0.015	0.018	0.016	0.0083
12	0.544	0.0058	0.0075	0.0096	0.0085	0.0050
13	0.602	0.013	0.020	0.027	0.024	0.016
14	0.724	0.024	0.033	0.037	0.028	0.019
15	0.902	0.031	0.048	0.061	0.053	0.036
16	1.16	0.029	0.040	0.046	0.035	0.022
17	1.298	0.037	0.053	0.062	0.053	0.036
18	1.497	0.042	0.050	0.046	0.032	0.022
19	1.655	0.026	0.017	0.023	0.018	0.015
20	1.775	0.043	0.064	0.077	0.066	0.042

Table 5.4 shows maximum storey drift of each storey in Y-direction for bare frame. The maximum storey drift obtained was 0.14 m at storey-3 for PGA 0.902g.

Table 5.4: Storey Drift in Y-direction for Bare Frame

SR.No.	**PGA (g)**	**Storey Drift (m) in Y-direction**				
		Storey-5	**Storey-4**	**Storey-3**	**Storey-2**	**Storey-1**
1	0.004	0.00038	0.00066	0.00090	0.00091	0.00084
2	0.041	0.0018	0.0021	0.0028	0.0033	0.0031
3	0.074	0.0024	0.0028	0.0031	0.0028	0.0027
4	0.095	0.0029	0.0040	0.0048	0.0044	0.0045
5	0.163	0.017	0.018	0.025	0.027	0.026
6	0.202	0.010	0.016	0.021	0.021	0.019
7	0.266	0.015	0.023	0.027	0.025	0.024
8	0.315	0.06	0.024	0.028	0.030	0.029
9	0.379	0.024	0.041	0.055	0.057	0.053
10	0.463	0.029	0.049	0.060	0.055	0.047
11	0.519	0.020	0.027	0.033	0.037	0.039
12	0.544	0.013	0.022	0.028	0.027	0.025
13	0.602	0.018	0.026	0.032	0.034	0.033
14	0.724	0.029	0.038	0.033	0.036	0.033
15	0.902	0.068	0.11	0.14	0.13	0.11
16	1.16	0.038	0.056	0.069	0.067	0.063
17	1.298	0.051	0.075	0.084	0.081	0.070
18	1.497	0.055	0.054	0.068	0.066	0.064
19	1.655	0.024	0.035	0.038	0.035	0.036
20	1.775	0.061	0.097	0.10	0.072	0.069

Table 5.5 shows maximum acceleration of each storey in X-direction for bare frame. The maximum acceleration obtained was 39.19 m/s^2 at storey-5 for PGA 1.655g.

Table 5.5: Acceleration in X-direction for Bare Frame

SR.No.	**PGA (g)**	**Acceleration (m/s^2) in X-direction**				
		Storey-5	**Storey-4**	**Storey-3**	**Storey-2**	**Storey-1**
1	0.004	0.091	0.081	0.085	0.063	0.027
2	0.041	0.948	0.772	0.654	0.511	0.236
3	0.074	1.234	1.064	0.8631	1.037	0.752
4	0.095	2.073	1.577	1.104	1.203	0.554
5	0.163	6.230	6.225	5.379	3.326	1.173
6	0.202	6.061	5.087	3.867	3.361	1.771
7	0.266	8.955	7.879	6.744	4.656	2.501
8	0.315	11.63	10.62	9.707	6.625	3.438
9	0.379	9.839	7.412	5.923	3.787	2.605
10	0.463	11.26	9.864	7.706	4.659	2.032
11	0.519	8.893	7.837	7.572	7.155	4.155
12	0.544	6.523	7.571	5.239	6.848	7.415
13	0.602	10.59	9.290	8.516	8.157	3.956
14	0.724	21.92	15.88	11.23	7.356	3.644
15	0.902	19.02	16.56	12.34	7.503	2.929
16	1.16	26.96	21.30	15.67	14.22	8.401
17	1.298	27.01	22.90	14.61	11.48	6.895
18	1.497	35.48	20.64	19.05	17.56	11.57
19	1.655	39.19	22.52	24.29	35.74	25.25
20	1.775	35.47	32.84	26.83	21.85	12.70

Table 5.6 shows maximum acceleration of each storey in Y-direction for bare frame. The maximum acceleration obtained was 31.18 m/s^2 at storey-3 for PGA 1.775g.

Table 5.6: Acceleration in Y-direction for Bare Frame

SR.No.	**PGA (g)**	**Acceleration (m/s^2) in Y-direction**				
		Storey-5	**Storey-4**	**Storey-3**	**Storey-2**	**Storey-1**
1	0.004	0.13	0.12	0.10	0.072	0.035
2	0.041	0.75	0.65	0.64	0.70	0.45
3	0.074	0.97	0.87	1.09	1.10	0.73
4	0.095	1.05	1.43	1.82	1.31	0.85
5	0.163	4.03	3.24	3.38	2.98	1.77
6	0.202	4.42	3.68	3.12	2.79	2.92
7	0.266	6.74	5.08	4.94	4.40	3.34
8	0.315	6.98	5.78	5.18	5.03	4.61
9	0.379	8.36	6.93	6.37	5.70	4.67
10	0.463	9.78	8.24	5.45	4.15	2.57
11	0.519	7.24	6.35	6.03	7.42	6.44
12	0.544	6.43	6.38	6.67	6.58	5.56
13	0.602	7.66	7.71	7.78	7.58	5.36
14	0.724	11.48	7.15	7.05	7.04	5.22
15	0.902	26.09	23.17	19.43	14.65	9.71
16	1.16	22.39	16.50	12.24	12.60	9.27
17	1.298	20.27	20.30	18.68	14.39	8.41
18	1.497	20.23	21.95	22.71	20.20	17.43
19	1.655	18.17	17.65	22.66	16.45	27.32
20	1.775	25.95	24.04	31.18	25.82	19.92

5.6 Time History Analysis and Results of Building with Infill Wall

Time History trace results of G+4 storey R.C.C. building for infill wall as membrane element, includes maximum displacement, maximum storey drift and maximum acceleration in two horizontal X and Y direction respectively.

Table 5.7: Displacement in X-direction for Membrane Wall

SR.No.	PGA (g)	Displacement (m) in X-direction				
		Storey-5	Storey-4	Storey-3	Storey-2	Storey-1
1	0.004	0.0015	0.0014	0.0010	0.00063	0.00025
2	0.041	0.010	0.0087	0.0064	0.0036	0.0014
3	0.074	0.010	0.0086	0.0065	0.0038	0.0015
4	0.095	0.012	0.011	0.0080	0.0047	0.0019
5	0.163	0.045	0.036	0.027	0.016	0.034
6	0.202	0.067	0.059	0.045	0.027	0.011
7	0.266	0.091	0.077	0.059	0.036	0.015
8	0.315	0.081	0.071	0.054	0.033	0.013
9	0.379	0.098	0.087	0.066	0.039	0.016
10	0.463	0.26	0.22	0.17	0.10	0.041
11	0.519	0.099	0.085	0.063	0.037	0.015
12	0.544	0.036	0.031	0.024	0.016	0.0067
13	0.602	0.095	0.084	0.064	0.039	0.016
14	0.724	0.16	0.13	0.10	0.058	0.023
15	0.902	0.30	0.26	0.20	0.12	0.048
16	1.16	0.12	0.11	0.079	0.048	0.056
17	1.298	0.31	0.28	0.22	0.14	0.056
18	1.497	0.21	0.17	0.12	0.079	0.034
19	1.655	0.090	0.068	0.051	0.034	0.015
20	1.775	0.35	0.31	0.24	0.14	0.058

Table 5.7 shows maximum displacement of each storey in X-direction for membrane wall. The maximum displacement obtained was 0.35 m at storey-5 for PGA 1.775g.

Table 5.8 shows maximum displacement of each storey in Y-direction for membrane wall. The maximum displacement obtained was 0.32 m at storey-5 for PGA 1.775g.

Table 5.8: Displacement in Y-direction for Membrane Wall

SR.No.	**PGA (g)**	**Displacement (m) in Y-direction**				
		Storey-5	**Storey-4**	**Storey-3**	**Storey-2**	**Storey-1**
1	0.004	0.0050	0.0045	0.0035	0.0023	0.0011
2	0.041	0.019	0.017	0.014	0.0094	0.0046
3	0.074	0.017	0.016	0.014	0.010	0.0055
4	0.095	0.037	0.034	0.028	0.019	0.0097
5	0.163	0.13	0.12	0.097	0.068	0.033
6	0.202	0.13	0.12	0.094	0.062	0.030
7	0.266	0.15	0.14	0.11	0.071	0.034
8	0.315	0.11	0.099	0.076	0.052	0.027
9	0.379	0.18	0.17	0.14	0.099	0.052
10	0.463	0.27	0.24	0.18	0.12	0.054
11	0.519	0.18	0.16	0.13	0.091	0.043
12	0.544	0.13	0.12	0.097	0.065	0.033
13	0.602	0.29	0.26	0.21	0.14	0.070
14	0.724	0.24	0.24	0.19	0.13	0.064
15	0.902	0.64	0.57	0.44	0.28	0.13
16	1.16	0.28	0.25	0.21	0.14	0.073
17	1.298	0.29	0.27	0.23	0.15	0.072
18	1.497	0.27	0.25	0.19	0.14	0.073
19	1.655	0.20	0.17	0.14	0.094	0.044
20	1.775	0.32	0.28	0.23	0.15	0.077

Table 5.9 shows maximum storey drift of each storey in X-direction for membrane wall. The maximum storey drift obtained was 0.097 m at storey-3 for PGA 1.775g.

Table 5.9: Storey Drift in X-direction for Membrane Wall

SR.No.	**PGA (g)**	**Storey Drift (m) in X-direction**				
		Storey-5	**Storey-4**	**Storey-3**	**Storey-2**	**Storey-1**
1	0.004	0.00021	0.00034	0.00043	0.00088	0.00025
2	0.041	0.0015	0.0024	0.0028	0.0022	0.0014
3	0.074	0.0018	0.0021	0.0026	0.0023	0.0015
4	0.095	0.0026	0.0028	0.0032	0.0028	0.0019
5	0.163	0.0084	0.011	0.012	0.041	0.034
6	0.202	0.0097	0.014	0.018	0.016	0.011
7	0.266	0.013	0.021	0.024	0.021	0.015
8	0.315	0.011	0.018	0.021	0.019	0.013
9	0.379	0.012	0.020	0.026	0.023	0.016
10	0.463	0.032	0.053	0.068	0.060	0.041
11	0.519	0.014	0.023	0.027	0.022	0.015
12	0.544	0.0053	0.0084	0.010	0.0092	0.0067
13	0.602	0.012	0.019	0.025	0.023	0.016
14	0.724	0.022	0.035	0.044	0.035	0.023
15	0.902	0.041	0.065	0.081	0.071	0.048
16	1.16	0.022	0.027	0.033	0.028	0.016
17	1.298	0.045	0.068	0.086	0.082	0.056
18	1.497	0.051	0.054	0.059	0.045	0.034
19	1.655	0.020	0.023	0.025	0.022	0.015
20	1.775	0.049	0.073	0.097	0.089	0.058

Table 5.10 shows maximum storey drift of each storey in Y-direction for membrane wall. The maximum storey drift obtained was 0.16 m at storey-3 for PGA 0.902g.

Table 5.10: Storey Drift in Y-direction for Membrane Wall

SR.No.	**PGA (g)**	**Storey Drift (m) in Y-direction**				
		Storey-5	**Storey-4**	**Storey-3**	**Storey-2**	**Storey-1**
1	0.004	0.00052	0.00097	0.0012	0.0013	0.0011
2	0.041	0.0024	0.0036	0.0047	0.0048	0.0046
3	0.074	0.0031	0.0038	0.0043	0.0055	0.0053
4	0.095	0.0037	0.0064	0.0091	0.010	0.0097
5	0.163	0.013	0.024	0.031	0.034	0.033
6	0.202	0.012	0.023	0.031	0.032	0.030
7	0.266	0.022	0.034	0.038	0.037	0.034
8	0.315	0.022	0.033	0.034	0.028	0.027
9	0.379	0.019	0.035	0.045	0.049	0.052
10	0.463	0.033	0.057	0.068	0.061	0.054
11	0.519	0.020	0.036	0.046	0.047	0.043
12	0.544	0.015	0.025	0.032	0.033	0.033
13	0.602	0.029	0.052	0.071	0.074	0.070
14	0.724	0.037	0.054	0.066	0.069	0.064
15	0.902	0.073	0.13	0.16	0.15	0.13
16	1.16	0.048	0.076	0.071	0.074	0.073
17	1.298	0.043	0.058	0.081	0.079	0.072
18	1.497	0.050	0.050	0.074	0.073	0.072
19	1.655	0.023	0.041	0.050	0.051	0.044
20	1.775	0.054	0.091	0.086	0.083	0.077

Table 5.11 shows maximum acceleration of each storey in X-direction for membrane wall. The maximum acceleration obtained was 40.03 m/s^2 at storey-5 for PGA 1.655g.

Table 5.11: Acceleration in X-direction for Membrane Wall

SR.No.	**PGA (g)**	**Acceleration (m/s^2) in X-direction**				
		Storey-5	**Storey-4**	**Storey-3**	**Storey-2**	**Storey-1**
1	0.004	0.102	0.088	0.066	0.047	0.022
2	0.041	1.071	0.81	0.67	0.43	0.20
3	0.074	1.37	1.2	0.83	0.97	0.74
4	0.095	2.27	1.42	1.38	1.36	0.79
5	0.163	6.29	4.45	3.19	2.39	1.25
6	0.202	5.88	5.53	4.79	4.15	2.20
7	0.266	8.81	6.86	6.64	5.26	2.79
8	0.315	8.67	8.06	7.81	6.72	3.81
9	0.379	8.49	7.74	4.97	3.58	3.25
10	0.463	17.30	14.19	10.59	6.34	2.67
11	0.519	9.96	8.47	7.44	6.87	4.42
12	0.544	7.53	7.11	5.55	6.86	7.44
13	0.602	8.86	9.56	8.02	5.22	3.54
14	0.724	17.99	16.93	11.31	8.15	4.60
15	0.902	20.63	15.48	13.49	9.13	3.97
16	1.16	20.09	15.94	13.60	17.92	11.20
17	1.298	26.75	23.15	21.61	18.71	7.80
18	1.497	36.46	19.62	19.74	20.83	13.86
19	1.655	29.06	21.92	26.06	27.94	23.09
20	1.775	33.94	35.91	40.03	28.59	11.07

Table 5.12 shows maximum acceleration of each storey in Y-direction for membrane wall. The maximum acceleration obtained was 26.05 m/s^2 at storey-5 for PGA 1.775g.

Table 5.12: Acceleration in Y-direction for Membrane Wall

SR.No.	**PGA (g)**	**Acceleration (m/s^2) in Y-direction**				
		Storey-5	**Storey-4**	**Storey-3**	**Storey-2**	**Storey-1**
1	0.004	0.15	0.13	0.099	0.081	0.044
2	0.041	0.67	0.52	0.60	0.68	0.42
3	0.074	0.88	0.76	0.97	1.01	0.83
4	0.095	1.02	1.09	1.61	1.32	1.09
5	0.163	3.95	3.35	2.94	2.45	1.26
6	0.202	3.87	3.65	3.08	2.83	2.51
7	0.266	6.27	5.41	5.13	4.24	3.06
8	0.315	7.81	5.32	4.39	5.07	4.28
9	0.379	7.34	5.28	6.17	5.97	4.62
10	0.463	9.55	7.28	5.37	4.42	2.88
11	0.519	7.33	5.73	5.68	7.29	6.64
12	0.544	5.48	6.42	6.81	5.75	5.35
13	0.602	9.13	7.74	7.20	7.26	5.56
14	0.724	11.40	9.43	11.54	11.43	7.31
15	0.902	25.09	20.72	18.76	15.59	9.68
16	1.16	21.53	13.81	14.42	13.93	12.15
17	1.298	19.61	20.11	17.48	13.18	9.67
18	1.497	22.51	20.54	20.60	18.84	16.21
19	1.655	16.98	17.10	19.59	17.52	26.05
20	1.775	22.45	23.80	25.51	25.96	21.68

Similarly, Time History trace results of G+4 storey R.C.C. building for infill wall as equivalent strut, includes maximum displacement, maximum storey drift and maximum acceleration in two horizontal X and Y direction respectively.

Table 5.13: Displacement in X-direction for Equivalent Strut

SR.No.	**PGA (g)**	**Displacement (m) in X-direction**				
		Storey-5	**Storey-4**	**Storey-3**	**Storey-2**	**Storey-1**
1	0.004	0.0014	0.0012	0.00094	0.00055	0.00022
2	0.041	0.0086	0.0074	0.0054	0.0031	0.0012
3	0.074	0.0081	0.0070	0.0053	0.0031	0.0012
4	0.095	0.012	0.010	0.0079	0.0047	0.0019
5	0.163	0.050	0.044	0.033	0.021	0.0083
6	0.202	0.072	0.062	0.047	0.029	0.011
7	0.266	0.098	0.083	0.061	0.034	0.013
8	0.315	0.090	0.075	0.053	0.029	0.012
9	0.379	0.093	0.082	0.063	0.038	0.015
10	0.463	0.23	0.20	0.15	0.091	0.036
11	0.519	0.093	0.080	0.060	0.035	0.014
12	0.544	0.035	0.031	0.023	0.014	0.0056
13	0.602	0.10	0.091	0.070	0.042	0.017
14	0.724	0.13	0.11	0.082	0.047	0.019
15	0.902	0.26	0.22	0.17	0.097	0.039
16	1.16	0.12	0.10	0.074	0.045	0.018
17	1.298	0.30	0.26	0.20	0.12	0.050
18	1.497	0.034	0.027	0.021	0.014	0.0062
19	1.655	0.080	0.066	0.047	0.031	0.013
20	1.775	0.31	0.27	0.21	0.13	0.054

Table 5.13 shows maximum displacement of each storey in X-direction for equivalent strut. The maximum displacement obtained was 0.31 m at storey-5 for PGA 1.775g.

Table 5.14 shows maximum displacement of each storey in Y-direction for equivalent strut. The maximum displacement obtained was 0.61 m at storey-5 for PGA 0.902g.

Table 5.14: Displacement in Y-direction for Equivalent Strut

SR.No.	**PGA (g)**	**Displacement (m) in Y-direction**				
		Storey-5	**Storey-4**	**Storey-3**	**Storey-2**	**Storey-1**
1	0.004	0.0051	0.0046	0.0036	0.0023	0.0011
2	0.041	0.015	0.014	0.012	0.0079	0.0028
3	0.074	0.013	0.012	0.011	0.0085	0.0044
4	0.095	0.031	0.028	0.023	0.016	0.0078
5	0.163	0.14	0.13	0.11	0.071	0.035
6	0.202	0.12	0.11	0.088	0.058	0.028
7	0.266	0.14	0.12	0.097	0.064	0.031
8	0.315	0.13	0.11	0.082	0.056	0.028
9	0.379	0.15	0.18	0.15	0.098	0.048
10	0.463	0.26	0.23	0.17	0.11	0.051
11	0.519	0.17	0.15	0.13	0.089	0.045
12	0.544	0.13	0.11	0.092	0.058	0.030
13	0.602	0.24	0.23	0.18	0.12	0.059
14	0.724	0.23	0.21	0.17	0.12	0.055
15	0.902	0.61	0.53	0.41	0.25	0.12
16	1.16	0.28	0.24	0.20	0.14	0.066
17	1.298	0.31	0.28	0.23	0.15	0.070
18	1.497	0.054	0.051	0.044	0.030	0.015
19	1.655	0.18	0.16	0.13	0.088	0.041
20	1.775	0.31	0.27	0.23	0.16	0.081

Table 5.15 shows maximum storey drift of each storey in X-direction for equivalent strut. The maximum storey drift obtained was 0.085 m at storey-3 for PGA 1.775g.

Table 5.15: Storey Drift in X-direction for Equivalent Strut

SR.No.	**PGA (g)**	**Storey Drift (m) in X-direction**				
		Storey-5	**Storey-4**	**Storey-3**	**Storey-2**	**Storey-1**
1	0.004	0.00018	0.00029	0.00037	0.00075	0.00022
2	0.041	0.0012	0.0019	0.0023	0.0019	0.0012
3	0.074	0.0016	0.0021	0.0022	0.0018	0.0012
4	0.095	0.0024	0.0027	0.0031	0.0028	0.0019
5	0.163	0.0085	0.012	0.013	0.012	0.0083
6	0.202	0.010	0.015	0.015	0.017	0.011
7	0.266	0.015	0.022	0.026	0.021	0.013
8	0.315	0.015	0.022	0.024	0.018	0.012
9	0.379	0.011	0.018	0.025	0.022	0.015
10	0.463	0.029	0.048	0.062	0.054	0.036
11	0.519	0.013	0.020	0.025	0.021	0.014
12	0.544	0.0052	0.0075	0.0096	0.0084	0.0056
13	0.602	0.013	0.021	0.027	0.025	0.017
14	0.724	0.022	0.031	0.034	0.028	0.019
15	0.902	0.036	0.057	0.070	0.058	0.039
16	1.16	0.022	0.029	0.032	0.026	0.018
17	1.298	0.044	0.066	0.082	0.072	0.050
18	1.497	0.0073	0.0092	0.0095	0.0085	0.0062
19	1.655	0.015	0.020	0.021	0.017	0.013
20	1.775	0.048	0.070	0.085	0.079	0.054

Table 5.16 shows maximum storey drift of each storey in Y-direction for equivalent strut. The maximum storey drift obtained was 0.16 m at storey-3 for PGA 0.902g.

Table 5.16: Storey Drift in Y-direction for Equivalent Strut

SR.No.	**PGA (g)**	**Storey Drift (m) in Y-direction**				
		Storey-5	**Storey-4**	**Storey-3**	**Storey-2**	**Storey-1**
1	0.004	0.00052	0.00097	0.0013	0.0012	0.0011
2	0.041	0.0019	0.003	0.004	0.0041	0.0038
3	0.074	0.0027	0.0032	0.0035	0.0041	0.0044
4	0.095	0.0035	0.0054	0.0073	0.0082	0.0078
5	0.163	0.015	0.026	0.033	0.036	0.035
6	0.202	0.012	0.022	0.030	0.031	0.028
7	0.266	0.020	0.032	0.037	0.033	0.031
8	0.315	0.022	0.034	0.035	0.028	0.027
9	0.379	0.020	0.037	0.050	0.051	0.048
10	0.463	0.033	0.056	0.067	0.060	0.051
11	0.519	0.019	0.034	0.043	0.045	0.045
12	0.544	0.014	0.024	0.031	0.032	0.030
13	0.602	0.026	0.046	0.061	0.063	0.053
14	0.724	0.036	0.052	0.057	0.061	0.055
15	0.902	0.078	0.12	0.16	0.14	0.12
16	1.16	0.047	0.071	0.072	0.073	0.066
17	1.298	0.046	0.064	0.084	0.081	0.070
18	1.497	0.010	0.011	0.016	0.015	0.014
19	1.655	0.024	0.040	0.046	0.047	0.041
20	1.775	0.06	0.099	0.095	0.082	0.081

Table 5.17 shows maximum acceleration of each storey in X-direction for equivalent strut. The maximum acceleration obtained was 37.90 m/s^2 at storey-3 for PGA 1.775g.

Table 5.17: Acceleration in X-direction for Equivalent Strut

SR.No.	PGA (g)	Acceleration (m/s^2) in X-direction				
		Storey-5	**Storey-4**	**Storey-3**	**Storey-2**	**Storey-1**
1	0.004	0.099	0.085	0.063	0.049	0.022
2	0.041	1.029	0.77	0.54	0.37	0.19
3	0.074	1.15	0.99	0.94	0.83	0.39
4	0.095	2.37	1.49	1.09	1.13	0.57
5	0.163	6.59	4.67	3.66	2.75	1.23
6	0.202	7.19	6.47	5.73	4.34	1.95
7	0.266	10.09	7.33	5.76	4.62	2.32
8	0.315	11.20	8.79	8.32	6.74	3.10
9	0.379	8.50	6.55	4.21	2.57	1.11
10	0.463	16.37	13.84	10.04	5.79	2.29
11	0.519	9.21	8.13	7.34	6.20	2.91
12	0.544	6.45	6.48	6.36	5.08	2.31
13	0.602	9.67	9.14	7.89	5.69	2.65
14	0.724	17.51	14.02	11.22	6.99	2.87
15	0.902	20.77	15.08	11.60	8.43	3.75
16	1.16	20.38	18.57	16.65	12.98	5.88
17	1.298	27.53	22.18	21.05	17.50	8.14
18	1.497	10.76	16.90	20.78	17.12	7.89
19	1.655	20.57	21.99	28.05	24.22	11.32
20	1.775	35.68	35.93	37.90	28.80	12.91

Table 5.18 shows maximum acceleration of each storey in Y-direction for membrane wall. The maximum acceleration obtained was 26.95 m/s^2 at storey-3 for PGA 1.775g.

Table 5.18: Acceleration in Y-direction for Equivalent Strut

SR.No.	**PGA (g)**	**Acceleration (m/s^2) in Y-direction**				
		Storey-5	**Storey-4**	**Storey-3**	**Storey-2**	**Storey-1**
1	0.004	0.15	0.14	0.10	0.072	0.041
2	0.041	0.66	0.64	0.64	0.70	0.43
3	0.074	0.91	0.78	1.03	1.04	0.86
4	0.095	0.93	1.27	1.68	1.22	1.24
5	0.163	4.53	3.69	3.26	2.49	1.36
6	0.202	3.93	3.57	3.07	2.95	2.58
7	0.266	6.93	5.44	4.41	4.61	3.56
8	0.315	6.17	5.53	4.55	4.76	4.42
9	0.379	7.46	5.82	6.10	6.04	4.64
10	0.463	9.75	7.70	5.34	4.33	2.81
11	0.519	6.74	5.95	6.52	7.41	6.67
12	0.544	5.66	6.34	6.93	5.98	5.46
13	0.602	8.30	7.43	7.26	7.43	5.25
14	0.724	12.94	8.13	10.01	10.49	6.89
15	0.902	26.63	21.17	17.61	14.85	9.62
16	1.16	22.31	15.18	14.60	16.60	12.34
17	1.298	20.44	20.08	17.74	13.01	9.59
18	1.497	14.43	14.21	14.28	16.14	17.50
19	1.655	17.44	17.24	20.28	17.02	26.39
20	1.775	21.66	25.23	26.95	25.99	21.10

5.7 Summary

This chapter covers Time History analysis of G+4 storey RCC building for twenty nos. of earthquake ground motions records are considered. Response of building under these earthquake ground motion in terms of peak storey drift and peak displacement are obtained.

The results of Time History analysis of three models of building, namely, building model without infill i.e, bare frame, building model with infill as membrane wall and building model with infill as equivalent strut shows that peak storey drift and peak displacement is less in bare frame as compared to membrane wall / equivalent strut.

Chapter 6

Fragility Curve For G+4 Storey R.C.C. Building

6.1 Introduction

Seismic risk assessments are an effective way to assess the vulnerability of structure to mitigate future losses. Fragility assessments play an important role in a seismic risk assessment by analyzing the response and probable damage of structures to provide loss estimation and aid in decision making. A fragility analysis is less complex, less costly, and more easily understood by decision makers than a complete risk assessment. Seismic fragilities can be broadly defined or redefined as needed to assess consequences by accounting for various structural characteristics and on the extent of rehabilitation. For a full seismic risk analysis, analysis of both the occurrence of the ground motion intensity level and the fragility of the system are necessary. The results of a fragility assessment are particularly helpful for decision-making. Fragility is defined as the conditional probability of a system or component meeting or exceeding a prescribed performance limit state given the occurrence of a particular demand or hazard. Advantages of a fragility analysis over a fully risk analysis, avoiding interpretation of small limit states, being less complex and costly, and involving fewer disciplines than a fully risk analysis.

6.2 Methods for Fragility Curve

Fragility curve generation is basically statistical analysis of the results obtained from the structural response assessment that is, of the variation of capacity of building under various ground motions using the methodology for structural response assessment. According to Bora **Gencturk, Amr S. Elnashai, and Junho** [**10**] Song There are two methods for fragility curve generation, namely (i) Conventional Fragility method, and (ii) HAZUS Fragility relationship method.

6.2.1 Conventional Fragility Method

In the field of earthquake engineering the most commonly accepted convention for the fragility relationships is to express the exceedance probabilities as a function of the hazard parameters, e.g. peak ground acceleration (PGA), peak ground velocity (PGV), spectral displacement (Sd), spectral acceleration (Sa) at certain period. This format is referred to as "conventional fragility relationship" and the methodology used for this purpose is described in section 6.3.

6.2.2 HAZUS Fragility Relationship Method

The other, less established format considered is from HAZUS (National Institute of Building Sciences, 2003), where exceedance probabilities are function of structural response. This is called "HAZUS compatible fragility relationships". HAZUS is the most widely used loss assessment software in USA. As opposed to conventional fragility relationships where the horizontal axis is the ground motion intensity (GMI), HAZUS fragility relationships associate structural response with the exceedance probabilities.

6.3 Conventional Fragility Curve Method

As mentioned above out of two methods, here the fragility curve is derived by conventional fragility method. Conventional fragility relationships relate the ground motion parameters to the exceedance probabilities. In this study, the ground motion records are scaled based on peak ground acceleration (PGA), and are therefore chosen as the representative parameter of the hazard.

6.3.1 Limit State Definition

A limit state is a criterion defined as the structural demand value where a system is unable to perform at a specified level. Both qualitative and quantitative approaches can be used to classify performance levels. **FEMA 356** [14] presents three main structural performance levels to approximate limiting levels of structural damage: immediate occupancy (IO), life safety (LS), and collapse prevention (CP). The post-earthquake damage state of a structure should remain safe to occupy and essentially retain the pre-earthquake design strength to be compliant with the acceptance criteria for the IO structural level. For LS performance level, damage to the structure could occur as long as the structure retains a margin against onset of partial or total collapse. The CP performance level indicates a structure could be on the verge of partial or total collapse, but the structure is still able to support gravity loads. FEMA 356 states a maximum interstorey drift limits were used to describe the IO, LS and CP performance levels; which are 1%, 2% and 4%, respectively, for a RC frame structure.

6.3.2 Probability Equation

The methodology by **Wen et al. (2004) [15]** is adopted for deriving fragility relationships in conventional format. Wen et al. (2004) provided the equation used to develop the fragility relationship as per Equation 6.1

$$P(LS_i/GMI) = 1 - \Phi\left(\frac{\lambda_{CL}^{i} - \lambda_{D/GMI}}{\sqrt{\beta_{D/GMI}^2 + \beta_{CL}^2 + \beta_M^2}}\right) \tag{6.1}$$

where:

$P(LS_i/GMI)$ = Probability of exceeding a particular limit state given the ground motion intensity (GMI)

Φ = Standard normal distribution function

λ^i_{CL} = ln(median drift capacity for a particular limit state), where drift capacity is expressed as a percentage of the storey height

β_{CL} = Uncertainty associated with the drift capacity criteria, taken as 0.3 in this study

β_M = Uncertainty associated with analytical modeling of the structure, taken as 0.3 in this study

Moderate to severe earthquakes often cause structures to behave nonlinearly. For a realistic model of a system, the nonlinear behavior must be included in a fragility assessment. Dynamic time history analysis using representative ground motions are analyzed to determine a relationship between structural response demand (D) and earthquake intensity (S). A nonlinear regression analysis is performed assuming a power-law form between the seismic intensity measure and the structural response demand

$$D = aS^b \tag{6.2}$$

where a and b are the unknown constant determined by a logarithmic transformation of Equation 6.2 to a linear form

$$ln(D) = ln(a) + bln(S) \tag{6.3}$$

Now the constant a and b can be found using a simple linear regression analysis to find the relationship between the structural response demand and the earthquake intensity. The probabilistic form of Equation 6.3 is as below.

$$\lambda_{D/GMI} = lna_1 + a_2 ln(GMI) \tag{6.4}$$

$$\beta_{D/GMI} = \sqrt{\frac{\sum_{k=1}^{n}[ln(GMI_k) - \lambda_{D/GMI}(GMI_k)]^2}{n-2}} \tag{6.5}$$

$$\Phi = \frac{1}{\sqrt{2\pi}} \times e^{-\frac{1}{2}(x^2)} \tag{6.6}$$

Finally $\lambda_{D/GMI}$ and $\beta_{D/GMI}$ are given by Equation 6.4 and Equation 6.5 respectively.

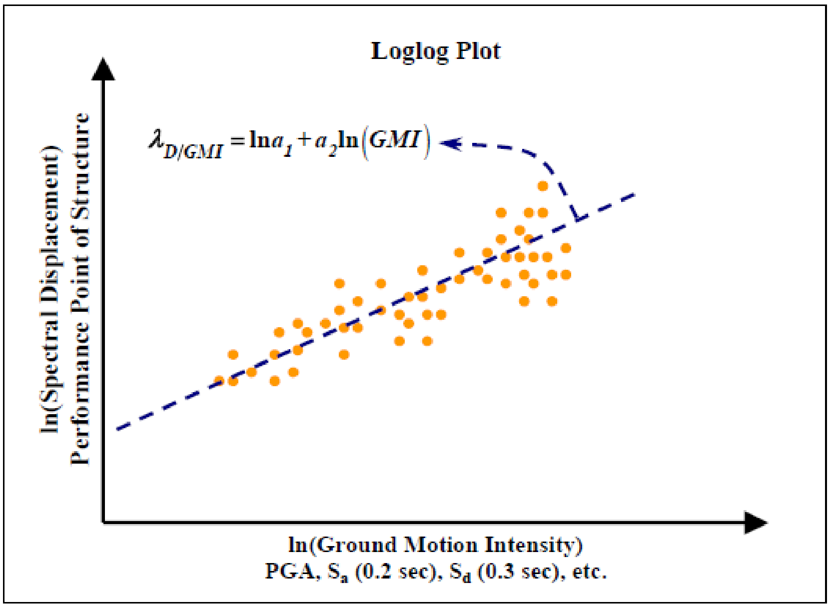

Figure 6.1: Linear regression analysis of structural response data

The constants a_1 and a_2 are calculated through a linear regression analysis, as shown in Figure (6.1). $\beta_{D/GMI}$ is called as the square root of the standard error and n in the given expression is the number of data points.

6.4 Fragility Analysis and Results of building without Infill Wall

Fragility curve obtained for G+4 storey building without infills i.e. bare frame is as below.

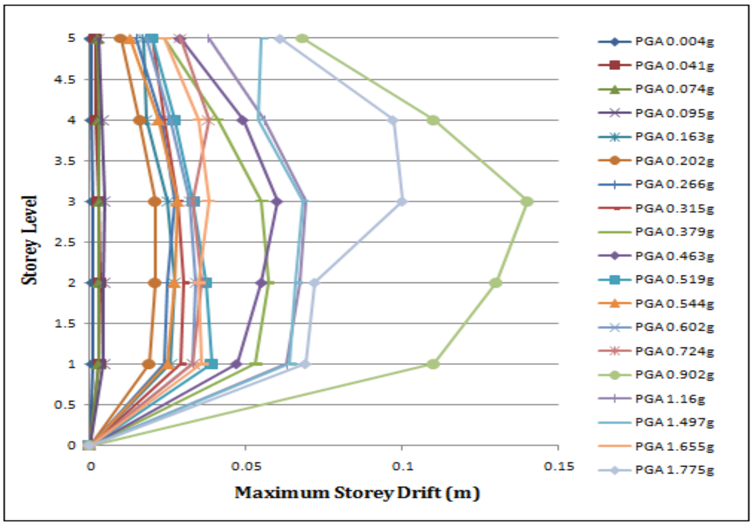

Figure 6.2: Maximum Storey Drift for Bare Frame

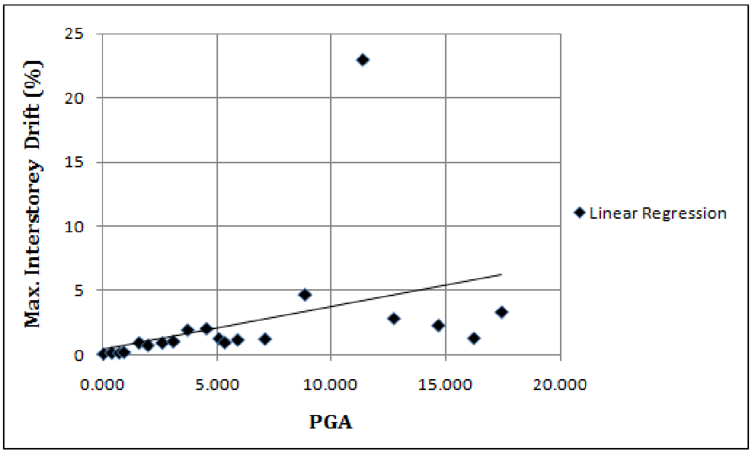

Figure 6.3: Linear regression plot of Max. Interstorey Drift Vs. PGA for Bare Frame

Table 6.1: Maximum Interstorey Drift for Bare Frame

SR.No.	PGA (g)	Max. Storey Drift (m)	PGA	Max. Interstorey Drift (%)
1	0.004	0.009	0.039	0.03
2	0.041	0.003	0.402	0.11
3	0.074	0.003	0.726	0.10
4	0.095	0.005	0.932	0.16
5	0.163	0.027	1.599	0.90
6	0.202	0.021	1.982	0.70
7	0.266	0.027	2.609	0.90
8	0.315	0.030	3.090	1.0
9	0.379	0.057	3.718	1.90
10	0.463	0.060	4.542	2.0
11	0.519	0.037	5.091	1.23
12	0.544	0.028	5.337	0.93
13	0.602	0.034	5.906	1.13
14	0.724	0.036	7.102	1.20
15	0.902	0.140	8.849	4.66
16	1.16	0.690	11.380	23
17	1.298	0.084	12.733	2.8
18	1.497	0.068	14.686	2.26
19	1.655	0.038	16.236	1.26
20	1.779	0.100	17.452	3.3

Figure (6.2) shows the plot of maximum storey drift Vs. storey level for bare frame as per Table 5.4 of chapter 5, which indicates maximum storey drift of 0.14 m was obtained at PGA 0.902g. Figure (6.3) shows linear regression plot of maximum interstorey drift Vs. PGA for bare frame. To calculate a probabilistic seismic demand model, the maximum interstorey drift of each record is plotted against the records demand to calculate a linear regression analysis between the seismic intensity measure and the structural response demand. A nonlinear regression analysis of the power-law form is used due to the nonlinear nature of the problem. Using a logarithmic transformation of the power-law Equation (6.3), a linear regression analysis determines the unknown constants.

Table 6.2: Linear Regression Calculation of Maximum Interstorey Drift for Bare Frame

SR.No.	PGA (X)	Max. Interstorey Drift (%) (Y)	X^2	Y^2	XY
1	0.039	0.03	0.0015	0.0009	0.0012
2	0.402	0.11	0.162	0.012	0.044
3	0.726	0.10	0.527	0.010	0.073
4	0.932	0.16	0.869	0.026	0.149
5	1.599	0.90	2.557	0.81	1.439
6	1.982	0.70	3.927	0.49	1.387
7	2.609	0.90	6.809	0.81	2.349
8	3.090	1.0	9.549	1.0	3.090
9	3.718	1.90	13.823	3.61	7.064
10	4.542	2.0	20.630	4.0	9.084
11	5.091	1.23	25.922	1.51	6.262
12	5.337	0.93	28.480	0.86	4.963
13	5.906	1.13	34.876	1.28	6.673
14	7.102	1.2	50.445	1.44	8.523
15	8.849	4.66	78.298	21.72	41.235
16	11.380	23	129.50	529	261.73
17	12.733	2.8	162.14	7.84	35.653
18	14.686	2.26	215.67	5.11	33.189
19	16.236	1.26	263.59	1.59	20.457
20	17.452	3.3	304.57	10.89	57.592
TOTAL	**124.41**	**49.57**	**1352.34**	**592.00**	**500.96**

The constants a_1 and a_2 are calculated through a linear regression analysis as per Table 6.2 and formulations which are given in Appendix C. The constants a_1 and a_2 are obtained 0.36 and 0.34 respectively.

Table 6.3: Probability Calculation of Structural Response (Drift) for Bare Frame

ln(PGA)	$\lambda_\mathbf{D}$	**(ln(PGA)-** $\lambda_D)^2$	**Φ(X)**	**(IO)**	**Φ(X)**	**(LS)**	**Φ(X)**	**(CP)**
-3.238	-2.123	1.244	-0.225	0.611	-0.290	0.617	0.001	0.601
-0.911	-1.331	0.177	-0.558	0.658	-0.623	0.671	-0.331	0.622
-0.320	-1.131	0.657	-0.642	0.675	-0.707	0.689	-0.416	0.634
-0.070	-1.046	0.951	-0.678	0.683	-0.743	0.697	-0.451	0.640
0.469	-0.862	1.773	-0.755	0.700	-0.820	0.715	-0.529	0.653
0.684	-0.789	2.170	-0.786	0.707	-0.850	0.722	-0.559	0.659
0.959	-0.696	2.738	-0.825	0.716	-0.890	0.731	-0.599	0.666
1.128	-0.638	3.120	-0.849	0.722	-0.914	0.737	-0.623	0.671
1.313	-0.575	3.566	-0.876	0.728	-0.940	0.744	-0.649	0.677
1.513	-0.507	4.082	-0.904	0.735	-0.969	0.750	-0.678	0.683
1.628	-0.468	4.393	-0.920	0.739	-0.985	0.754	-0.694	0.686
1.675	-0.452	4.524	-0.927	0.740	-0.992	0.756	-0.701	0.688
1.776	-0.418	4.813	-0.942	0.744	-1.006	0.760	-0.715	0.691
1.960	-0.355	5.362	-0.968	0.750	-1.033	0.766	-0.742	0.697
2.180	-0.280	6.055	-0.999	0.758	-1.064	0.773	-0.773	0.704
2.432	-0.195	6.899	-1.035	0.767	-1.100	0.782	-0.809	0.712
2.544	-0.157	7.295	-1.051	0.770	-1.116	0.786	-0.825	0.716
2.687	-0.108	7.812	-1.072	0.775	-1.137	0.791	-0.845	0.721
2.787	-0.074	8.186	-1.086	0.779	-1.151	0.794	-0.860	0.724
2.859	-0.049	8.462	-1.096	0.781	-1.161	0.797	-0.870	0.727

Table 6.3 shows probability calculation of twenty nos. of earthquake ground motion records for three drift limits namely Immediate Occupancy (1%), Life Safety (2%) and Collapse Prevention (4%) as specified in FEMA 356. The value of $\beta_{D/GMI}$ is obtained 2.16 from Table 6.3. The capacity uncertainty (β_{cl}) and modeling uncertainty (β_m) are taken as 0.3 respectively.

Table 6.4: Probability of Structural Response (Drift) for Bare Frame

SR.No.	**PGA (g)**	**Probability**		
		Immediate Occupancy (IO)	**Life Safety (LS)**	**Collapse Prevention (CP)**
1	0.004	0.673	0.620	0.601
2	0.041	0.755	0.682	0.626
3	0.074	0.777	0.702	0.639
4	0.095	0.786	0.711	0.646
5	0.163	0.806	0.731	0.661
6	0.202	0.814	0.739	0.668
7	0.266	0.823	0.749	0.676
8	0.315	0.829	0.755	0.682
9	0.379	0.836	0.762	0.688
10	0.463	0.842	0.770	0.695
11	0.519	0.846	0.774	0.699
12	0.544	0.848	0.776	0.701
13	0.602	0.851	0.779	0.704
14	0.724	0.857	0.786	0.711
15	0.902	0.864	0.794	0.719
16	1.16	0.871	0.803	0.728
17	1.298	0.875	0.807	0.732
18	1.497	0.879	0.812	0.737
19	1.655	0.882	0.816	0.741
20	1.779	0.884	0.819	0.744

Table 6.4 shows the probability of exceeding a particular limit state for three drift limits.

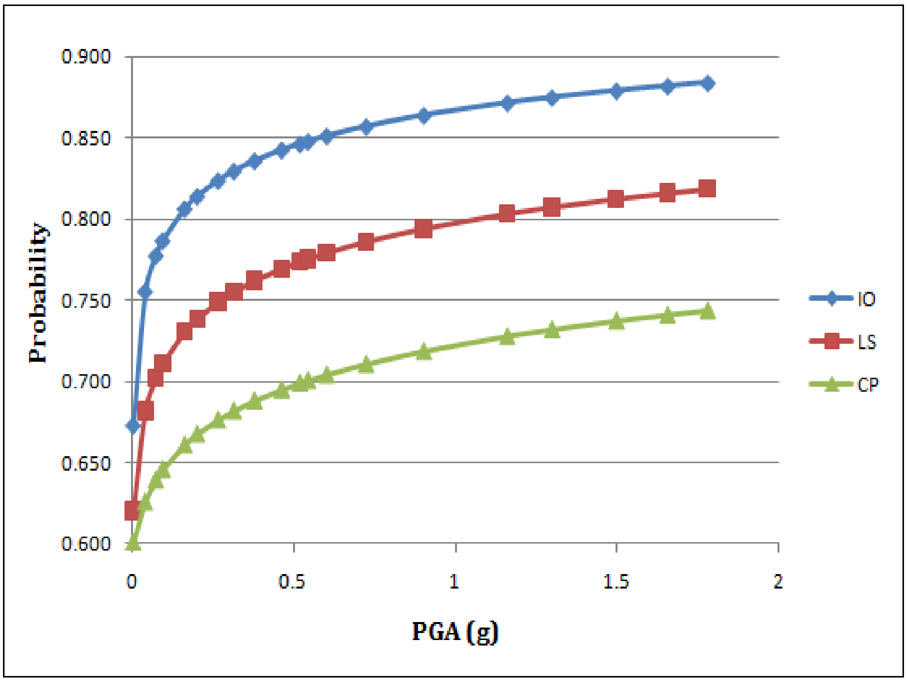

Figure 6.4: Fragility Curve of Structural Response (Drift) for Bare Frame

Figure (6.4) indicates that the probability of exceeding a particular limit state in bare frame model, IO, LS and CP were found to be 0.67 to 0.88 percent , 0.62 to 0.81 percent and 0.60 to 0.74 percent respectively.

Similarly, probability calculation of structural response (Displacement) for bare frame is carried out to find probability at performance point.

Table 6.5: Maximum Displacement for Bare Frame

SR.No.	PGA (g)	Max.Displ (m)	PGA	Max.Displ (%)
1	0.004	0.000965	0.039	0.032
2	0.041	0.0075	0.402	0.250
3	0.074	0.007	0.726	0.233
4	0.095	0.01	0.932	0.333
5	0.163	0.057	1.599	1.900
6	0.202	0.048	1.982	1.600
7	0.266	0.067	2.609	2.233
8	0.315	0.091	3.090	3.033
9	0.379	0.08	3.718	2.667
10	0.463	0.15	4.542	5.000
11	0.519	0.067	5.091	2.233
12	0.544	0.036	5.337	1.200
13	0.602	0.094	5.906	3.133
14	0.724	0.13	7.102	4.333
15	0.902	0.23	8.849	7.667
16	1.16	0.17	11.380	5.667
17	1.298	0.23	12.733	7.667
18	1.497	0.18	14.686	6.000
19	1.655	0.076	16.236	2.533
20	1.779	0.28	17.452	9.333

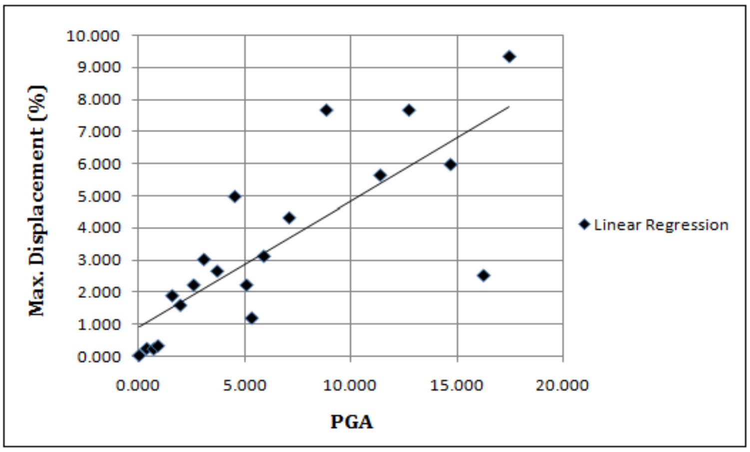

Figure 6.5: Linear regression plot of Maximum Displacement Vs. PGA for Bare Frame

Table 6.6: Linear Regression Calculation of Maximum Displacement for Bare Frame

SR.No.	**PGA (X)**	**Maximum Displacement (%) (Y)**	**X^2**	**Y^2**	**XY**
1	0.039	0.032	0.002	0.001	0.001
2	0.402	0.250	0.162	0.063	0.101
3	0.726	0.233	0.527	0.054	0.169
4	0.932	0.333	0.869	0.111	0.311
5	1.599	1.900	2.557	3.610	3.038
6	1.982	1.600	3.927	2.560	3.171
7	2.609	2.233	6.809	4.988	5.828
8	3.090	3.033	9.549	9.201	9.373
9	3.718	2.667	13.823	7.111	9.915
10	4.542	5.000	20.630	25.0	22.710
11	5.091	2.233	25.922	4.988	11.371
12	5.337	1.200	28.480	1.440	6.404
13	5.906	3.133	34.876	9.818	18.504
14	7.102	4.333	50.445	18.778	30.777
15	8.849	7.667	78.298	58.778	67.839
16	11.380	5.667	129.50	32.111	64.484
17	12.733	7.667	162.14	58.778	97.623
18	14.686	6.000	215.67	36.000	88.113
19	16.236	2.533	263.59	6.418	41.130
20	17.452	9.333	304.57	87.111	162.89
TOTAL	**124.41**	**67.05**	**1352.34**	**366.92**	**643.75**

Figure (6.5) shows linear regression plot of maximum displacement Vs. PGA for bare frame. The constants a_1 and a_2 are calculated through a linear regression analysis as per Table 6.6 and formulations which are given in Appendix C. The constants a_1 and a_2 are obtained 0.93 and 0.39 respectively.

Table 6.7: Probability Calculation of Structural Response (Displacement) for Bare Frame

ln(PGA)	$\lambda_\mathbf{D}$	**(ln(PGA)-** $\lambda_D)^2$	$\mathbf{\Phi}$**(X)**	**Probability**
-3.238	-1.335	3.620	-0.996	0.757
-0.911	-0.428	0.233	-1.678	0.902
-0.320	-0.197	0.015	-1.852	0.928
-0.070	-0.100	0.001	-1.925	0.937
0.469	0.110	0.129	-2.083	0.954
0.684	0.194	0.240	-2.146	0.960
0.959	0.301	0.433	-2.227	0.967
1.128	0.367	0.579	-2.277	0.970
1.313	0.440	0.763	-2.331	0.974
1.513	0.518	0.991	-2.390	0.977
1.628	0.562	1.135	-2.423	0.979
1.675	0.581	1.197	-2.437	0.980
1.776	0.620	1.336	-2.467	0.981
1.960	0.692	1.609	-2.521	0.983
2.180	0.778	1.967	-2.585	0.986
2.432	0.876	2.421	-2.659	0.988
2.544	0.920	2.639	-2.692	0.989
2.687	0.975	2.929	-2.734	0.990
2.787	1.014	3.143	-2.763	0.991
2.859	1.043	3.301	-2.784	0.992

Table 6.7 shows the probability calculation of structural response (Displacement) for bare frame. The value of $\beta_{D/GMI}$ is obtained 1.26 from Table 6.7. The capacity uncertainty (β_{cl}) and modeling uncertainty (β_m) are taken as 0.3 respectively. The value of λ_{cl} is take as 0.07.

Table 6.8: Probability of Structural Response (Displacement) for Bare Frame

SR.No.	**PGA (g)**	**Probability**
1	0.004	0.757
2	0.041	0.902
3	0.074	0.928
4	0.095	0.937
5	0.163	0.954
6	0.202	0.960
7	0.266	0.967
8	0.315	0.970
9	0.379	0.974
10	0.463	0.977
11	0.519	0.979
12	0.544	0.980
13	0.602	0.981
14	0.724	0.983
15	0.902	0.986
16	1.16	0.988
17	1.298	0.989
18	1.497	0.990
19	1.655	0.991
20	1.779	0.992

Table 6.8 shows probability of exceeding a particular limit state for bare frame at performance point.

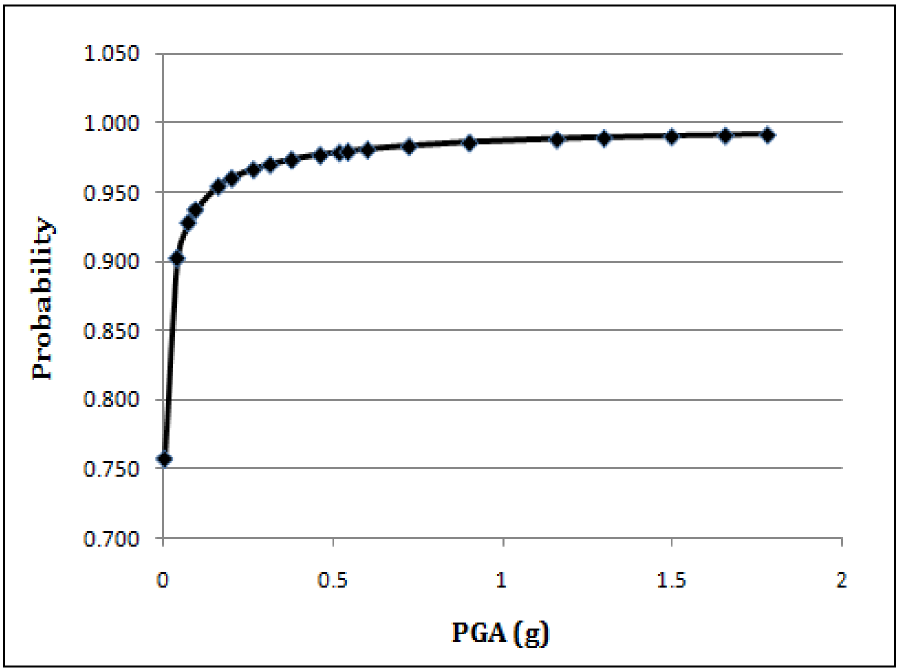

Figure 6.6: Fragility Curve of Structural Response (Displacement) for Bare Frame

Figure (6.6) shows that the probability of structural response (Displacement) for bare frame model to exceeding a limit state was found to be 0.75 to 0.99 percent.

6.5 Fragility Analysis and Results of Building with Infill Wall

Fragility curve obtained for G+4 storey building without infills as membrane wall is as below.

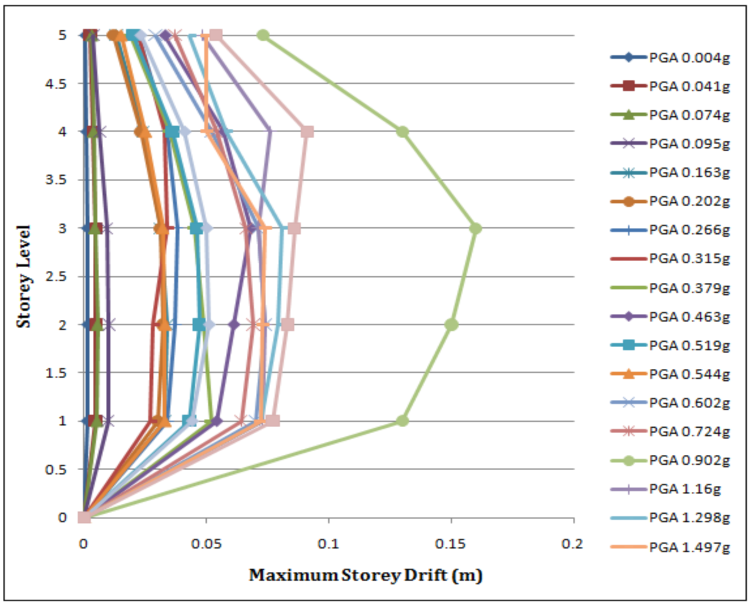

Figure 6.7: Maximum Storey Drift for Membrane Wall

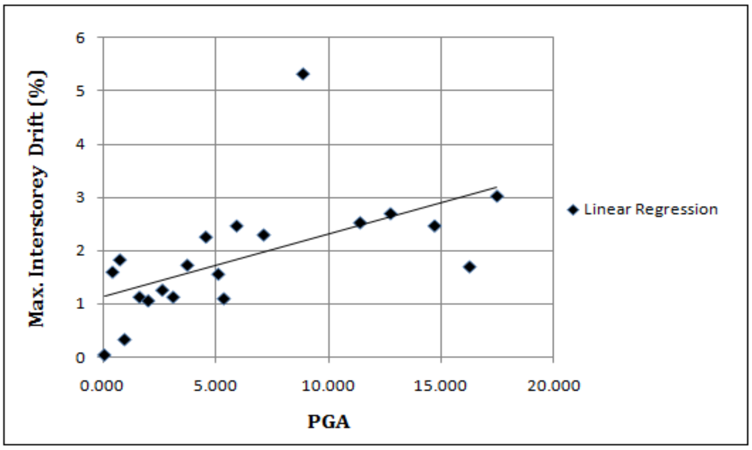

Figure 6.8: Linear regression plot of Maximum Interstorey Drift Vs. PGA for Membrane Wall

Table 6.9: Maximum Interstorey Drift for Membrane Wall

SR.No.	PGA (g)	Max. Storey Drift (m)	PGA	Max. Interstorey Drift (%)
1	0.004	0.001	0.039	0.04
2	0.041	0.005	0.402	1.60
3	0.074	0.006	0.726	1.83
4	0.095	0.010	0.932	0.33
5	0.163	0.034	1.599	1.13
6	0.202	0.032	1.982	1.06
7	0.266	0.038	2.609	1.26
8	0.315	0.034	3.090	1.13
9	0.379	0.052	3.718	1.73
10	0.463	0.068	4.542	2.26
11	0.519	0.047	5.091	1.56
12	0.544	0.033	5.337	1.10
13	0.602	0.074	5.906	2.47
14	0.724	0.069	7.102	2.30
15	0.902	0.16	8.849	5.33
16	1.16	0.076	11.380	2.53
17	1.298	0.081	12.733	2.70
18	1.497	0.074	14.686	2.47
19	1.655	0.051	16.236	1.70
20	1.779	0.091	17.452	3.03

Figure (6.7) shows the plot of maximum storey drift Vs. storey level for membrane wall as per Table 5.10 of chapter 5, which indicates maximum storey drift of 0.16 m was obtained at PGA 0.902g. Figure (6.8) shows linear regression plot of maximum interstorey drift Vs. PGA for membrane wall.

Table 6.10: Linear Regression Calculation of Maximum Interstorey Drift for Membrane Wall

SR.No.	PGA (X)	Max. Interstorey Drift (%) (Y)	X^2	Y^2	XY
1	0.039	0.04	0.002	0.002	0.0016
2	0.402	1.60	0.162	2.56	0.644
3	0.726	1.83	0.527	3.35	1.328
4	0.932	0.33	0.869	0.11	0.308
5	1.599	1.13	2.557	1.28	1.807
6	1.982	1.06	3.927	1.12	2.101
7	2.609	1.26	6.809	1.59	3.288
8	3.090	1.13	9.549	1.28	3.492
9	3.718	1.73	13.823	2.99	6.432
10	4.542	2.26	20.630	5.11	10.26
11	5.091	1.56	25.922	2.43	7.943
12	5.337	1.10	28.480	1.21	5.870
13	5.906	2.47	34.876	6.10	14.59
14	7.102	2.3	50.445	5.29	16.34
15	8.849	5.33	78.298	28.41	47.16
16	11.380	2.53	129.50	6.40	28.79
17	12.733	2.70	162.14	7.29	34.38
18	14.686	2.47	215.67	6.10	36.27
19	16.236	1.70	263.59	2.89	27.60
20	17.452	3.03	304.57	9.18	52.88
TOTAL	**124.410**	**37.56**	**1352.34**	**94.69**	**301.49**

The constants a_1 and a_2 are calculated through a linear regression analysis as per Table 6.10 and formulations which are given in Appendix C. The constants a_1 and a_2 are obtained 1.13 and 0.12 respectively.

Table 6.11: Probability Calculation of Structural Response (Drift) for Membrane Wall

ln(PGA)	$\lambda_{\mathbf{D}}$	**(ln(PGA)-** $\lambda_D)^2$	**Φ(X)**	**(IO)**	**Φ(X)**	**(LS)**	**Φ(X)**	**(CP)**
-3.238	-0.266	8.831	-1.849	0.928	-1.454	0.861	-1.058	0.772
-0.911	0.013	0.853	-2.009	0.947	-1.613	0.891	-1.217	0.810
-0.320	0.084	0.163	-2.049	0.951	-1.654	0.898	-1.258	0.819
-0.070	0.114	0.034	-2.066	0.953	-1.671	0.901	-1.275	0.823
0.469	0.179	0.085	-2.103	0.956	-1.708	0.907	-1.312	0.831
0.684	0.204	0.230	-2.118	0.958	-1.722	0.909	-1.327	0.834
0.959	0.237	0.521	-2.137	0.959	-1.741	0.912	-1.346	0.839
1.128	0.258	0.758	-2.148	0.960	-1.753	0.914	-1.357	0.841
1.313	0.280	1.068	-2.161	0.961	-1.765	0.916	-1.370	0.844
1.513	0.304	1.463	-2.175	0.962	-1.779	0.918	-1.383	0.847
1.628	0.318	1.716	-2.183	0.963	-1.787	0.919	-1.391	0.848
1.675	0.323	1.826	-2.186	0.963	-1.790	0.920	-1.395	0.849
1.776	0.335	2.075	-2.193	0.964	-1.797	0.921	-1.401	0.851
1.960	0.357	2.570	-2.205	0.965	-1.810	0.922	-1.414	0.853
2.180	0.384	3.227	-2.220	0.966	-1.825	0.924	-1.429	0.856
2.432	0.414	4.071	-2.238	0.967	-1.842	0.927	-1.446	0.860
2.544	0.428	4.480	-2.245	0.968	-1.850	0.928	-1.454	0.861
2.687	0.445	5.028	-2.255	0.969	-1.859	0.929	-1.464	0.863
2.787	0.457	5.431	-2.262	0.969	-1.866	0.930	-1.471	0.865
2.859	0.465	5.732	-2.267	0.969	-1.871	0.931	-1.476	0.866

Table 6.11 shows probability calculation of twenty nos. of earthquake ground motion records for three drift limits namely Immediate Occupancy (1%), Life Safety (2%) and Collapse Prevention (4%) as specified in FEMA 356. The value of $\beta_{D/GMI}$ is obtained 1.70 from Table 6.11. The capacity uncertainty (β_{cl}) and modeling uncertainty (β_m) are taken as 0.3 respectively.

Table 6.12: Probability of Structural Response (Drift) for Membrane Wall

SR.No.	**PGA (g)**	**Probability**		
		Immediate Occupancy (IO)	**Life Safety (LS)**	**Collapse Prevention (CP)**
1	0.004	0.928	0.861	0.772
2	0.041	0.947	0.891	0.810
3	0.074	0.951	0.898	0.819
4	0.095	0.953	0.901	0.823
5	0.163	0.956	0.907	0.831
6	0.202	0.958	0.909	0.834
7	0.266	0.959	0.912	0.839
8	0.315	0.960	0.914	0.841
9	0.379	0.961	0.916	0.844
10	0.463	0.962	0.918	0.847
11	0.519	0.963	0.919	0.848
12	0.544	0.963	0.920	0.849
13	0.602	0.964	0.921	0.851
14	0.724	0.965	0.922	0.853
15	0.902	0.966	0.924	0.856
16	1.16	0.967	0.927	0.860
17	1.298	0.968	0.928	0.861
18	1.497	0.969	0.929	0.863
19	1.655	0.969	0.930	0.865
20	1.779	0.969	0.931	0.866

Table 6.12 shows the probability of exceeding a particular limit state for three drift limits.

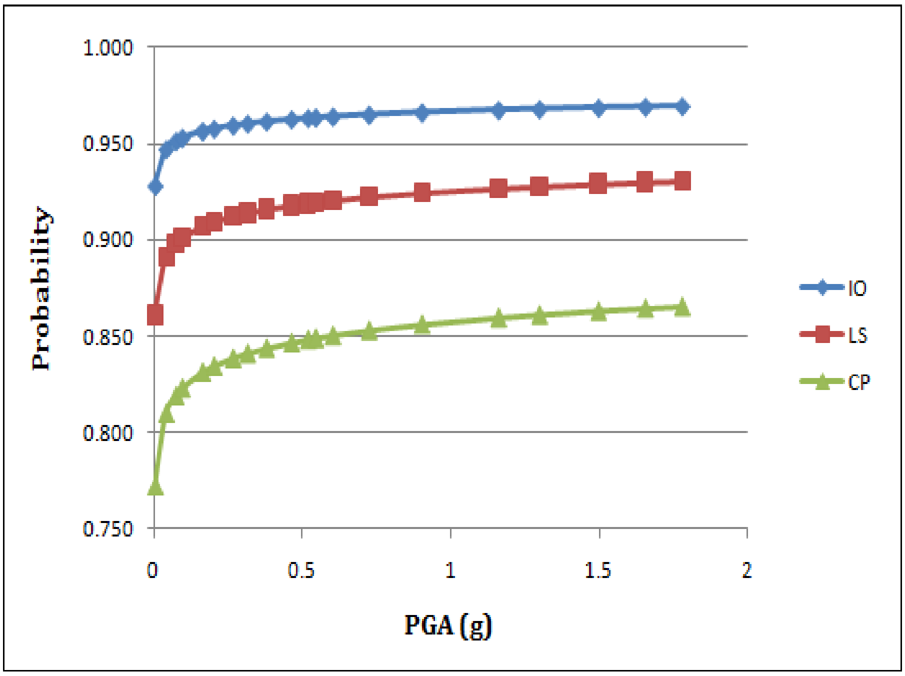

Figure 6.9: Fragility Curve of Structural Response (Drift) for Membrane Wall

Figure (6.9) indicates that the probability of exceeding a particular limit state in infill wall model, IO, LS and CP were found to be 0.92 to 0.96 percent , 0.86 to 0.93 percent and 0.77 to 0.86 percent respectively.

Similarly, probability calculation of structural response (Displacement) for membrane wall is carried out to find probability at performance point.

Table 6.13: Maximum Displacement for Membrane Wall

SR.No.	PGA (g)	Max. Displ (m)	PGA	Max. Displ (%)
1	0.004	0.002	0.039	0.05
2	0.041	0.010	0.402	0.33
3	0.074	0.010	0.726	0.33
4	0.095	0.012	0.932	0.4
5	0.163	0.045	1.599	1.5
6	0.202	0.067	1.982	2.23
7	0.266	0.091	2.609	3.03
8	0.315	0.081	3.090	2.70
9	0.379	0.098	3.718	3.27
10	0.463	0.26	4.542	8.67
11	0.519	0.099	5.091	3.3
12	0.544	0.036	5.337	1.2
13	0.602	0.095	5.906	3.17
14	0.724	0.16	7.102	5.33
15	0.902	0.3	8.849	10
16	1.16	0.12	11.380	4
17	1.298	0.31	12.733	10.33
18	1.497	0.21	14.686	7
19	1.655	0.09	16.236	3
20	1.779	0.35	17.452	11.67

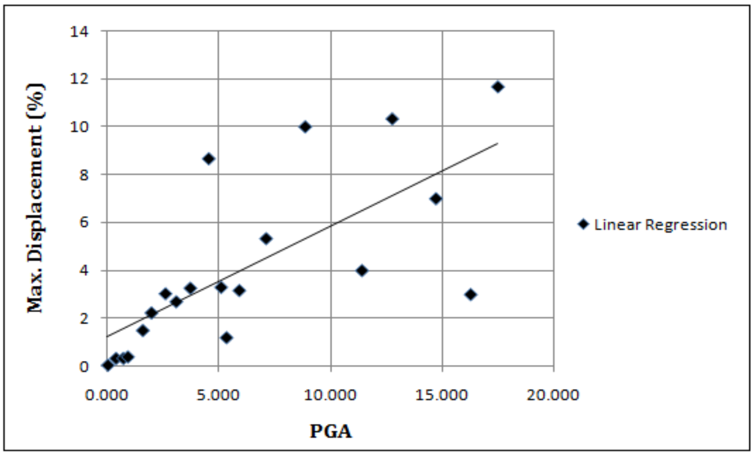

Figure 6.10: Linear regression plot of Maximum Displacement Vs. PGA for Membrane Wall

Table 6.14: Linear Regression Calculation of Maximum Displacement for Membrane Wall

SR.No.	**PGA (X)**	**Max. Displacement (%) (Y)**	$\mathbf{X^2}$	$\mathbf{Y^2}$	**XY**
1	0.039	0.05	0.002	0.0025	0.002
2	0.402	0.33	0.162	0.11	0.134
3	0.726	0.33	0.527	0.11	0.242
4	0.932	0.4	0.869	0.16	0.373
5	1.599	1.5	2.557	2.25	2.399
6	1.982	2.23	3.927	4.99	4.426
7	2.609	3.03	6.809	9.20	7.915
8	3.090	2.7	9.549	7.29	8.343
9	3.718	3.27	13.823	10.67	12.145
10	4.542	8.67	20.630	75.11	39.364
11	5.091	3.3	25.922	10.89	16.802
12	5.337	1.2	28.480	1.44	6.404
13	5.906	3.17	34.876	10.03	18.701
14	7.102	5.33	50.445	28.44	37.880
15	8.849	10	78.298	100	88.486
16	11.380	4.0	129.495	16	45.518
17	12.733	10.33	162.139	106.78	131.578
18	14.686	7.0	215.666	49	102.799
19	16.236	3.0	263.593	9	48.707
20	17.452	11.67	304.572	136.11	203.607
TOTAL	**124.41**	**81.52**	**1352.34**	**577.59**	**775.82**

Figure (6.14) shows linear regression plot of maximum displacement Vs. PGA for membrane wall. The constants a_1 and a_2 are calculated through a linear regression analysis as per Table 6.14 and formulations which are given in Appendix C. The constants a_1 and a_2 are obtained 1.21 and 0.46 respectively.

Table 6.15: Probability Calculation of Structural Response (Displacement) for Membrane Wall

ln(PGA)	$\lambda_{\mathbf{D}}$	**(ln(PGA)-** $\lambda_D)^2$	$\mathbf{\Phi}$**(X)**	**Probability**
-3.238	-1.299	3.760	-1.443	0.859
-0.911	-0.228	0.466	-2.463	0.981
-0.320	0.043	0.132	-2.722	0.990
-0.070	0.158	0.052	-2.831	0.993
0.469	0.407	0.004	-3.068	0.996
0.684	0.505	0.032	-3.162	0.997
0.959	0.632	0.107	-3.283	0.998
1.128	0.710	0.175	-3.357	0.999
1.313	0.795	0.269	-3.438	0.999
1.513	0.887	0.393	-3.525	0.999
1.628	0.939	0.474	-3.575	0.999
1.675	0.961	0.509	-3.596	0.999
1.776	1.008	0.590	-3.640	0.999
1.960	1.092	0.753	-3.721	1.000
2.180	1.194	0.974	-3.818	1.000
2.432	1.309	1.260	-3.928	1.000
2.544	1.361	1.400	-3.977	1.000
2.687	1.427	1.588	-4.040	1.000
2.787	1.473	1.728	-4.084	1.000
2.859	1.506	1.832	-4.115	1.000

Table 6.15 shows the probability calculation of structural response (Displacement) for membrane wall. The value of $\beta_{D/GMI}$ is obtained 0.96 from Table 6.15. The capacity uncertainty (β_{cl}) and modeling uncertainty (β_m) are taken as 0.3 respectively. The value of β_{cl} is take as 0.03.

Table 6.16: Probability of Structural Response (Displacement) for Membrane Wall

SR.No.	**PGA (g)**	**Probability**
1	0.004	0.859
2	0.041	0.981
3	0.074	0.990
4	0.095	0.993
5	0.163	0.996
6	0.202	0.997
7	0.266	0.998
8	0.315	0.999
9	0.379	0.999
10	0.463	0.999
11	0.519	0.999
12	0.544	0.999
13	0.602	0.999
14	0.724	1.000
15	0.902	1.000
16	1.16	1.000
17	1.298	1.000
18	1.497	1.000
19	1.655	1.000
20	1.779	1.000

Table 6.16 shows probability of exceeding a particular limit state for bare frame at performance point.

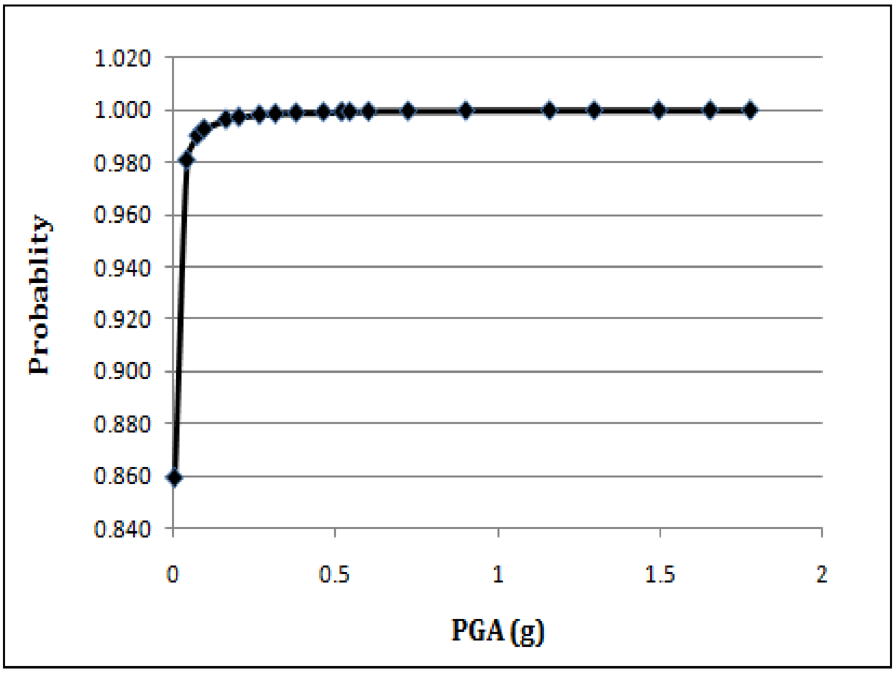

Figure 6.11: Fragility Curve of Structural Response (Displacement) for Infill Wall

Figure (6.11) shows that the probability of structural response (Displacement) for infill wall model to exceeding a limit state was found to be 0.85 to 1.0 percent.

Fragility curve obtained for G+4 storey building without infills as equivalent strut is as below.

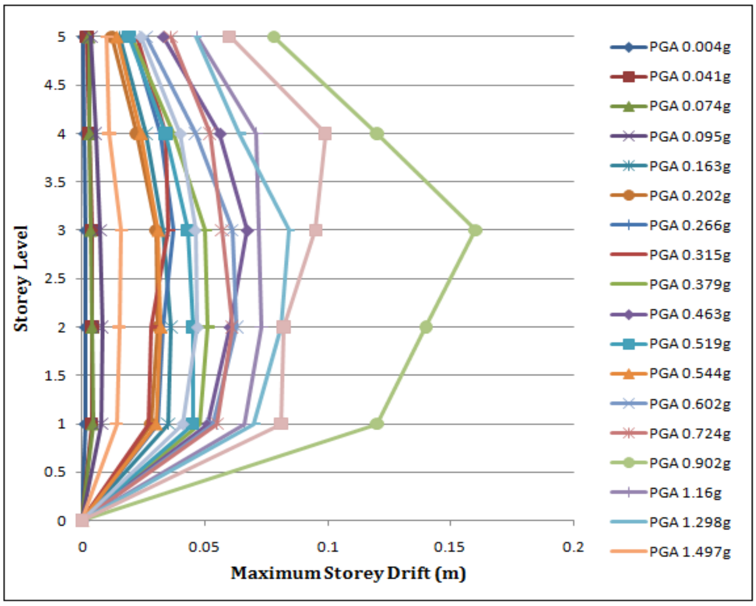

Figure 6.12: Maximum Storey Drift for Equivalent Strut

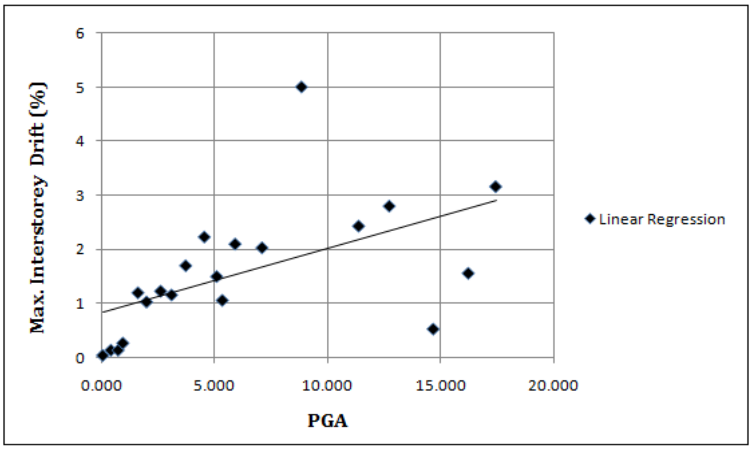

Figure 6.13: Linear regression plot of Maximum Interstorey Drift Vs. PGA for Equivalent Strut

Table 6.17: Maximum Interstorey Drift for Equivalent Strut

SR.No.	PGA (g)	Max. Storey Drift (m)	PGA	Max. Interstorey Drift (%)
1	0.004	0.0013	0.039	0.043
2	0.041	0.0041	0.402	0.14
3	0.074	0.0041	0.726	0.14
4	0.095	0.0082	0.932	0.27
5	0.163	0.036	1.599	1.20
6	0.202	0.031	1.982	1.03
7	0.266	0.037	2.609	1.23
8	0.315	0.035	3.090	1.16
9	0.379	0.051	3.718	1.70
10	0.463	0.067	4.542	2.23
11	0.519	0.045	5.091	1.50
12	0.544	0.032	5.337	1.06
13	0.602	0.063	5.906	2.10
14	0.724	0.061	7.102	2.03
15	0.902	0.15	8.849	5.0
16	1.16	0.073	11.380	2.43
17	1.298	0.084	12.733	2.80
18	1.497	0.016	14.686	0.53
19	1.655	0.047	16.236	1.56
20	1.779	0.095	17.452	3.16

Figure (6.12) shows the plot of maximum storey drift Vs. storey level for equivalent strut as per Table 5.14 of chapter 5, which indicates maximum storey drift of 0.16 m was obtained at PGA 0.902g. Figure (6.13) shows linear regression plot of maximum interstorey drift Vs. PGA for equivalent strut.

Table 6.18: Linear Regression Calculation of Maximum Interstorey Drift for Equivalent Strut

SR.No.	PGA (X)	Max.Interstorey Drift (%) (Y)	X^2	Y^2	XY
1	0.039	0.043	0.002	0.002	0.002
2	0.402	0.14	0.162	0.020	0.056
3	0.726	0.14	0.527	0.020	0.102
4	0.932	0.27	0.869	0.073	0.252
5	1.599	1.20	2.557	1.440	1.919
6	1.982	1.03	3.927	1.061	2.041
7	2.609	1.23	6.809	1.513	3.210
8	3.090	1.16	9.549	1.346	3.585
9	3.718	1.70	13.823	2.890	6.321
10	4.542	2.23	20.630	4.973	10.129
11	5.091	1.50	25.922	2.250	7.637
12	5.337	1.06	28.480	1.124	5.657
13	5.906	2.10	34.876	4.410	12.402
14	7.102	2.03	50.445	4.121	14.418
15	8.849	5.0	78.298	25.0	44.243
16	11.380	2.43	129.50	5.905	27.652
17	12.733	2.80	162.14	7.840	35.653
18	14.686	0.53	215.67	0.281	7.783
19	16.236	1.56	263.59	2.434	25.327
20	17.452	3.16	304.57	9.986	55.148
TOTAL	**124.41**	**31.31**	**1352.34**	**76.69**	**263.54**

The constants a_1 and a_2 are calculated through a linear regression analysis as per Table 6.18 and formulations which are given in Appendix C. The constants a_1 and a_2 are obtained 0.82 and 0.12 respectively.

Table 6.19: Probability Calculation of Structural Response (Drift) for Equivalent Strut

ln(PGA)	$\lambda_{\mathbf{D}}$	**(ln(PGA)-** $\lambda_D)^2$	$\mathbf{\Phi}$**(X)**	**(IO)**	$\mathbf{\Phi}$**(X)**	**(LS)**	$\mathbf{\Phi}$**(X)**	**(CP)**
-3.238	-0.5870	7.028	-1.515	0.873	-1.155	0.795	-0.796	0.709
-0.911	-0.3077	0.364	-1.660	0.899	-1.300	0.829	-0.940	0.744
-0.320	-0.2369	0.007	-1.697	0.905	-1.337	0.837	-0.977	0.752
-0.070	-0.2069	0.019	-1.712	0.908	-1.352	0.840	-0.993	0.756
0.469	-0.1421	0.374	-1.746	0.913	-1.386	0.847	-1.026	0.764
0.684	-0.1164	0.640	-1.759	0.915	-1.399	0.850	-1.040	0.768
0.959	-0.0834	1.087	-1.776	0.918	-1.417	0.854	-1.057	0.772
1.128	-0.0631	1.419	-1.787	0.919	-1.427	0.856	-1.067	0.774
1.313	-0.0409	1.833	-1.798	0.921	-1.439	0.858	-1.079	0.777
1.513	-0.0168	2.342	-1.811	0.923	-1.451	0.861	-1.091	0.780
1.628	-0.0031	2.659	-1.818	0.924	-1.458	0.862	-1.099	0.782
1.675	0.0025	2.796	-1.821	0.924	-1.461	0.863	-1.101	0.782
1.776	0.0147	3.102	-1.827	0.925	-1.467	0.864	-1.108	0.784
1.960	0.0368	3.700	-1.839	0.926	-1.479	0.866	-1.119	0.787
2.180	0.0632	4.482	-1.852	0.928	-1.493	0.869	-1.133	0.790
2.432	0.0934	5.468	-1.868	0.930	-1.508	0.872	-1.149	0.794
2.544	0.1069	5.941	-1.875	0.931	-1.515	0.873	-1.156	0.795
2.687	0.1240	6.568	-1.884	0.932	-1.524	0.875	-1.164	0.797
2.787	0.1360	7.029	-1.890	0.933	-1.530	0.876	-1.171	0.799
2.859	0.1447	7.370	-1.895	0.934	-1.535	0.877	-1.175	0.800

Table 6.19 shows probability calculation of twenty nos. of earthquake ground motion records for three drift limits namely Immediate Occupancy (1%), Life Safety (2%) and Collapse Prevention (4%) as specified in FEMA 356. The value of $\beta_{D/GMI}$ is obtained 1.88 from Table 6.19. The capacity uncertainty (β_{cl}) and modeling uncertainty (β_m) are taken as 0.3 respectively.

Table 6.20: Probability of Structural Response (Drift) for Equivalent Strut

SR.No.	PGA (g)	Probability		
		Immediate Occupancy (IO)	Life Safety (LS)	Collapse Prevention (CP)
1	0.004	0.873	0.795	0.709
2	0.041	0.899	0.829	0.744
3	0.074	0.905	0.837	0.752
4	0.095	0.908	0.840	0.756
5	0.163	0.913	0.847	0.764
6	0.202	0.915	0.850	0.768
7	0.266	0.918	0.854	0.772
8	0.315	0.919	0.856	0.774
9	0.379	0.921	0.858	0.777
10	0.463	0.923	0.861	0.780
11	0.519	0.924	0.862	0.782
12	0.544	0.924	0.863	0.782
13	0.602	0.925	0.864	0.784
14	0.724	0.926	0.866	0.787
15	0.902	0.928	0.869	0.790
16	1.16	0.930	0.872	0.794
17	1.298	0.931	0.873	0.795
18	1.497	0.932	0.875	0.797
19	1.655	0.933	0.876	0.799
20	1.779	0.934	0.877	0.800

Table 6.20 shows the probability of exceeding a particular limit state for three drift limits.

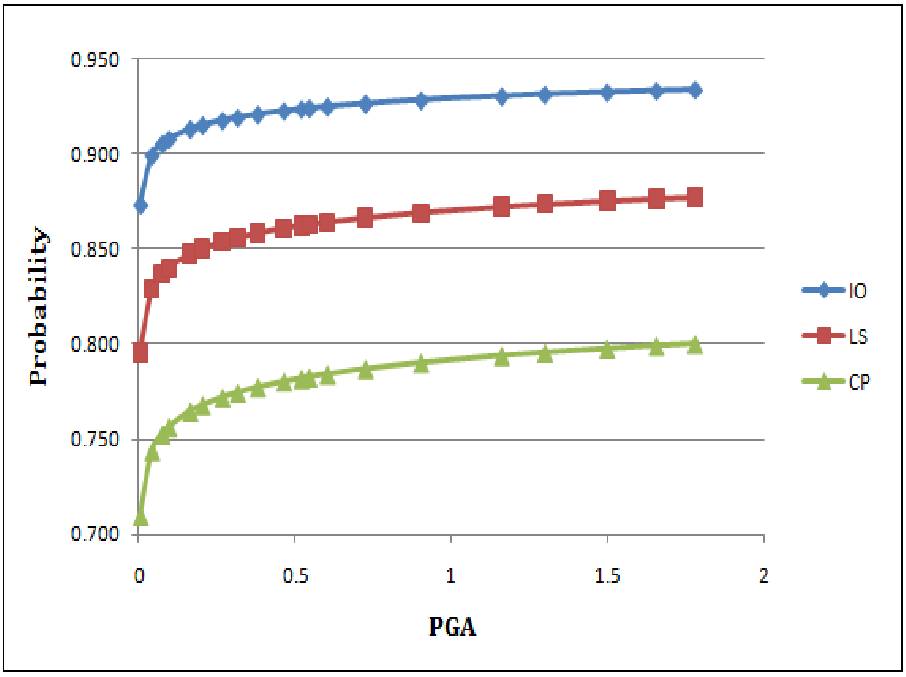

Figure 6.14: Fragility Curve of Structural Response (Drift) for Equivalent Strut

Figure (6.14) indicates that the probability of exceeding a particular limit state in equivalent strut model, IO, LS and CP were found to be 0.87 to 0.93 percent , 0.79 to 0.87 percent and 0.70 to 0.80 percent respectively.

Similarly, probability calculation of structural response (Displacement) for equivalent strut is carried out to find probability at performance point.

Table 6.21: Maximum Displacement for Equivalent Strut

SR.No.	PGA (g)	Max. Displ (m)	PGA	Max. Displ (%)
1	0.004	0.0051	0.039	0.17
2	0.041	0.015	0.402	0.5
3	0.074	0.013	0.726	0.43
4	0.095	0.031	0.932	1.03
5	0.163	0.14	1.599	4.66
6	0.202	0.12	1.982	4
7	0.266	0.14	2.609	4.66
8	0.315	0.13	3.090	4.33
9	0.379	0.15	3.718	5
10	0.463	0.26	4.542	8.66
11	0.519	0.17	5.091	5.66
12	0.544	0.13	5.337	4.33
13	0.602	0.24	5.906	8
14	0.724	0.23	7.102	7.66
15	0.902	0.61	8.849	20.33
16	1.16	0.28	11.380	9.33
17	1.298	0.31	12.733	10.33
18	1.497	0.054	14.686	1.8
19	1.655	0.18	16.236	6
20	1.779	0.31	17.452	10.33

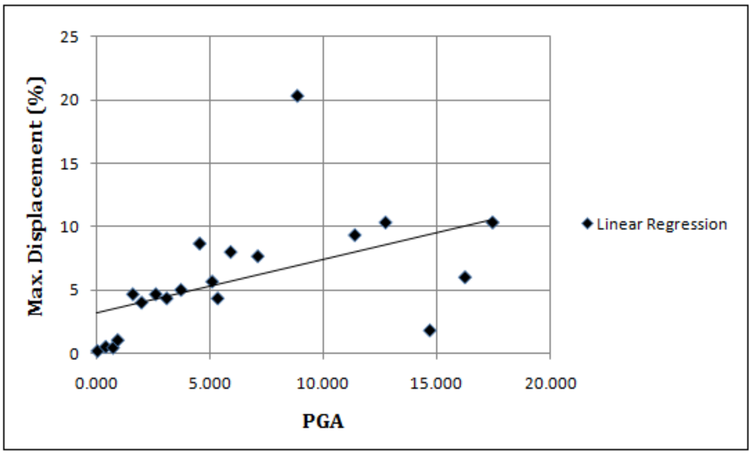

Figure 6.15: Linear regression plot of Maximum Displacement Vs. PGA for Equivalent Strut

Table 6.22: Linear Regression Calculation of Maximum Displacement for Equivalent Strut

SR.No.	**PGA (X)**	**Max. Displacement (%) (Y)**	$\mathbf{X^2}$	$\mathbf{Y^2}$	**XY**
1	0.039	0.17	0.002	0.029	0.007
2	0.402	0.5	0.162	0.250	0.201
3	0.726	0.43	0.527	0.185	0.312
4	0.932	1.03	0.869	1.061	0.960
5	1.599	4.66	2.557	21.716	7.451
6	1.982	4.0	3.927	16.000	7.926
7	2.609	4.66	6.809	21.716	12.16
8	3.090	4.33	9.549	18.749	13.38
9	3.718	5.0	13.82	25.000	18.59
10	4.542	8.66	20.63	74.996	39.33
11	5.091	5.66	25.92	32.036	28.82
12	5.337	4.33	28.48	18.749	23.11
13	5.906	8.0	34.88	64.000	47.24
14	7.102	7.66	50.44	58.676	54.40
15	8.849	20.33	78.30	413.31	179.89
16	11.380	9.33	129.50	87.049	106.17
17	12.733	10.33	162.14	106.71	131.54
18	14.686	1.8	215.67	3.240	26.43
19	16.236	6.0	263.59	36	97.41
20	17.452	10.33	304.57	107	180.28
TOTAL	**124.410**	**117.21**	**1352.34**	**1106.18**	**975.62**

Figure (6.15) shows linear regression plot of maximum displacement Vs. PGA for equivalent strut. The constants a_1 and a_2 are calculated through a linear regression analysis as per Table C.1 and formulations which are given in Appendix C. The constants a_1 and a_2 are obtained 3.18 and 0.43 respectively.

Table 6.23: Probability Calculation of Structural Response (Displacement) for Equivalent Strut

ln(PGA)	$\lambda_{\mathbf{D}}$	**(ln(PGA)-** $\lambda_D)^2$	$\mathbf{\Phi}$**(X)**	**Probability**
-3.238	-0.235	9.015	-0.627	0.672
-0.911	0.765	2.809	-1.548	0.880
-0.320	1.019	1.794	-1.782	0.918
-0.070	1.127	1.433	-1.881	0.932
0.469	1.359	0.791	-2.094	0.955
0.684	1.451	0.588	-2.179	0.963
0.959	1.569	0.372	-2.288	0.971
1.128	1.642	0.264	-2.355	0.975
1.313	1.722	0.167	-2.428	0.979
1.513	1.808	0.087	-2.508	0.983
1.628	1.857	0.053	-2.553	0.985
1.675	1.877	0.041	-2.571	0.985
1.776	1.921	0.021	-2.611	0.987
1.960	2.000	0.002	-2.685	0.989
2.180	2.094	0.007	-2.772	0.991
2.432	2.203	0.053	-2.871	0.994
2.544	2.251	0.086	-2.916	0.994
2.687	2.312	0.140	-2.972	0.995
2.787	2.355	0.186	-3.012	0.996
2.859	2.386	0.224	-3.040	0.996

Table 6.23 shows the probability calculation of structural response (Displacement) for equivalent strut. The value of $\beta_{D/GMI}$ is obtained 1.0 from Table 6.23. The capacity uncertainty (β_{cl}) and modeling uncertainty (β_m) are taken as 0.3 respectively. The value of λ_{cl} is take as 0.05.

Table 6.24: Probability of Structural Response (Displacement) for Equivalent Strut

SR.No.	**PGA (g)**	Probability
1	0.004	0.672
2	0.041	0.880
3	0.074	0.918
4	0.095	0.932
5	0.163	0.955
6	0.202	0.963
7	0.266	0.971
8	0.315	0.975
9	0.379	0.979
10	0.463	0.983
11	0.519	0.985
12	0.544	0.985
13	0.602	0.987
14	0.724	0.989
15	0.902	0.991
16	1.16	0.994
17	1.298	0.994
18	1.497	0.995
19	1.655	0.996
20	1.779	0.996

Table 6.24 shows probability of exceeding a particular limit state for bare frame at performance point

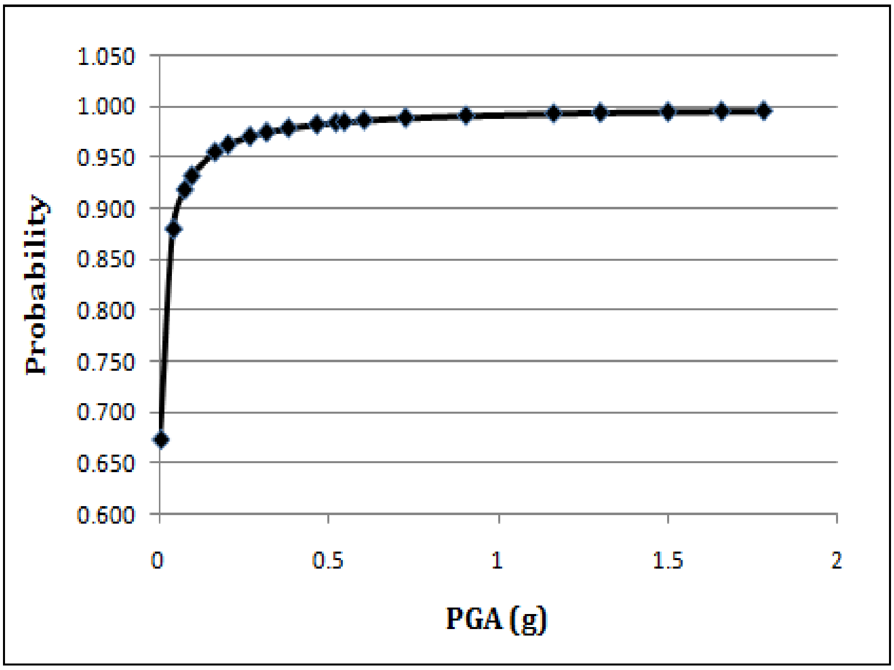

Figure 6.16: Fragility Curve of Structural Response (Displacement) for Equivalent Strut

Figure (6.16) shows that the probability of structural response (Displacement) for equivalent strut model to exceeding a limit state was found to be 0.67 to 0.99 percent.

6.6 Uncertainty In a Fragility Analysis

Modeling Uncertainty:

To examine the influence of modeling uncertainty on the fragility analysis, the capacity uncertainty is first defined as zero. The modeling uncertainty is varied from 0 to 1.0 and the results are plotted in Figure(6.17)

Table 6.25: Modeling Uncertainty in Bare Frame

SR. No.	**PGA (g)**	**Probability**					
		βm = 0	βm = 0.2	βm = 0.4	βm = 0.6	βm = 0.8	βm = 1
1	0.004	0.675	0.674	0.673	0.670	0.667	0.663
2	0.041	0.760	0.759	0.756	0.751	0.745	0.737
3	0.074	0.782	0.781	0.778	0.772	0.766	0.758
4	0.095	0.791	0.790	0.787	0.782	0.774	0.766
5	0.163	0.811	0.810	0.807	0.801	0.794	0.785
6	0.202	0.819	0.818	0.814	0.809	0.801	0.792
7	0.266	0.829	0.828	0.824	0.818	0.810	0.801
8	0.315	0.835	0.834	0.830	0.824	0.816	0.807
9	0.379	0.841	0.840	0.836	0.830	0.822	0.813
10	0.463	0.848	0.847	0.843	0.837	0.829	0.820
11	0.519	0.852	0.850	0.847	0.841	0.833	0.823
12	0.544	0.853	0.852	0.848	0.842	0.834	0.825
13	0.602	0.856	0.855	0.852	0.846	0.838	0.828
14	0.724	0.862	0.861	0.857	0.851	0.843	0.834
15	0.902	0.869	0.868	0.864	0.858	0.850	0.841
16	1.16	0.877	0.876	0.872	0.866	0.858	0.848
17	1.298	0.880	0.879	0.875	0.869	0.861	0.852
18	1.497	0.884	0.883	0.879	0.874	0.866	0.856
19	1.655	0.887	0.886	0.882	0.876	0.869	0.859
20	1.779	0.889	0.888	0.884	0.878	0.871	0.861

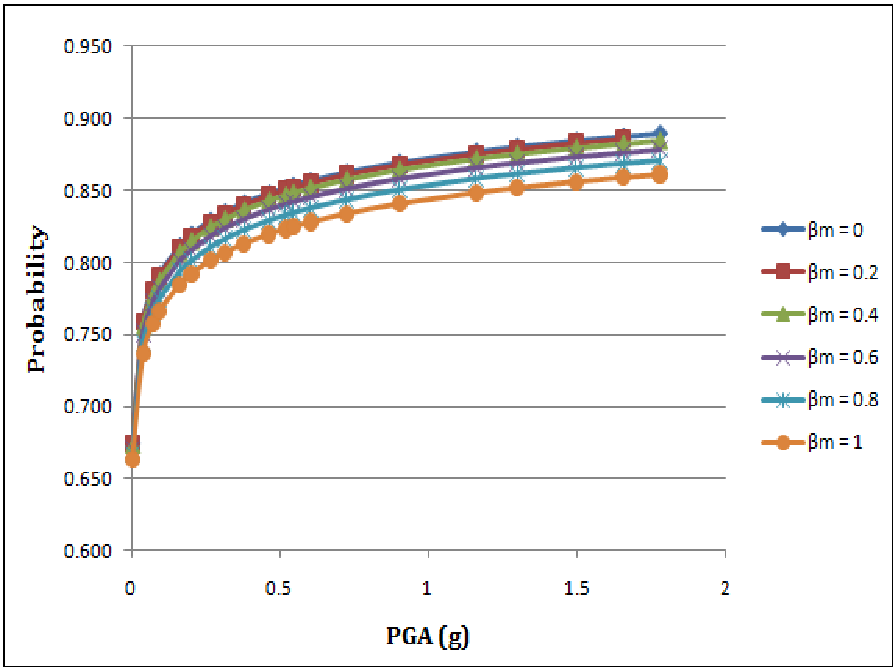

Figure 6.17: Fragility Curve for Modeling Uncertainty in Bare Frame

Capacity Uncertainty:

capacity uncertainty is varied from zero to 1.0 as shown in Figure (6.18). FEMA 356 defines inter-story drift values that are typical values of the overall performance of the structure associated with a particular performance level, but inherent uncertainties cause variation between the model and the structures performance. Therefore, the difficulty arises in determining an appropriate value for the capacity uncertainty. A value of 100% is a large value for the capacity uncertainty and zero uncertainty in not realistic. A smaller range of capacity uncertainty values is shown in Figure (6.18) and the effect of a smaller range in the capacity uncertainty can be seen as negligible.

Table 6.26: Capacity Uncertainty in Bare Frame

SR. No.	**PGA (g)**	**Probability**					
		βcl = 0	βcl = 0.2	βcl = 0.4	βcl = 0.6	βcl = 0.8	βcl = 1
1	0.004	0.613	0.613	0.613	0.612	0.612	0.611
2	0.041	0.670	0.669	0.668	0.665	0.662	0.658
3	0.074	0.689	0.689	0.687	0.684	0.680	0.675
4	0.095	0.698	0.697	0.695	0.692	0.688	0.683
5	0.163	0.718	0.717	0.714	0.711	0.706	0.700
6	0.202	0.726	0.725	0.722	0.718	0.713	0.707
7	0.266	0.736	0.735	0.732	0.728	0.723	0.716
8	0.315	0.742	0.741	0.739	0.734	0.728	0.722
9	0.379	0.749	0.748	0.746	0.741	0.735	0.728
10	0.463	0.757	0.756	0.753	0.748	0.742	0.735
11	0.519	0.761	0.760	0.757	0.752	0.746	0.739
12	0.544	0.763	0.762	0.759	0.754	0.748	0.740
13	0.602	0.767	0.766	0.763	0.758	0.751	0.744
14	0.724	0.774	0.773	0.770	0.765	0.758	0.750
15	0.902	0.782	0.781	0.778	0.773	0.766	0.758
16	1.16	0.792	0.791	0.787	0.782	0.775	0.767
17	1.298	0.796	0.795	0.791	0.786	0.779	0.770
18	1.497	0.801	0.800	0.797	0.791	0.784	0.775
19	1.655	0.805	0.804	0.800	0.795	0.787	0.779
20	1.779	0.808	0.806	0.803	0.797	0.790	0.781

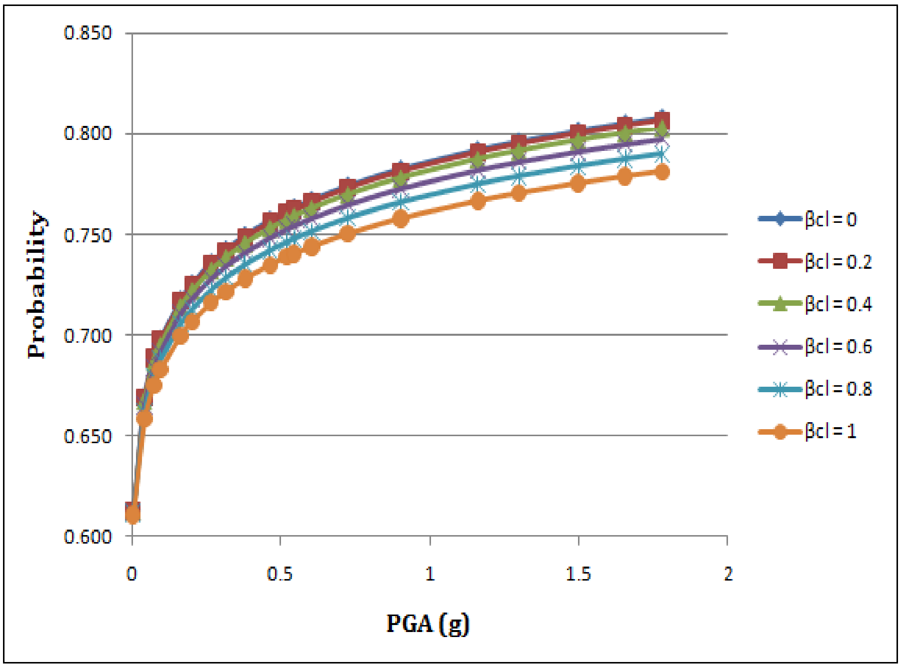

Figure 6.18: Fragility Curve for Capacity Uncertainty in Bare Frame

6.7 Summary

This chapter includes generation of Fragility Curve methodology as available in literature. It also include fragility curve generated for limit state of peak interstorey drift and peak displacement of G+4 storey RCC building. The chapter also discuss the modeling uncertainty and capacity uncertainty that need to be incorporate while generating fragility curves.

The results of the Fragility Analysis shows that, fragility curves generated for building models for three specified limit states follows similar trend that given in literature. Fragility curves generated for bare frame for three specified limit states, namely, IO, LS and CP, shows that probability of exceeding these limit state is least as compared to that of building with infill walls. Building with infill as membrane wall seems maximum probability of exceeding a specified limit state.

Chapter 7

Summary and Conclusions

7.1 Summary

This thesis is an attempt to understand Performance Based Design of G+4 storey R.C.C. building and implement such limit states to generate Fragility Curve. The main objective of the work is to obtain fragility curve by conventional method for limit states specified of response quantities like peak interstorey drift and peak displacement. Linear Static and Dynamic analysis is performed using the codal seismic coefficient method. To carry out pushover analysis different nonlinear hinge properties like default Moment (M_3) hinges and Shear (V_2) hinges were added to beams, default Axial Moment Interaction (PMM) hinges were added to columns and Axial (P) hinges in diagonal struts were provided. Time History Analysis considering twenty nos. of earthquake ground motion records were performed on three different models of building i.e, bare frame and infill wall as a membrane wall and equivalent strut, in ETABS (Version 9.5).

Pushover Curve, Capacity Spectrum Curve, Performance point and Time History traces for each storey level in terms of maximum displacement and maximum acceleration were obtained for building models in ETABS. In order to understand the influence of lateral loading patterns on pushover analysis, three lateral loading patterns, namely, parabolic, triangular and rectangular were considered and plots for V/W Vs. displacements were obtained.

A Fragility Curves, which are indicators of exceeding specified limit states under various ground motions (seismic hazards) were drawn for three different building models. The limit state on maximum interstorey drift and displacement at performance point obtained through pushover analysis are considered to generate fragility curves. Also, influence of modeling uncertainty and capacity uncertainty on fragility curves are explained through parametric study.

7.2 Conclusions

Following conclusions are made based on work carried out:

- Different building model developed based on different modeling aspects showed distinct modeling effect on overall results of the building.
- As new building has designed for an earthquake forces prior to nonlinear analysis its performance was found satisfactory.
- Building model without infill i.e, bare frame has an overall performance in Life Safety to Collapse Prevention.
- Building model with infill as membrane wall has an overall performance in Immediate Occupancy level.
- Building model with infill as equivalent strut has an overall performance in Immediate Occupancy level.
- It has been observed that, performance point of three models of building lies in nonlinear range.
- Rectangular loading pattern gives higher base shear to weight ratio as compared to other loading patterns, namely, parabolic and triangular loading pattern.
- Parabolic loading pattern gives the least base shear to weight ratio as compared to other loading patterns.

- It was observed that displacement capacity under parabolic loading pattern is maximum among all other loading pattern considered.
- The rectangular loading pattern is best fitted in case of obtaining maximum seismic demands as it extract maximum capacity of the building.
- Time history analysis of three models of building for twenty nos. of earthquake ground motions shows that peak interstorey drift and peak displacement is less in bare frame as compared to membrane wall / equivalent strut.
- Fragility Curves generated for building models for three specified limit states follows similar trend that given in literature.
- Fragility Curve generated for bare frame for three specified limit states, namely, IO, LS and CP, shows that probability of exceeding these limit state is least as compared to that of building with infill walls.
- Building with infill as membrane wall seems maximum probability of exceeding specified limit state.

7.3 Future scope of Work

Following works can be taken up as future scope of work related to present study of work.

- Generate fragility curves for G+4 storey R.C.C. building considering Incremental Dynamic Analysis (IDA) based response quantities.
- Generate fragility relationships for controlled structures.
- Using performance based analysis suggest retrofit measures for a building and develop fragility relationship of retrofitted building.

Appendix A

Appendix-A

MODELING OF INFILL WALLS

For lateral load resisting frame, the stiffness of infill wall and strength contribution has to be considered. Non-integral infill frame subjected to lateral load behaves like a diagonally braced frame. Hence, appropriately, infill wall can be replaced by an equivalent compression only strut in the analysis model.

MODULUS OF ELASTICITY OF MASONRY

The modulus of elasticity of masonry is calculated from the formula given below:

$$E_m = 750 f_m$$

where, f_m = Compressive strength of brickwork Brick masonry walls are commonly constructed in India using cement mortar of 1:6 and bricks (first or second class) of size 210 x 110 x 60 mm. So, compressive strength (f_m) of brick masonry constructed in India will be 1.85 N/mm^2 for first class bricks and 1.65 N/mm^2 for second class brick [16]. For calculation of the strut parameter here f_m has been taken as 1.65 N/mm^2 to be on conservative side. So, all the strut should be modelled with modulus of elasticity, $E_m = 750 \times 1.65$ N/mm^2 = 1237.5 MPa

EQUIVALENT WIDTH OF STRUT

The key to the equivalent diagonal strut approach lies in determination of effective width of the equivalent diagonal strut. For solid walls width of equivalent diagonal strut (w) can be taken as one third of the diagonal length (d) of the infill wall [17].

$$w = d/3$$

FAILURE PROPERTIES OF STRUT

The equivalent struts has to be modeled with axial hinges, which has brittle load-deformation relation only for compression. Figure A.1 shows a typical load-deformation relation for the axial hinge in strut. R and Δ_y represent the yield load and the yield deformation, respectively, of the strut.

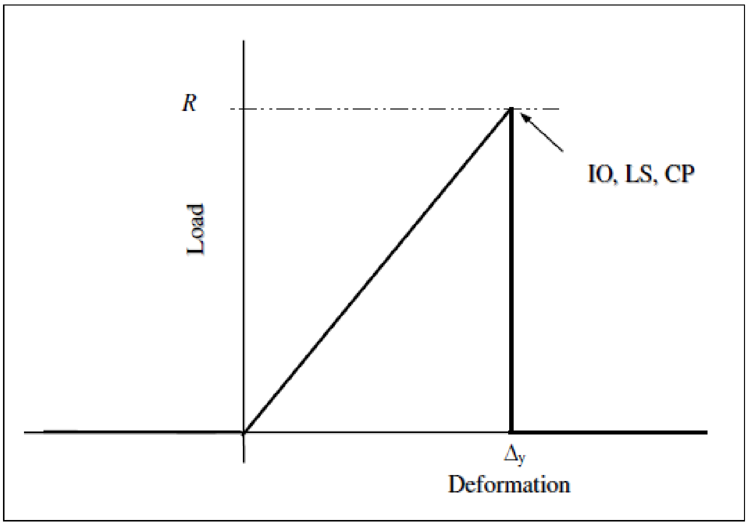

Figure A.1: A typical stress-strain relation for axial hinges in equivalent struts

Lower of the failure loads corresponding to the following failure modes is taken as the strength(R) of the masonry infill.

I. Local crushing of the masonry at one of the compression corners of the infill wall.

II. Shear cracking along the bed-joints of the bricks.

I. Crushing failure

The diagonal load causing local crushing (R_c) is given by the following equation [16]

$$R_c = \alpha_c t sec\theta f_m \tag{A.1}$$

The length of the contact at the column (α_c) at the compression diagonal corner is calculated using the following formula.

$$\frac{\alpha_c}{h} = \frac{\pi}{2\lambda h} \tag{A.2}$$

Hence λ is the relative stiffness of the infill to the frame. It can be expressed as

$$\lambda = \sqrt[4]{\frac{E_m t sin2\theta}{4E_c I_c h'}} \tag{A.3}$$

Here,

E_c = Modulus of elasticity of concrete in the column

h = Height of column (between centerlines of beams)

h' = Clear height of infill wall

I_c = Moment of inertia of the column section (Lowest of the two Column)

l = Length of beam (between centerlines of columns)

t = Thickness of infill wall

θ = Slope of the infill diagonal to the horizontal

II. Shear failure

Shear failure load R$_s$ cab be estimated by a relation which is obtained from simple and non-dimensional curve. Following relationship of R$_s$ proposed [16]

$$\frac{R_s}{f'_{bs}ht} = 1.65(l'/h')^{0.6}(\lambda h)^{-0.05(l'/h')0.5} \tag{A.4}$$

Where, f'_{bs} is the bond strength between the masonry and mortar. It is varies from 0.24 MPa for low strength mortar to 0.69 MPa for high strength mortar [16]. Again to be in conservative side f'_{bs} is taken as 0.24 for the calculation.

Lower of R_c and R_s is the axial strength (R) of the equivalent strut. Yield deformation (Δ_y) is to be calculated using the following formula.

$$\Delta_y = \frac{R}{AE/d} = \frac{R \times d}{W \times t \times E} \tag{A.5}$$

Appendix B

Appendix-B

Calculation of Ca and Cv:

According to **ATC-40** [**7**], an Elastic Response Spectrum, for each earthquake hazard level of interest at a site is based on the site seismic coefficients Ca and Cv. The seismic coefficient Ca represents the effective peak acceleration (EPA) of the ground. A factor of about 2.5 times Ca represents the average value of peak response of a 5% damped short period system in the acceleration domain. The seismic coefficient Cv represents 5% damped response of a 1-second system and when divided by period defines acceleration response in the velocity domain.

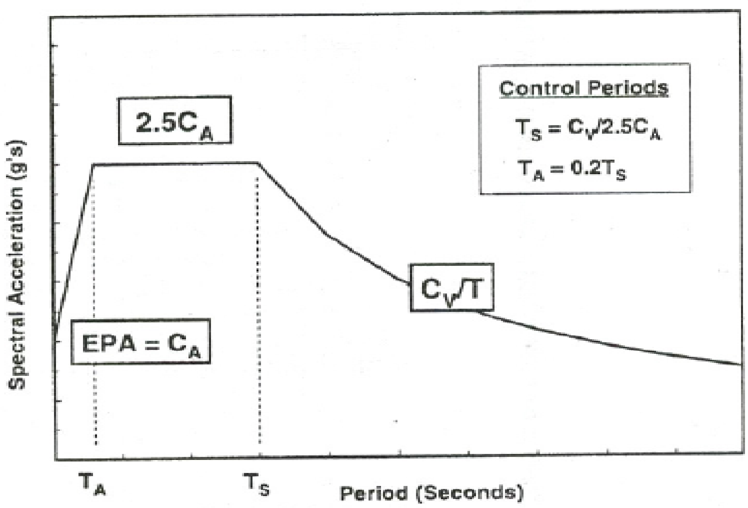

Figure B.1: Construction of a 5% damped Elastic Response Spectrum

The Response Spectrum for 5% damping given in IS:1893(Part-I):2002 is shown in Figure (B.2)

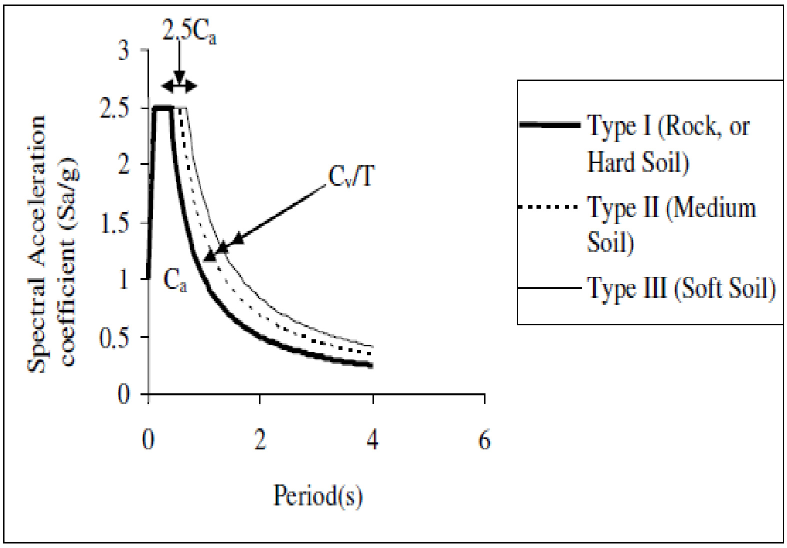

Figure B.2: Response Spectrum Curve of IS:1893(Part-I):2002

Coefficient of acceleration (Ca) = Z

Coefficient of velocity (Cv) = 2.5 Ca Cv

For Zone III (Rock, or Hard Soil)

Ca = 0.16

T = 1 sec

Cv = 2.5X0.16X1 = 0.4

Appendix C

Appendix-C

Linear Regression:

A technique for estimating the equation of a "best fit" straight line to express the relationship between two variable; i.e. X & Y.

Equation of a Straight Line:

$$Y = a + bX \tag{C.1}$$

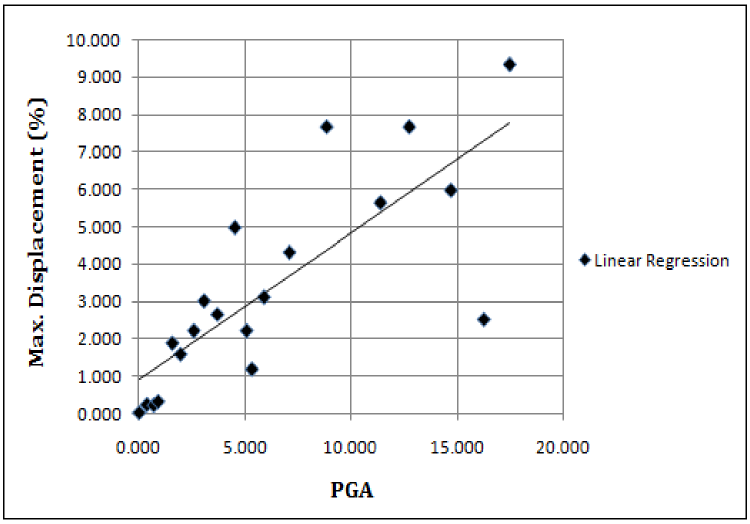

Figure C.1: Linear Regression Analysis of Structural Response Data

Y = vertical axis; e.g. Max. Interstorey Drift

X = horizontal axis; e.g. Peak Ground Acceleration(PGA)

a = the intercept, the point at which the line intersects the Y axis

b = the slope of the line, the rate of increase or decrease in Y as a function of a unit change in X

Equations for Estimating the "Best Fit" Straight Line:

The slope (b) of the "best fit" line is also called the regression coefficient,

$$b = [XY - (\Sigma X)(\Sigma Y)/N]/[\Sigma X^2 - (\Sigma X)^2/N] \tag{C.2}$$

The intercept (a) of the "best fit" line is also called the regression constant,

$$a = \overline{Y} - (b)(\overline{X}) \tag{C.3}$$

where, $\overline{Y}$ = Mean of Y,
$\overline{X}$ = Mean of X,
N = Number of data points.

References

[1] Advanced in Performance Based Earthquake Engineering.

[2] B.Gencturk, A.S.Elanshai and J.Song, *The* 14^{th} *World Conference on Earthquake Engineering*, October 12-17, 2008.

[3] FEMA 445, Federal Emergency Management Agency, Next-Generation Performance Based Seimic Design Guidelines, August 2006.

[4] E.D. Thomson, A.J. Carr and P.J. Moss, P-$\triangle$ Effects in the Seismic Response of Ductile Reinforced Concrete Frames, Pacific Conference on Earthquake Engineering, New Zealand, November 1991.

[5] Yogendra Singh, Earthquake Resistant Design and Retrofitting of Reinforced Concrete Buildings, Push Over Analysis of RC Buildings, July 2003.

[6] Farzad Naeim, Performance Based Seismic Engineering, Earthquake Ground Motions and Performance Based Design, 1998.

[7] ATC-40, Applied Technology Council, Seismic Evaluation and Retrofit of Concrete Buildings, Volume 1, 1996.

[8] Murat Serdar Kircil and Zekeriya Polat, Fragility analysis of mid-rise RC frame buildings, Engineering Strucures, January 2006.

[9] Sathish K. Ramamoorthy, Paolo Gardoni and Joseph M. Bracci, Probabilistic Demand Models and Fragility Curves for Reinforced Concrete Frames, *Journal Of Structural Engineering (ASCE)*, October 2006.

[10] Bora Gencturk, Amr S. Elnashai, and Junho Song, Fragility Relationship For Populations of Buildings Based On Inelastic Response, Mid-American Earthquake Center, August 2007.

[11] Ashraf Habibullah and Stephen Pyle, Practival Three Dimentional Nonlinear Static Pushover Analysis, *Structure Magazine*, Winter, 1998.

[12] ETABS Users Manual, "Integrated Building Design Software, Computer and Structure Inc. Berkeley, USA

[13] Pacific Earthquake Engineering Research (PEER) Center, PEER Strong Motion Database Records.

[14] FEMA 356, Federal Emergency Management Agency, Prestandard And Commentary For The Seismic Rehabilition of Buildings, November 2000.

[15] Wen. Y.K., Ellingwood, B.R. and Bracci, J. (2004), "Vulnerability Function Framework for Consequences-based Engineering," MAE Center Projects DS-4 Report, Mid-American Earthquake Center, University of Illinois at Urbana-Champaign.

[16] Sivaji C V., "Evaluation of Seismic Vulnerability of Existing Building", M. Tech Thesis, Indian Institute of Technology Madras, 2004 Chennai, India.

[17] Code and Commentary on IS:1893 (Part 1):2002 IITK-GSDMA-EQ05-V2.

[18] FEMA 273, Federal Emergency Management Agency,NEHRP Guidelines For The Seismec Rehabilitation Of Buildings, Octomber 1997.

[19] Pacific Earthquake Engineering Research Center, "US-Japan workshop on Performance-Based Earthquake Engineering Methodology for Reinforced Concrete Building Structures, September 1999.

[20] IS:1893 (Part 1):2002, Criteria For Earquake Resistant Design Of Structures, June 2002.

[21] IS:456:2000, Plain And Reinforced Concrete Code of Practice, July 2000.

[22] IS:875 (Part 2):1987, Code Of Practive For Design Loads (Other Than Earthquake) For Buildings And Structures, June 1998.